

---

Electronic Thesis and Dissertation Repository

---

2-4-2016 12:00 AM

## Aerobic Oxidations Mediated by Allylnickel(N-Heterocyclic Carbene)Chloride Complexes: Investigating the Role of a Pendent Amine Group

Richard J. Hazlehurst  
*The University of Western Ontario*

Supervisor  
Johanna Blacquiere  
*The University of Western Ontario*

Graduate Program in Chemistry  
A thesis submitted in partial fulfillment of the requirements for the degree in Master of Science  
© Richard J. Hazlehurst 2016

Follow this and additional works at: <https://ir.lib.uwo.ca/etd>

 Part of the [Inorganic Chemistry Commons](#)

---

### Recommended Citation

Hazlehurst, Richard J., "Aerobic Oxidations Mediated by Allylnickel(N-Heterocyclic Carbene)Chloride Complexes: Investigating the Role of a Pendent Amine Group" (2016). *Electronic Thesis and Dissertation Repository*. 3492.

<https://ir.lib.uwo.ca/etd/3492>

This Dissertation/Thesis is brought to you for free and open access by Scholarship@Western. It has been accepted for inclusion in Electronic Thesis and Dissertation Repository by an authorized administrator of Scholarship@Western. For more information, please contact [wlsadmin@uwo.ca](mailto:wlsadmin@uwo.ca).

## Abstract

Molecular oxygen (O<sub>2</sub>) represents the most ideal "green" oxidant for the large-scale oxidation of organic compounds, due to its inexpensive and environmentally benign characteristics. However, a number of challenges remain for its use in the fine chemical and pharmaceutical industry, including the development of highly selective catalytic transformations. NiCl(allyl)(NHC) complexes have been shown to react with O<sub>2</sub> to promote the oxidation of the allylic ligand, however non-catalytically.

This report details the synthesis and characterization of novel NiCl(cinnamyl/allyl)(NHC) complexes, containing a pendent 2° amine arm on the NHC ligand to act as a hydrogen-bond donor group. The complexes prove to exhibit dynamic behavior, with the pendent amine showing the ability for hydrogen-bonding and/or hemi-labile ligand coordination to the metal. Dioxygen reactivity studies indicate that the complexes are active for aerobic oxidation, and that the product distribution is different than that of previously reported systems. However, the observed reactivity currently is non-catalytic.

## Keywords

Nickel (II) complexes, N-heterocyclic carbene ligands, molecular oxygen, allylic C-H oxidation, hydrogen bonding, hemi-labile coordination, variable temperature NMR spectroscopy, X-ray crystallography

## Acknowledgments

First and foremost, I would like to sincerely thank my supervisor for this project, Dr. Johanna Blacquiere. She was always more than willing to help me with any facet of my research, whether it be in the lab, or with writing and presentations. Her support throughout the entire process, coupled with her vast knowledge of the area, has definitely made this thesis possible. I could have not asked for a better supervisor.

I would also like to greatly thank the research staff, and faculty in the chemistry department that have assisted me over my graduate career. Specifically Dr. Mathew Willans for assistance for everything related to NMR spectroscopy, Kristina Jurcic and Jasmine Wang for running MALDI-MS samples, and Doug Hairsine for help with GC/MS experiments. A special thanks goes to Dr. Paul Boyle for his assistance in X-ray crystallography, including training in the use of the equipment, helping me solve the obtained data, as well as solving/running my samples in some cases. Additionally, thanks to Dr. Paul Ragogna and his research group for letting me use their glovebox in the early days of my research. Also thanks to Dr. Richard Puddephatt and his research group for the use of many of their chemicals and equipment over the two years.

A thank you to the many members of the Blacquiere group that I had the pleasure of working with the past two years. Specifically graduate students James Stubbs, Ava Behnia, John-Paul Bow, David Bocking, and Scott Hendriks, in addition to the past and present undergraduate students of the lab. These people made it enjoyable to come into the lab, and helped me with many things along the way. We have had a number of great times both in the lab, as well as outside of school, and I hope we can continue to be friends in the future.

Lastly, I need to thank my family and friends (both in chemistry and outside of chemistry) for their endless support over both my graduate and undergraduate career, especially my parents Brian and Paulette. All of you have helped me get through university and enjoy it along the way.

# Table of Contents

Abstract.....	i
Acknowledgments.....	ii
Table of Contents.....	iii
List of Tables.....	vi
List of Figures.....	vii
List of Schemes.....	xi
List of Abbreviations.....	xiii
<b>Chapter 1</b> .....	<b>1</b>
1 Introduction.....	1
1.1 Catalysis.....	1
1.1.1 Organometallic Catalysis.....	2
1.2 Allylic C-H Oxidation Chemistry.....	3
1.2.1 Catalytic Allylic C-H Oxidations with Specialty Oxidants.....	4
1.2.2 Dioxygen as an Oxidant.....	5
1.2.3 Catalytic Aerobic Oxidations.....	6
1.3 Ni Dioxygen Reactivity.....	8
1.4 Hydrogen-Bonding Groups.....	11
1.5 Project Goals.....	12
1.5.1 Synthesis of NiX(allyl/cinnamyl)(NHC) Complexes.....	12
1.5.2 O <sub>2</sub> Reactivity of NiCl(allyl/cinnamyl)(NHC) Complexes.....	13
1.6 References.....	15
<b>Chapter 2</b> .....	<b>18</b>
2 Synthesis and Characterization of Dynamic NiX(allyl)(NHC) and NiCl(cinnamyl)(NHC) Complexes.....	18
2.1 Ligand Synthesis.....	18

2.2	Synthesis of NiCl(allyl/cinnamyl)(NHC) Complexes .....	20
2.2.1	Synthesis of Complex 2a .....	20
2.2.2	Synthesis of Complexes 3a and 3b .....	20
2.2.3	Attempted Synthesis of Complex 3c.....	21
2.3	Characterization of NiCl(allyl/cinnamyl)(NHC) Complexes .....	21
2.3.1	MALDI Mass Spectrometry Analysis of Complexes 2a, 3a, and 3b.....	21
2.3.2	Solid-State Analysis of Complexes 2a, 3a, and 3b .....	23
2.3.3	<sup>1</sup> H NMR Characterization and Dynamics of Complexes 2a, 3a, and 3b ..	27
2.4	Efforts Towards Reducing Dynamic Processes for <sup>1</sup> H NMR Characterization of 2a.....	30
2.4.1	Attempted Deprotonation of 2a with Base.....	30
2.4.2	Synthesis and Characterization of a NiI(allyl)(NHC) Complex .....	31
2.5	Conclusions.....	37
2.6	References.....	39
<b>Chapter 3</b>	.....	<b>40</b>
3	Dioxygen Reactivity Studies.....	40
3.1	Reactivity of NiCl(allyl/cinnamyl)(NHC) complexes with O <sub>2</sub> .....	40
3.2	Time Scale of the Aerobic Oxidation of 3a .....	41
3.3	Effect of Solvent in the Aerobic Oxidation of 3a .....	43
3.4	Effect of Changing R <sup>2</sup> in Aerobic Oxidations .....	45
3.5	Control Experiments .....	46
3.6	Attempted Catalytic Aerobic Oxidations.....	47
3.7	Determining the Fate of Nickel after Oxidation .....	51
3.8	Conclusions.....	53
3.9	References.....	54
<b>Chapter 4</b>	.....	<b>55</b>

4	General Conclusions and Future Work .....	55
4.1	General Conclusions .....	55
4.2	Future Work .....	57
4.3	References.....	59
5	<b>Experimental</b> .....	60
6	<b>Appendix</b> .....	74
6.1	Crystallographic Data for 2a.....	74
6.2	Crystallographic Data for 3b.....	76
6.3	Crystallographic Data for 3a.....	81
6.4	MALDI-MS Data.....	84
6.5	<sup>1</sup> H NMR Spectra .....	87
6.6	<sup>13</sup> C NMR Spectrum for Complex 4a.....	92
6.7	GC-FID Calibration Data for Aerobic Oxidation Reactions .....	93
6.8	Data for Aerobic Oxidation Reactions.....	96
6.9	References.....	97
	Curriculum Vitae .....	98

## List of Tables

Table 2.1 Selected bond lengths (Å) and bond angles (deg) for solid-state structures discussed .....	27
Table 3.1 Results of control experiments for aerobic oxidation reactions .....	47
Table 3.2 Data for attempted catalytic aerobic oxidations of <b>3b</b> .....	50
Table 6.1 Summary of crystal data for <b>2a</b> .....	75
Table 6.2 Summary of crystal data for <b>3b</b> .....	78
Table 6.3 Selected bond lengths (Å) and bond angles (deg) for molecule B ( <b>3b</b> ) .....	81
Table 6.4 Summary of crystal data for <b>3a</b> .....	82
Table 6.5 Data for aerobic oxidation reactions of complexes <b>3a</b> and <b>3b</b> .....	96

## List of Figures

Figure 1.1 Generic Gibbs free energy profile for transformation of reactant A to product B, showing different reaction pathway for non-catalytic (black) and catalytic (red) reactions ....	1
Figure 1.2 Known reaction products and binding modes of Ni with dioxygen.....	9
Figure 1.3 Effect of bulkiness of NHC ligand and observed O <sub>2</sub> reactivity of corresponding NiCl(allyl)(NHC) complexes.....	11
Figure 1.4 Monomeric M-OH complexes stabilized by H-bonding.....	12
Figure 1.5 NHC compounds and NiX(allyl/cinnamyl)(NHC) complexes studied in this report .....	13
Figure 1.6 Coordination of pendent amine arm of NHC ligand to metal centre .....	13
Figure 2.1 MALDI MS of <b>2a</b> with pyrene as the matrix. The inset depicts the simulated and observed isotope pattern for the most abundant signal. Signals that do not contain Ni or Cl (as judged by the isotope pattern) are labeled with an asterisk (*).....	22
Figure 2.2 ORTEP drawing of <b>2a</b> showing naming and numbering scheme for selected atoms of interest. Ellipsoids are at the 50% probability level and hydrogen atoms were omitted for clarity (with the exception of the hydrogen atom on N3). Disordered atom position C2' is omitted for clarity .....	24
Figure 2.3 ORTEP drawing of <b>3b</b> (Molecule A) showing naming and numbering scheme for selected atoms of interest. Ellipsoids are at the 50% probability level and hydrogen atoms were omitted for clarity (with the exception of the hydrogen atom on N3). Disordered atom positions omitted for clarity .....	25
Figure 2.4 ORTEP drawing of <b>3a</b> showing naming and numbering scheme for selected atoms of interest. Ellipsoids are at the 50% probability level and hydrogen atoms were omitted for clarity (with the exception of the hydrogen atom on N3).....	26
Figure 2.5 <sup>1</sup> H NMR spectrum of <b>2a</b> in C <sub>6</sub> D <sub>6</sub> at room temperature, 600 MHz.....	28



Figure 2.6 Potential bonding modes and ligand rotations (green arrows) of Ni(allyl)(NHC) species. A: thermodynamically stable complex (based on x-ray) B: isomerisation of NHC and allyl ligands .....	29
Figure 2.7 Variable-Temperature $^1\text{H}$ NMR experiment for complex <b>2a</b> , in $\text{CD}_2\text{Cl}_2$ , 400 MHz .....	30
Figure 2.8 Variable-Temperature $^1\text{H}$ NMR experiment for complex <b>4a</b> , in $\text{CD}_2\text{Cl}_2$ , 400 MHz .....	33
Figure 2.9 Relevant portion of $^1\text{H}$ - $^1\text{H}$ COSY NMR spectrum of <b>4a</b> (in $\text{CD}_2\text{Cl}_2$ ) showing $\text{H}^3$ of allyl group coupling to other allylic peaks, coupling of methylene protons, and coupling of NH to $\text{H}^{8/9}$ of adjacent methylene group.....	34
Figure 2.10 Comparison of $^1\text{H}$ NMR spectra for <b>2a</b> and <b>4a</b> at $-70^\circ\text{C}$ , 400 MHz.....	37
Figure 3.1 Effect of reaction time on conversion in the oxidation of <b>3a</b> and $\text{O}_2$ . Points represent the average conversion to cinnamaldehyde ( <b>6</b> , red) and phenyl vinyl ketone ( <b>5</b> , blue) oxidation products. The experiments were performed in duplicate and the error bars represent the span of the duplicate runs .....	42
Figure 3.2 Effect of solvent on conversion in the oxidation of <b>3a</b> and $\text{O}_2$ . Bars represent the average conversion to cinnamaldehyde ( <b>6</b> , red) and phenyl vinyl ketone ( <b>5</b> , blue) oxidation products. The experiments were performed in duplicate and the error bars represent the span of the duplicate runs.....	44
Figure 3.3 Effect of changing R group in the reaction of <b>3a</b> ( $\text{R}^2 = \text{tBu}$ ), and <b>3b</b> ( $\text{R}^2 = \text{Mes}$ ) with $\text{O}_2$ . Bars represent the average conversion to cinnamaldehyde ( <b>6</b> , red) and phenyl vinyl ketone ( <b>5</b> , blue) oxidation products. The experiments were performed in duplicate and the error bars represent the span of the duplicate runs. Solvent is THF.....	45
Figure 3.4 $^1\text{H}$ NMR study monitoring aerobic oxidation of <b>2a</b> in $\text{CD}_3\text{CN}$ over time .....	52
Figure 6.1 ORTEP drawing of <b>2a</b> showing naming and numbering scheme. Ellipsoids are at the 50% probability level and hydrogen atoms were omitted for clarity. Disordered atom position is depicted using “hollow” ellipsoids and bonds .....	76

Figure 6.2 ORTEP drawing of molecule A ( <b>3b</b> ) showing naming and numbering scheme. Ellipsoids are at the 50% probability level and hydrogen atoms were omitted for clarity. Disordered part of the structures is depicted by “hollow” atoms and bonds .....	79
Figure 6.3 ORTEP drawing of molecule B ( <b>3b</b> ) showing naming and numbering scheme. Ellipsoids are at the 50% probability level and hydrogen atoms were omitted for clarity. Disordered part of the structures is depicted by “hollow” atoms and bonds .....	80
Figure 6.4 MALDI-MS of <b>3a</b> with anthracene as the matrix. The inset depicts the simulated and observed isotope pattern for the most abundant signal .....	84
Figure 6.5 MALDI-MS of <b>3b</b> with anthracene as the matrix. The inset depicts the simulated and observed isotope pattern for the signal at $m/z = 440.1$ .....	85
Figure 6.6 MALDI MS of <b>4a</b> with pyrene as the matrix. The inset depicts the simulated and observed isotope pattern for the most abundant signal.....	86
Figure 6.7 $^1\text{H}$ NMR Spectrum (in $\text{C}_6\text{D}_6$ ) for Complex <b>3a</b> , 600 MHz.....	87
Figure 6.8 $^1\text{H}$ NMR Spectrum (in $\text{C}_6\text{D}_6$ ) for Complex <b>3b</b> , 600 MHz.....	88
Figure 6.9 $^1\text{H}$ NMR Spectrum (in $\text{C}_6\text{D}_6$ ) for reaction of <b>2a</b> with KH, 400 MHz .....	89
Figure 6.10 $^1\text{H}$ NMR Spectrum (in $\text{C}_6\text{D}_6$ ) for reaction of <b>2a</b> with $\text{K}_2\text{CO}_3$ , 600 MHz .....	90
Figure 6.11 High Temperature Variable-Temperature $^1\text{H}$ NMR Spectra for <b>4a</b> in $\text{C}_7\text{D}_8$ , 400 MHz .....	91
Figure 6.12 $^{13}\text{C}$ NMR Spectrum (in $\text{CD}_2\text{Cl}_2$ ) for Complex <b>4a</b> at $-50\text{ }^\circ\text{C}$ .....	92
Figure 6.13 Plot of tetradecane area count vs concentration. Red and blue dots represent data from two separate runs. Triple injections of each concentration were made. Acetone was the solvent. Dotted coloured lines represent linear trendline for respective run .....	93
Figure 6.14 Plot of cinnamaldehyde ( <b>6</b> ) area count vs concentration. Red and blue dots represent data from two separate runs. Triple injections of each concentration were made. Acetone was the solvent. Dotted coloured lines represent linear trendline for respective run	94

Figure 6.15 Plot of phenyl vinyl ketone (**5**) area count vs concentration. Red and blue dots represent data from two separate runs. Triple injections of each concentration were made. Acetone was the solvent. Dotted coloured lines represent linear trendline for respective run95

Figure 6.16 Representative  $^{19}\text{F}$  NMR Spectrum for Attempted Catalytic Aerobic Oxidation of 1-allyl-4-(trifluoromethyl)benzene with **3b**..... 97

## List of Schemes

Scheme 1.1 SHOP oligomerization of ethylene to give 1-alkenes of various lengths (C6 to C20).....	3
Scheme 1.2 One-step oxidation of a C-H group to a carbonyl group.....	3
Scheme 1.3 Allylic C-H oxidation of 1-butene to methyl vinyl ketone and 2-butenal .....	4
Scheme 1.4 Direct oxidation of an allylic C-H bond with PdCl <sub>2</sub> and DDQ .....	5
Scheme 1.5 Aerobic allylic acetoxylation of allyl benzene with a Pd-4,5-diazafluorenone catalyst .....	6
Scheme 1.6 Oxygenase type oxidation of cyclohexene with a manganese catalyst.....	7
Scheme 1.7 Generic reaction scheme for desired oxidation of a substrate to the oxidation product with O <sub>2</sub> as the sole oxidant .....	7
Scheme 1.8 Binding of superoxo to active site of nickel superoxide dismutases (NiSOD) to form a Ni-superoxo species .....	8
Scheme 1.9 Reaction of NiCl(cinnamyl/allyl)(NHC) with O <sub>2</sub> .....	10
Scheme 1.10 Proposed mechanism for allylic oxidation in the formation of cinnamaldehyde .....	10
Scheme 1.11 Proposed mechanism for oxidation of allylic ligand.....	14
Scheme 1.12 C-H activation of an allylic substrate to give the resulting Pd(allyl)(OAc) complex.....	15
Scheme 2.1 Multi-step synthesis of free NHC ligands <b>1a</b> , <b>1b</b> , and <b>1c</b> . Parenthetical numbers are isolated yields for the given step.....	19
Scheme 2.2 Two-step, one-pot synthesis of <b>2a</b> .....	20
Scheme 2.3 Two-step, one-pot synthesis of <b>3a</b> and <b>3b</b> .....	21

Scheme 2.4 Attempted two-step, one-pot synthesis of <b>3c</b> .....	21
Scheme 2.5 Attempted deprotonation of <b>2a</b> using KH .....	31
Scheme 2.6 Synthesis of <b>4a</b> through halide substitution of chloride for iodide .....	32
Scheme 2.7 Potential formation of five-coordinate Ni(II) species at low temperatures.....	36
Scheme 3.1 Reaction conditions tested in aerobic oxidation of <b>3a/b</b> .....	41
Scheme 3.2 Postulated mechanism for catalytic oxidation of <b>3a</b> and <b>3b</b> .....	48
Scheme 3.3 Attempted catalytic aerobic oxidation of allylbenzene with <b>3a/b</b> , with conditions tested .....	49
Scheme 3.4 Attempted catalytic aerobic oxidation of 1-allyl-4-(trifluoromethyl)benzene with <b>3b</b> .....	50
Scheme 4.1 NaOH deprotonation of ammonium-imidazolium intermediate .....	58

## List of Abbreviations

a, b, c,  $\alpha$ ,  $\beta$ ,  $\gamma$  = unit cell parameters

Å = Ångstrom =  $10^{-8}$  meters

$\mu$  = absorption coefficient (X-ray crystallography)

br = broad

<sup>t</sup>Bu = *tertiary*-butyl

BQ = 1,4-benzoquinone

°C = degrees Celsius

$\delta$  = chemical shift

cod = 1,5-cyclooctadiene

COSY = correlation spectroscopy

d = doublet

$\rho$  = density

$\kappa$  = denticity

DDQ = 2,3-dichloro-5,6-dicyano-1,4-benzoquinone

EA = elemental analysis

$E_a$  = activation energy

$\eta$  = hapticity

FID = flame ionization detector

g = gram

$\Delta G$  = Gibbs free energy

GC = gas chromatography

h = hour

H-bond = hydrogen bond

HMBC = heteronuclear multiple-bond correlation spectroscopy

Hz = hertz

IR = infrared spectroscopy

IAd = 1,3-di(adamantyl)imidazol-2-ylidene

IiPr = 1,3-bis(2,6-diisopropylphenyl)imidazole-2-ylidene

I*t*Bu = 1,3-bis(*tert*-butyl)imidazol-2-ylidene

IMes = 1,3-bis(2,4,6-trimethylphenyl)imidazol-2-ylidene

IMe = 1,3-bis(methyl)imidazol-2-ylidene

$J$  = coupling constant (in Hz)

K = degrees Kelvin

L = ligand

MS = mass spectrometry

m = multiplet

mg = milligram

Me = methyl

Mes = mesityl (2,4,6-trimethylphenyl)

MHz = megahertz

min = minutes

mL = millilitre

$\mu$ L = microlitre

mmol = millimole

M = molarity

mM = millimolar

mol = mole

MALDI = matrix-assisted laser desorption/ionization

$m/z$  = mass to charge ratio

NMR = nuclear magnetic resonance spectroscopy

NHC = *N*-heterocyclic carbene

NiSOD = nickel superoxide dismutases

o = ortho

ov = overlapping

p = para

ppm = parts per million

Ph = phenyl

q = quartet

R = alkyl/aryl group or hydrogen, as specified



s = singlet

SHOP = Shell higher olefin process

t = triplet

TBHP = *tert*-butyl hydroperoxide

*tert* = tertiary

UV-Vis = Ultraviolet–visible spectroscopy

VT = variable temperature

$\lambda$  = wavelength

X = halogen

## Chapter 1

### 1 Introduction

#### 1.1 Catalysis

A catalyst is defined as a substance that is used in sub-stoichiometric amounts that increases the rate of a reaction, or allows a reaction to proceed at lower temperature, all whilst not being consumed itself.<sup>1</sup> Catalysts increase the rate of reactions by operating under a different pathway with a lower activation energy ( $E_a$ ), than the non-catalyzed reaction (Figure 1.1). The reaction mechanism for a catalytic process involves a number of lower energy transition states (number depends on the catalyst/reaction being performed), in comparison to a higher energy intermediate(s) for the non-catalytic pathway. Catalysts only affect the kinetics of the reaction, as the thermodynamics ( $\Delta G$ ) do not change between catalytic and non-catalytic processes.

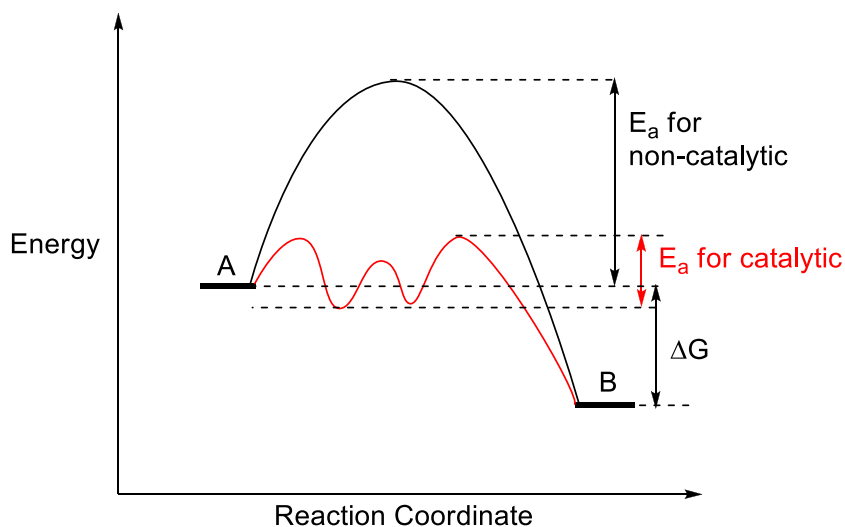


**Figure 1.1** Generic Gibbs free energy profile for transformation of reactant A to product B, showing different reaction pathway for non-catalytic (black) and catalytic (red) reactions.

Catalysts can also control the selectivity of the products formed, or allow for reactions that are not possible under non-catalytic conditions.<sup>1</sup> As a result of the aforementioned benefits

from using catalysts, they are widely used in nature (enzymes), bulk industrial synthesis, and laboratory synthesis for more specialized products. There are two main classes of catalysts: homogeneous and heterogeneous.

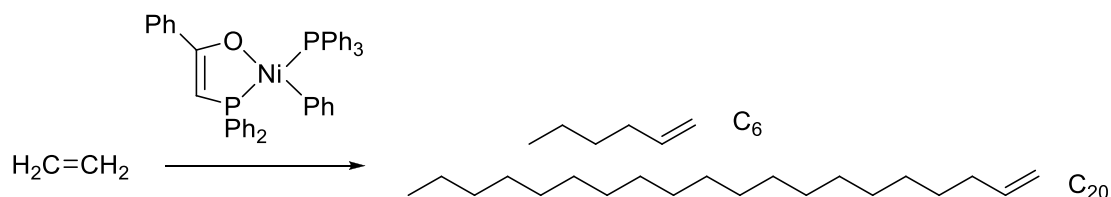
A catalyst is defined as heterogeneous if it is present in a different phase than that of the reactants.<sup>1</sup> Typically this means a solid catalyst, such as finely divided metals or metals deposited on a surface, with liquid or gaseous reactants. Heterogeneous catalysts are currently much more widespread than homogeneous for bulk chemical synthesis in industry. This widespread use is due to the robustness of the catalysts at high temperatures, allowing for repeated use under harsh reaction conditions (high temperature/pressure). Additionally, no extra steps are required for product separation, as they are in a different phase than the catalyst. The most common example encountered in day-to-day life is the catalytic converter, found on all automobiles that burn gasoline. The catalytic converter is made up of a mixture of palladium, platinum, and rhodium nanoparticles deposited on a silica/alumina surface. As the engine exhaust passes over the catalyst(s), toxic emissions such as CO and nitrogen oxides are converted to less harmful gases such as O<sub>2</sub>, N<sub>2</sub>, and CO<sub>2</sub>.

Homogeneous catalysts are present in the same phase as the reactants, usually dissolved in a solution for liquid reaction mixtures.<sup>1</sup> Within the homogeneous class there are many different types of catalysts including: acid/base (the most commonly used), organic, and organometallic complexes. Benefits of homogeneous catalysts as compared to heterogeneous systems, include: high product selectivity, easier heat dissipation in very exothermic reactions, simpler catalytic mechanism determination and variation of the catalyst structure.<sup>1,2</sup> The major drawback to homogeneous catalysis is a difficult separation step is required to isolate the product.

### 1.1.1 Organometallic Catalysis

An organometallic complex is defined as compound that contains a coordinated organic molecule (ligand) to a metal centre, with the presence of at least one metal-carbon bond.<sup>2</sup> One of the most important applications of organometallic complexes has been in the catalysis of organic reactions. Organometallics are well suited to this area, due to the ability

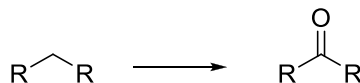
to tune both the organic ligands and the metal used, to achieve the desired reactivity. Catalysis with organometallic compounds dates back to the 1930's with the hydroformylation of alkenes with  $\text{Co}_2(\text{CO})_8$ .<sup>2</sup> Since then organometallic complexes have been instrumental in a number of important catalytic reactions, with three Nobel Prizes in chemistry being awarded since 2001 for research in this area. Organometallic catalysts have also found use in large-scale industrial processes. One such application is the Shell higher olefins process (SHOP), in which a nickel complex catalyzes the oligomerization of ethylene to 1-alkenes of various chain lengths ( $\text{C}_6$ – $\text{C}_{20}$ ) (Scheme 1.1), with a production level of millions of tons/year.<sup>2</sup> These alkenes then undergo subsequent isomerization, metathesis, and hydroformylation steps (with different catalysts) to produce  $\text{C}_{11}$ – $\text{C}_{15}$  alcohols (used in detergent manufacturing).



**Scheme 1.1** SHOP oligomerization of ethylene to give 1-alkenes of various lengths ( $\text{C}_6$  to  $\text{C}_{20}$ ).<sup>2</sup>

## 1.2 Allylic C-H Oxidation Chemistry

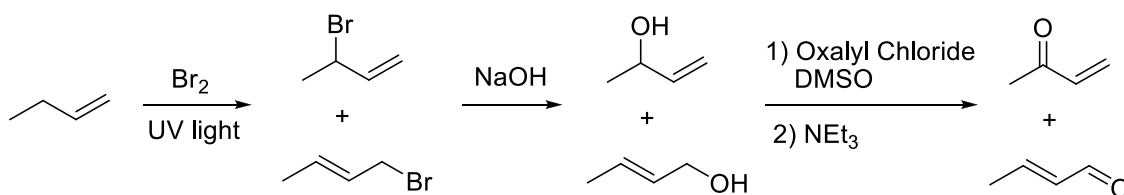
The direct oxidation of a C-H bond to C-O groups such as alcohols and carbonyls, is a highly desired process (Scheme 1.2).<sup>3</sup> By the addition of C-O functional groups to cheap hydrocarbons (from petrochemicals for example), higher value oxygen functionalized products are generated. The oxygenated products generated can undergo further use in the synthesis of complex organic molecules in industries such as pharmaceuticals.



**Scheme 1.2** One-step oxidation of a C-H group to a carbonyl group.

Selective oxidation of C-H bonds is often difficult due to the thermodynamic strength (high bond dissociation energy) and kinetic inertness of the bond.<sup>4,5</sup> As a result, many researchers target somewhat activated C-H functionalities such as allylic groups ( $\alpha$  carbon to a C=C group), which in turn will be easier to oxidize.

A theoretical non-catalytic allylic C-H oxidation to a ketone/aldehyde functional group is shown below in Scheme 1.3. The first step is a free-radical bromination of 1-butene to give one of two possible allyl bromide products. Second would be a nucleophilic substitution reaction to produce a 2° or 1° alcohol. Lastly would be an alcohol oxidation to the respective ketone or aldehyde, using one of a number of oxidation techniques (a Swern oxidation is shown below).



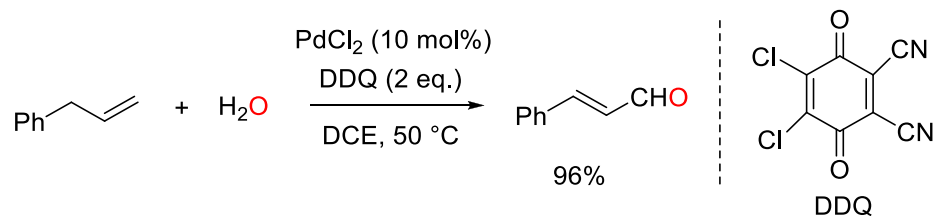
**Scheme 1.3** Allylic C-H oxidation of 1-butene to methyl vinyl ketone and 2-butenal.

Problems with the above reaction include selectivity issues and multiple synthetic steps. Another potential route is through a Riley oxidation in which  $\text{SeO}_2$  can selectively oxidize an allylic group to an alcohol in one step (followed by oxidation to the carbonyl), reducing the number of steps by one for the above reaction. The downside of using  $\text{SeO}_2$  is the generation of stoichiometric amounts of toxic selenium by-products. Direct oxidation via catalysis represents an ideal solution to reducing number of steps and improving selectivity

### 1.2.1 Catalytic Allylic C-H Oxidations with Specialty Oxidants

There are multiple recent literature reports that investigate the one-step oxidation of allylic C-H bonds to a variety of functional groups.<sup>6-10</sup> Complexes containing late-transition metals such as palladium, rhodium, and iron have been employed to perform this chemistry. One such example is shown below with a  $\text{PdCl}_2$  catalyst and DDQ (2,3-dichloro-5,6-dicyano-1,4-benzoquinone) as an oxidant (Scheme 1.4).<sup>6</sup> In this reaction, C-H activation of allyl benzene (among many other allylic substrates) is achieved, to generate

a PdCl( $\pi$ -allyl) species. This is followed by nucleophilic attack by water on the allylic ligand, with further oxidation by DDQ, to give the resulting aldehyde product in high yields and stereoselectivity.



**Scheme 1.4** Direct oxidation of an allylic C-H bond with PdCl<sub>2</sub> and DDQ.<sup>6</sup>

The main drawback with the above example, as well as all other literature methods of this type, is the use of stoichiometric amounts of oxidants such as DDQ, BQ (1,4-benzoquinone), and TBHP (*tert*-butyl hydroperoxide), or even toxic oxidants such as permanganate or dichromate.<sup>3</sup> The large amounts of by-products as a result of these reactions represents an environmental issue, therefore development of systems using more “green” oxidants is required.

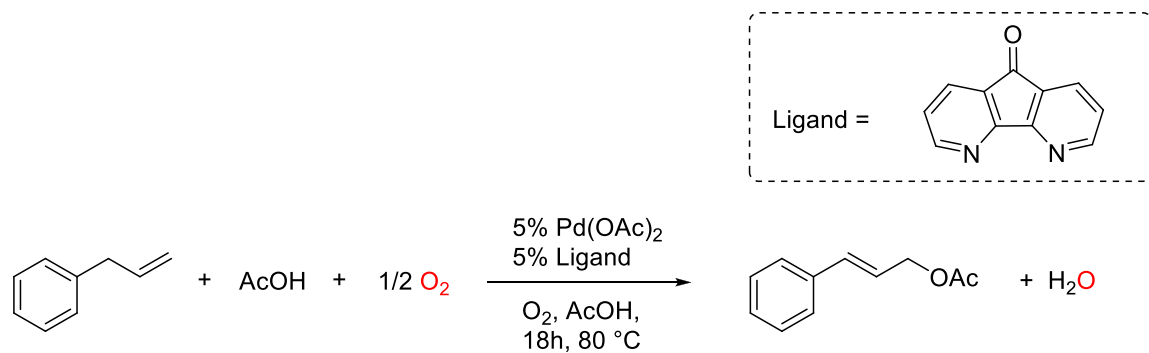
### 1.2.2 Dioxygen as an Oxidant

Dioxygen (O<sub>2</sub>) represents the ideal oxidant for large scale oxidation reactions, due to its environmentally benign and inexpensive characteristics.<sup>11</sup> There are however some challenges with using O<sub>2</sub> as an oxidant that need to be overcome. O<sub>2</sub> activation or direct oxidation of organic substances with O<sub>2</sub> under mild conditions, in the absence of additional additives or co-catalysts, is difficult due to molecular oxygen being kinetically unreactive.<sup>5,12</sup> Product selectivity is often poor, especially if free oxygen radicals are present, as many undesired side-products may be formed. Furthermore, use of O<sub>2</sub> on large scales in industrial processes is of major concern, as O<sub>2</sub> is a very strong oxidant which promotes the rapid combustion of organics. A safe way to reduce the risk of using O<sub>2</sub> is by using a non-flammable mixture, referred to as dilute air (5–8% O<sub>2</sub> in N<sub>2</sub>).<sup>13</sup> To ensure sufficient oxygen content for reactions, dilute air has to be used at high pressures. Standard large stirred-tank reactors used in industry are not equipped to handle the pressures required to use dilute air for aerobic oxidations.<sup>13</sup> Continuous flow chemistry represents an ideal

solution to the issue, in which the components of the reaction are continuously injected into/out of a reactor. Recent research has explored this process, as Stahl *et. al.* have developed a flow chemistry system for the Pd-catalyzed aerobic oxidation of alcohols, utilizing dilute air.<sup>13</sup>

### 1.2.3 Catalytic Aerobic Oxidations

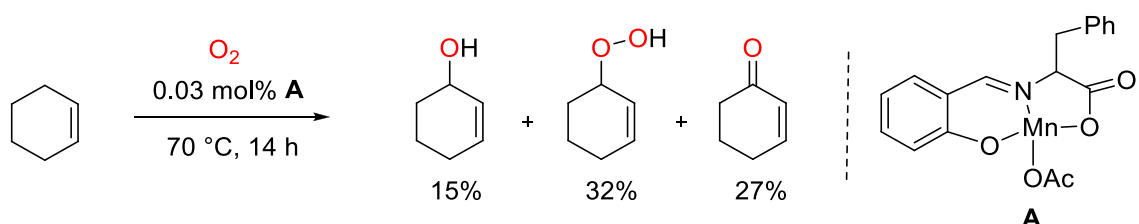
There are two main types of catalytic aerobic oxidation processes: oxidase, and oxygenase catalysis.<sup>14</sup> In oxidase catalysis  $O_2$  acts as the oxidant without the O atom being incorporated into the organic product. The most notable oxidase catalytic reaction is the Wacker process, in which ethylene is converted to acetaldehyde with a  $PdCl_2$  catalyst and  $CuCl_2$  co-catalyst. For this reaction the O atom comes from water, and oxygen only acts as the terminal oxidant to regenerate the copper co-catalyst. An example of a recent oxidase allylic oxidation was shown in work by Stahl *et. al.*<sup>15</sup> Through the use of a Pd catalyst containing a 4,5-diazafluorenone ligand, Stahl was able to show aerobic allylic acetoxylation of terminal olefins, achieving the product in good yield and selectivity (Scheme 1.5).



**Scheme 1.5** Aerobic allylic acetoxylation of allyl benzene with a Pd-4,5-diazafluorenone catalyst.<sup>15</sup>

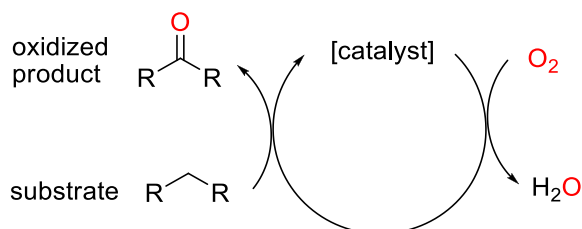
In oxygenase catalysis,  $O_2$  acts as both the oxidant and O-atom source, representing a very atom economical process. Examples of oxygenase catalysis are fewer than for oxidase catalysis. In the examples that do exist, there are still issues remaining such as the use of other additives or co-catalysts, poor selectivity and yields, and/or high temperatures.<sup>16-19</sup> Specific to catalytic oxygenase allylic oxidations, there are few examples of high

performing systems. One example is shown below for the transformation of cyclohexene into three oxidation products (cyclohexenol, cyclohexenone, and cyclohexenyl hydroperoxide) by use of only oxygen and a manganese catalyst (Scheme 1.6).<sup>16</sup> While an overall yield of ~75% is achieved, the lack of selectivity between products is a major problem moving forward. Other systems with cobalt, and molybdenum/vanadium catalysts are similar in terms of performance/selectivity.<sup>17-19</sup>



**Scheme 1.6** Oxygenase type oxidation of cyclohexene with a manganese catalyst.<sup>16</sup>

The ideal catalytic reaction (Scheme 1.7) would make use of only a catalyst and  $\text{O}_2$  to generate an oxidized substrate at high selectivity and yield, under mild conditions. In addition, the only by-product generated would be water, extremely attractive from an environmental standpoint.

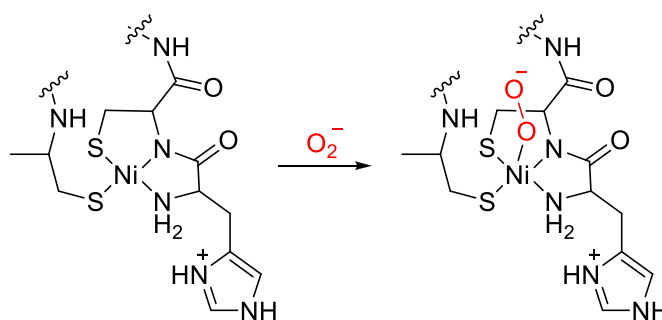


**Scheme 1.7** Generic reaction scheme for desired oxidation of a substrate to the oxidation product with  $\text{O}_2$  as the sole oxidant.



### 1.3 Ni Dioxygen Reactivity

Catalysis with nickel is highly attractive since the metal is cheap and readily available compared to other commonly used metals. Specifically, nickel is up to 2000 times cheaper than palladium, one of the most widely used metals for catalysis. Investigation into metal dioxygen reactivity is currently mostly dominated by iron and copper complexes, with ligand designs inspired by enzymes.<sup>20</sup> This is in large part due to the abundance of examples in nature of Fe or Cu based enzymes that bind and activate O<sub>2</sub>. In contrast, nickel enzymes are much less common in nature, and are predominately used in anaerobic processes. There does exist an aerobic nickel enzyme, nickel superoxide dismutases (NiSOD), that catalyzes the disproportionation of superoxide to hydrogen peroxide and O<sub>2</sub>.<sup>21</sup> The first step of the catalytic cycle, the binding of superoxo to the nickel centre to form a Ni(II)-superoxo, is shown below in Scheme 1.8.



**Scheme 1.8** Binding of superoxo to active site of nickel superoxide dismutases (NiSOD) to form a Ni-superoxo species.<sup>21</sup>

Ni(0) or Ni(I) readily reacts with O<sub>2</sub> to generate a number of possible Ni-O<sub>2</sub> species (Figure 1.2).<sup>20,22</sup> In contrast, Nickel (II) complexes generally tend to be non-reactive towards O<sub>2</sub>, however an electron rich metal centre (due to strongly electron-donating ligands) can favour this reactivity.<sup>20</sup> This is achieved by lowering the Ni<sup>III/II</sup> redox potential, allowing oxidation by O<sub>2</sub> to be a thermodynamically favourable process.

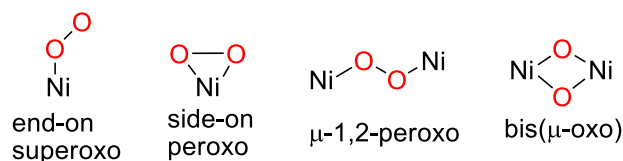
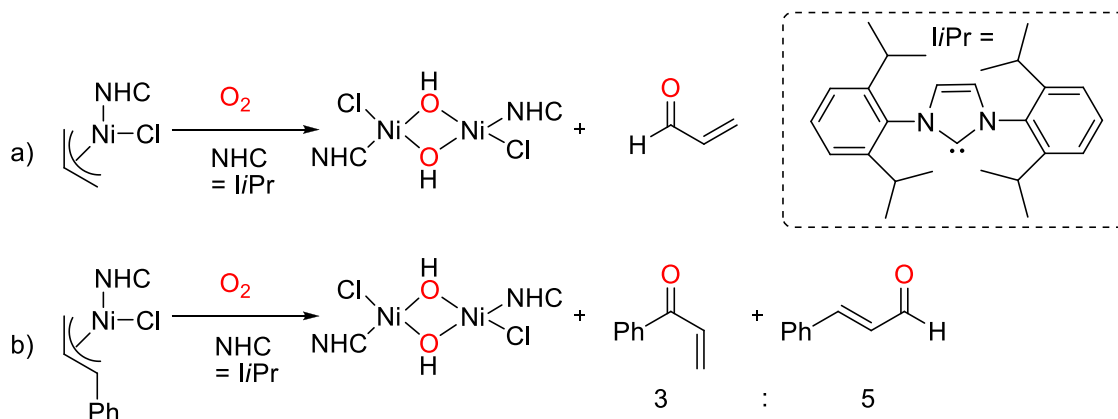


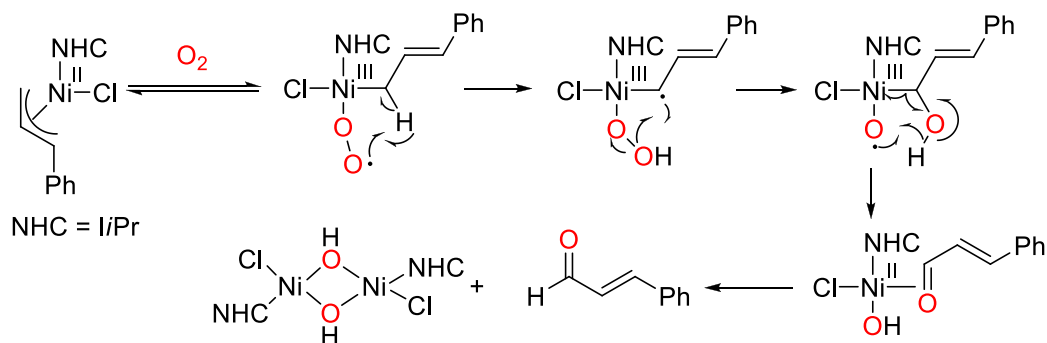
**Figure 1.2** Known reaction products and binding modes of Ni with dioxygen.<sup>20,22</sup>

A ligand class that is highly suited for this chemistry is *N*-heterocyclic carbenes (NHC), as they are strong  $\sigma$ -donors leading to an electron-rich metal centre. Coordinated NHCs tend to be stable towards O<sub>2</sub>, an extremely useful property for aerobic chemistry. A report has proved this theory, as a NiCl(allyl)(*IiPr*) (*IiPr* = 1,3-bis(2,6-diisopropylphenyl)imidazol-2-ylidene) complex was shown to react with O<sub>2</sub> (Scheme 1.9).<sup>23</sup> Oxidation of the allyl ligand is observed (Scheme 1.9, reaction a)), and gives 2-propenal as the resulting oxidation product. To elucidate the selectivity of the oxidation step, Sigman *et. al.* focused on oxidation of a cinnamyl ligand (Scheme 1.9, reaction b)). In the aerobic oxidation of NiCl(cinnamyl)(*IiPr*) there are two observed products: cinnamaldehyde and phenyl vinyl ketone. <sup>18</sup>O labelling studies confirms the incorporation of oxygen into the oxidized product is due to O<sub>2</sub>. Importantly, there is no formation of other potential oxidation products including epoxide, hydroxo, and hydroperoxo species. The lack of other products points to an improvement to the selectivity over many previous catalysts, in the area of aerobic allylic oxidation.<sup>16-19</sup> Furthermore, the small product distribution suggests metal mediated oxidation chemistry, in contrast to the presence of free oxygen radicals, which lead to very poor selectivity. In both reactions, there is the formation of an unreactive dark purple Ni-OH dimer, identified by X-ray crystallography. Additionally, the presence of a peak at -7.8 ppm (C<sub>6</sub>D<sub>6</sub>) in the <sup>1</sup>H NMR, and a sharp stretch at 3645 cm<sup>-1</sup> in the IR spectrum, gives further evidence for a Ni-OH dimer.



**Scheme 1.9** Reaction of NiCl(cinnamyl/allyl)(NHC) with O<sub>2</sub>.<sup>23</sup>

Product formation is achieved through a proposed reactive Ni-O<sub>2</sub> intermediate, a Ni(III)-superoxo, that is suggested to promote an inner-sphere H-atom abstraction that ultimately leads to either the ketone and/or aldehyde products. The postulated mechanism for this process is supported by kinetics data (UV-Vis spectroscopy), and is shown below in Scheme 1.10.



**Scheme 1.10** Proposed mechanism for allylic oxidation in the formation of cinnamaldehyde.<sup>23</sup>

A study of a number of NiCl(allyl)(NHC) derivatives, with a variety of NHC ligands, revealed that the steric properties of the NHC ligand were very important in the O<sub>2</sub> reactivity of the corresponding Ni complex.<sup>24</sup> Bulky NHC ligands (ItBu, IAd) with restricted rotation about the Ni-NHC bond were found to be air stable. In contrast, the

smaller freely rotating NHC ligands (IMes, IiPr, IMe) react very rapidly with O<sub>2</sub> and NHC ligands with intermediate rotation show intermediate reactivity. The authors attribute this behaviour to the bulky ligands, with hindered rotation, blocking the empty axial sites above or below the square plane of the complex. This prevents the binding of oxygen to the Ni centre. Examples of each class of NHC and the time to react with O<sub>2</sub> are shown in Figure 1.3.

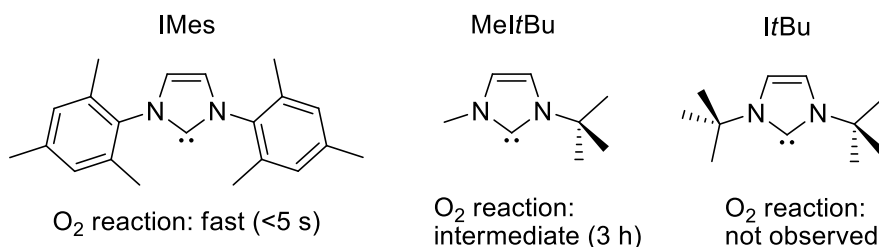


**Figure 1.3** Effect of bulkiness of NHC ligand and observed O<sub>2</sub> reactivity of corresponding NiCl(allyl)(NHC) complexes.<sup>24</sup>

There are a number of issues that make this system non ideal: poor selectivity between aldehyde and ketone (5:3 ratio) products and the system is not catalytic. Turnover is prevented by the instability of the monomeric Ni-OH intermediate that quickly dimerizes to an unreactive  $\mu$ -hydroxo Ni(II) species that subsequently decomposes. Stabilization of the Ni-OH monomer could give an opportunity to promote catalytic turnover.

## 1.4 Hydrogen-Bonding Groups

One method to overcome the problem of an unstable metal-hydroxo complex is the use of hydrogen-bonding groups. Typically monomeric metal-OH complexes are difficult to isolate due to the tendency of hydroxo ligands to bridge between two metal atoms.<sup>25</sup> Studies on biological molecules, such as lipoxygenase, show stable monomeric Fe-OH complexes.<sup>26</sup> In these systems it is observed that there is an intramolecular hydrogen bond between the OH ligand, and a directing group in the secondary-coordination sphere. Therefore, this represents an effective method for laboratory synthesis of stable metal-OH complexes. A number of recent reports<sup>25,27-29</sup> relating to metal-OH complexes, indeed do show that a hydrogen-bond donor in the second-coordination sphere can stabilize reactive

O<sub>2</sub>-derived intermediates, allowing for the isolation and characterization of these complexes (example complexes shown in Figure 1.4).

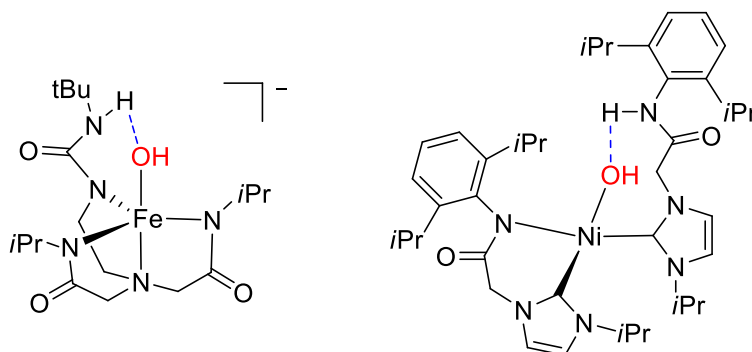


**Figure 1.4** Monomeric M-OH complexes stabilized by H-bonding.<sup>25,29</sup>

## 1.5 Project Goals

The goals of the project can be split into two subcategories. The first being the synthesis of novel NiX(allyl/cinnamyl)(NHC) (X= I, Cl) complexes with hydrogen-bond donor groups in the second-coordination sphere, and, secondly, investigate the reactivity of these complexes towards O<sub>2</sub>.

### 1.5.1 Synthesis of NiX(allyl/cinnamyl)(NHC) Complexes

The proposed nickel complexes (**2a**, **3a/b/c**, **4a**) would have the same general structure as the complexes reported by Sigman,<sup>23,24</sup> however with one main difference: the NHC ligand used contains a pendent 2° amine arm (Figure 1.5).

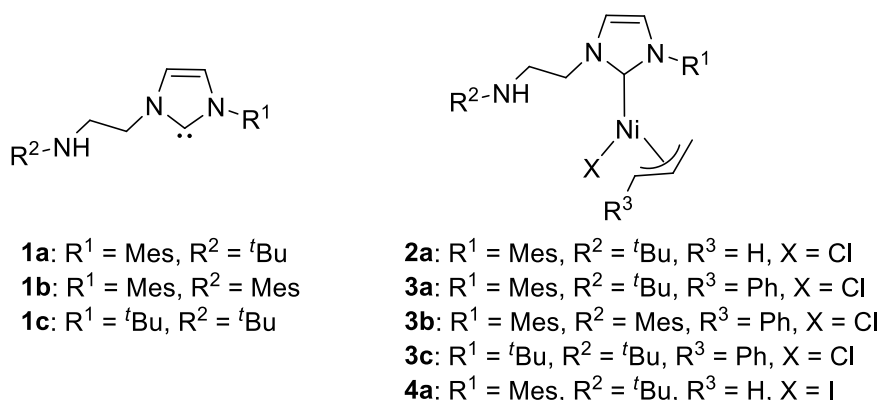


**Figure 1.5** NHC compounds and NiX(allyl/cinnamyl)(NHC) complexes studied in this report

The hypothesis is that the pendent amine arm can act as a hydrogen-bond donor, which can stabilize the reactive Ni-OH monomer formed following aerobic oxidation. The NHC ligands (**1a/b/c**) chosen have already been reported in literature, and have been isolated as the free NHC, easing the synthesis of the corresponding nickel complex.<sup>30-32</sup> While these reported NHCs have not been previously shown to act as H-bond donors, the ability of the amine arm to coordinate to the metal centre has been demonstrated (Figure 1.6).<sup>33,34</sup> In the case of the ruthenium complex, the coordination of the amine is shown to be hemi-labile.<sup>34</sup>

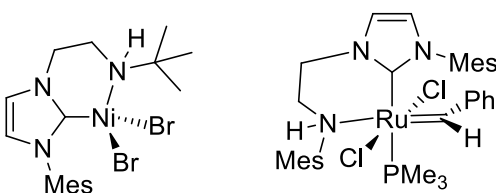
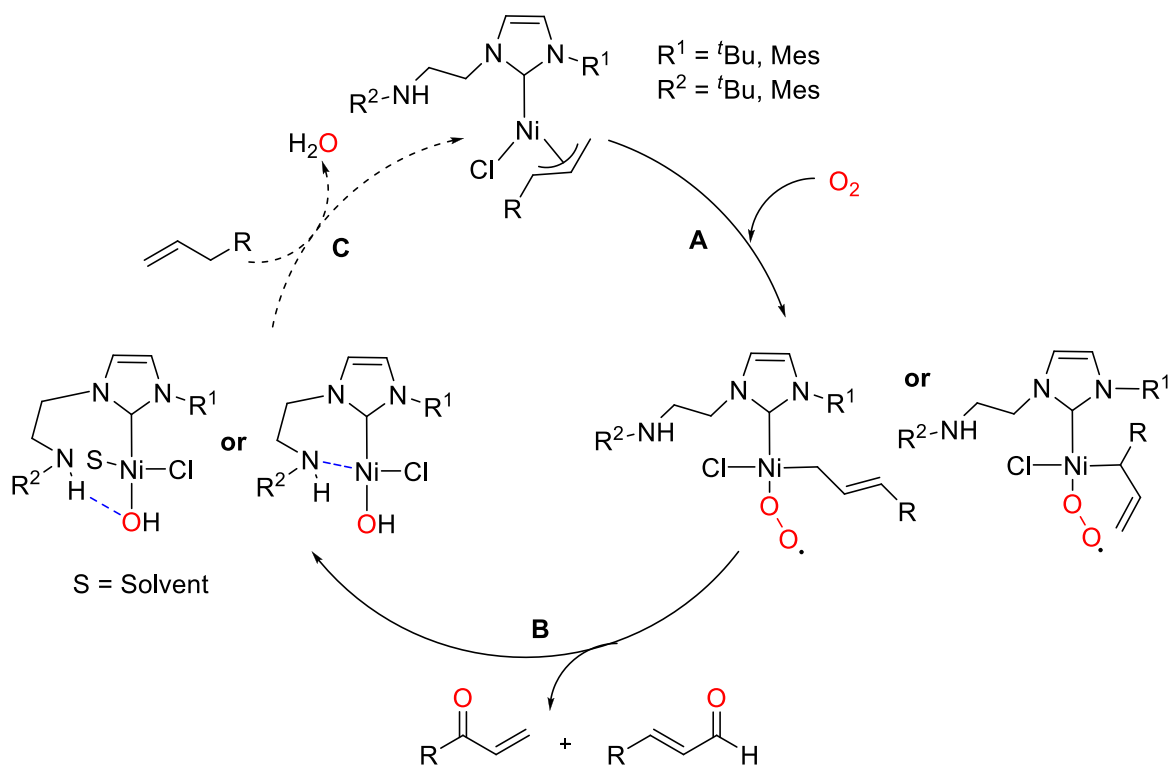


**Figure 1.6** Coordination of pendent amine arm of NHC ligand to metal centre.<sup>33,34</sup>

### 1.5.2 $\text{O}_2$ Reactivity of NiCl(allyl/cinnamyl)(NHC) Complexes

Reactivity of the target metal complexes (**2a**, **3a-c**, **4a**) is proposed to be similar to that of the Sigman systems,<sup>23,24</sup> however the inclusion of the pendent amine is hoped to alter the selectivity between products, and allow the system to be catalytic by stabilizing the reactive Ni-OH intermediate.

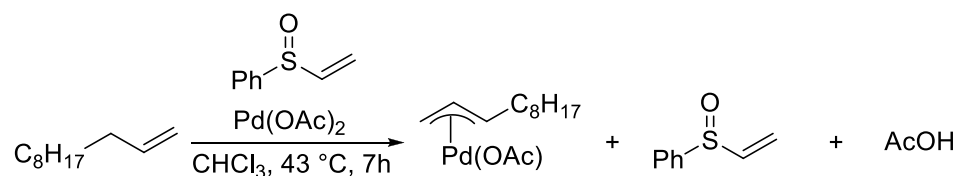
A proposed catalytic cycle (Scheme 1.11) is shown below, in which activation of  $O_2$  to form a Ni-superoxo species is the first step (step **A**, Scheme 1.11). Additionally at this step isomerisation of the allylic ligand to a  $\eta^1$  bonding mode would occur, in either a linear or branched fashion. Secondly, oxidation of the bound allylic ligand, followed by release of the oxidized product (step **B**, Scheme 1.11), will hopefully generate a monomeric Ni-OH species, stabilized by the amine arm on the NHC ligand. Steps A and B are analogous to that observed by Sigman. The final step (step **C**, Scheme 1.11) is proposed and would include C-H activation of a substrate and release of water to regenerate the catalyst.



**Scheme 1.11** Proposed mechanism for oxidation of allylic ligand.

This final step has not been observed for Ni complexes, however a similar C-H activation step has been observed for a Pd system (Scheme 1.12).<sup>7</sup> With  $Pd(OAc)_2$  and a vinyl sulfoxide as the ligand, C-H activation of 1-undecene was achieved after heating at 43 °C for 7 hours to give the resulting  $\pi$ -allylpalladium complex. A Ni-OH intermediate should

be quite reactive towards C-H activation, due to the nucleophilicity of Ni-OH species.<sup>29</sup>



**Scheme 1.12** C-H activation of an allylic substrate to give the resulting Pd(allyl)(OAc) complex.<sup>7</sup>

## 1.6 References

1. Atkins, P.; Overton, T.; Rourke, J.; Weller, M.; Armstrong, F.; Hagerman, M. *Inorganic Chemistry, Fifth Edition*; W.H Freeman and Company: New York. **2010**
2. Crabtree, R.H. *The Organometallic Chemistry of the Transition Metals, 6th edition*; John Wiley and Sons, Inc.: New Jersey. **2014**
3. Punniyamurthy, T.; Velusamy, S.; Iqbal, J. *Chem. Rev.* **2005**, *105*, 2329-2363
4. White, C. M. *Science*, **2012**, *335*, 807-809
5. Roduner, E.; Kaim, W.; Sarkar, B.; Urlacher, B.; Pleiss, J.; Gläser, R.; Einicke, W.-D.; Sprenger, G. A.; Beifus, U.; Klemm, E.; Liebner, C.; Hieronymus, H.; Hsu, S.-F.; Plietker, B.; Laschat, S. *Chem. Cat. Chem.* **2013**, *5*, 82-112
6. Chen, H.; Jiang, H.; Cai, C.; Dong, J.; Fu, W. *Org. Lett.* **2011**, *13*, 992-994
7. Chen, M. S.; Prabakaran, N.; Labenz, N. A.; White, C. M. *J. Am. Chem. Soc.* **2005**, *127*, 6970-6971
8. Vermeulen, N. A.; Delcamp, J. H.; White, C. M. *J. Am. Chem. Soc.* **2010**, *132*, 11323-11328
9. Wang, T.; Xiang, S.-K.; Qin, C.; Ma, J.-A.; Zhang, L.-H.; Jiao, N. *Tetrahedron Lett.* **2011**, *52*, 3208-3211
10. Choi, H.; Doyle, M. P.; *Org. Lett.* **2007**, *9*, 5349-5352
11. Shi, Z.; Zhang, C.; Tang, C.; Jiao, N. *Chem. Soc. Rev.* **2012**, *41*, 3381-3430
12. Drago, R. S.; *Coord. Chem. Rev.* **1992**, *117*, 185-213
13. Ye, X.; Johnson, M. D.; Diao, T.; Yates, M. H.; Stahl, S. S. *Green Chem.* **2010**, *12*, 1180-1186



14. Scheuermann, M. L.; Goldberg, K. I. *Chem. Eur. J.* **2014**, *20*, 14556-14568
15. Campbell, A. N.; White, P. B.; Guzei, I. A.; Stahl, S. S. *J. Am. Chem. Soc.* **2010**, *132*, 15116-15119
16. Wang, R.-M.; Hao, C.-J.; Wang, Y.-P.; Li, S.-B. *J. Mol. Catal. A: Chem.* **1999**, *147*, 173-178
17. Hanyu, A.; Sakurai, Y.; Fujibayashi, S.; Sakaguchi, S.; Ishii, Y. *Tetrahedron Lett.* **1997**, *38*, 5659-5662
18. Lajunen, M. K.; Maunula, T.; Koskinen, A. M. P. *Tetrahedron* **2000**, *56*, 8167-8171
19. Joseph, T.; Halligudi, S. B.; Satyanarayan, C.; Sawant, D. P.; Gopinathan, S. *J. Mol. Catal. A: Chem.* **2001**, *168*, 87-97
20. Kieber-Emmons, M. T.; Riordan, C. G. *Acc. Chem. Res.* **2007**, *40*, 618-625
21. Barondeau, D. P.; Kassmann, C. J.; Bruns, C. K.; Tainer, J. A.; Getzoff, E. D. *Biochemistry* **2004**, *43*, 8038-8047
22. Suzuki, M. *Acc. Chem. Res.* **2007**, *40*, 609-617
23. Dible, B. R.; Sigman, M. S. *J. Am. Chem. Soc.* **2003**, *125*, 872-873
24. Dible, B. R.; Sigman, M. S. *Inorg. Chem.* **2006**, *45*, 8430-8441
25. Mukherjee, J.; Lucas, R. L.; Zart, M. K.; Powell, D. R.; Day, V. W.; Borovik, A. S. *Inorg. Chem.* **2008**, *47*, 5780-5786
26. Tomchick, D. R.; Phan, P.; Cymborowski, M.; Minor, W.; Holman, T. R. *Biochemistry* **2001**, *40*, 7509-7517
27. Park, Y. J.; Cook, S. A.; Sickerman, N. S.; Sano, Y.; Ziller, J. W.; Borovik, A. S. *Chem. Sci.* **2013**, *4*, 717-726
28. Matson, E. M.; Bertke, J. A.; Fout, A. R. *Inorg. Chem.* **2014**, *53*, 4450-4458
29. Samantaray, M. K.; Shaikh, M. M.; Ghosh, P. *Organometallics* **2009**, *28*, 2267-2275
30. Jong, H.; Patrick, B. O.; Fryzuk, M. D. *Can. J. Chem.* **2008**, *86*, 803-810
31. Shih, W.-C.; Wang, C.-H.; Chang, Y.-T.; Yap, G. P. A.; Ong, T.-G. *Organometallics* **2009**, *28*, 1060-1067
32. Arnold, P. L.; Mungur, S. A.; Blake, A. J.; Wilson, C. *Angew. Chem.* **2003**, *115*, 6163-6166
33. Huang, Y.-P.; Tsai, C.-C.; Shih, W.-C.; Chang, Y.-C.; Lin, S.-T.; Yap, G. P. A.; Chao, I.; Ong, T.-G. *Organometallics* **2009**, *28*, 4316-4323

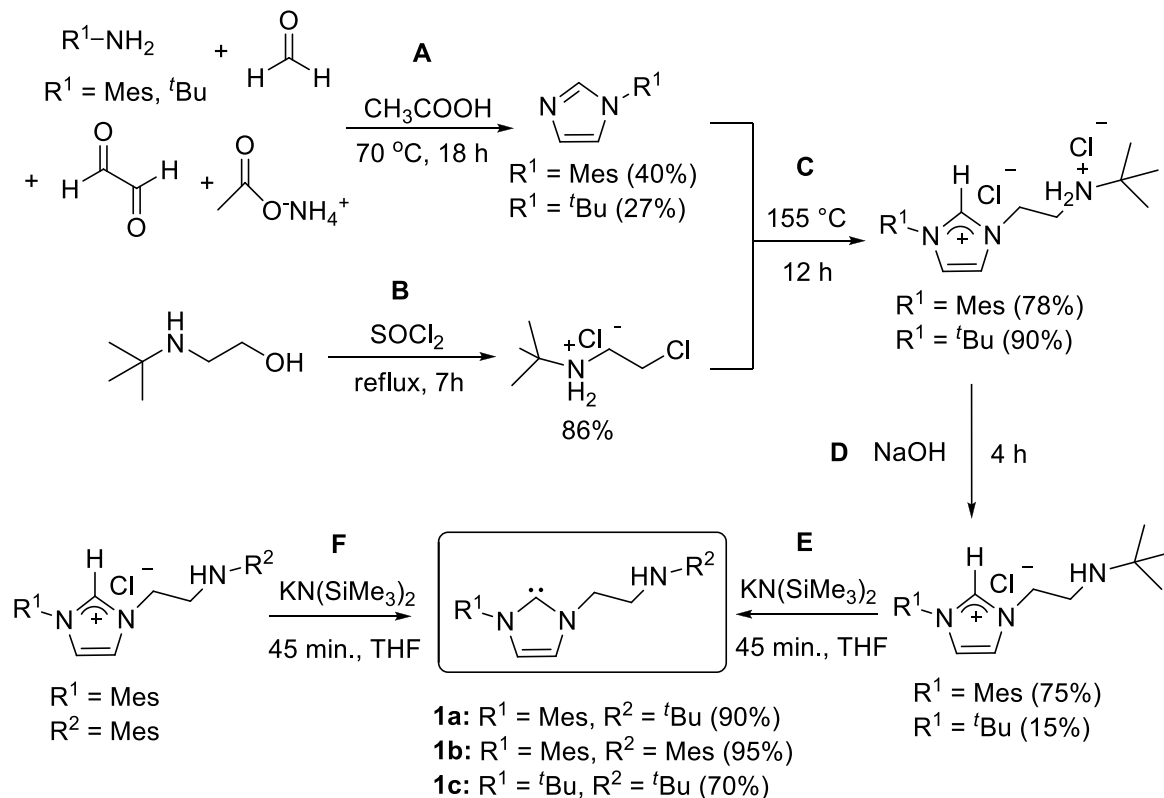
34. Jong, H.; Patrick, B. O.; Fryzuk, M. D. *Organometallics* **2011**, *30*, 2333-2341

## Chapter 2

### 2 Synthesis and Characterization of Dynamic NiX(allyl)(NHC) and NiCl(cinnamyl)(NHC) Complexes

#### 2.1 Ligand Synthesis

The NHC ligands used throughout this report were synthesized using a multi-step procedure based on the literature methods (Scheme 2.1). In our hands the reported chlorination of 2-(*tert*-butylamino)ethanol with 1 equivalent of thionyl chloride in dichloromethane at room temperature, proceeded in low yields and routinely afforded the protonated starting material as judged by  $^1\text{H}$  NMR spectroscopy and mass spectrometry. The synthesis of 2-(*tert*-butylamino)ethyl chloride hydrochloride was instead achieved by chlorination in neat thionyl chloride (Scheme 2.1, Step **B**). The chlorinated product was obtained in good yields and the  $^1\text{H}$  NMR spectrum matched that of literature values.<sup>25</sup> The remainder of the synthetic steps (A, C-E) for carbene **1a** ( $\text{R}^1 = \text{Mes}$ ,  $\text{R}^2 = \text{tBu}$ ) proceeded in good yields as reported. The free *N*-heterocyclic carbene, **1a**, was isolated as a light brown solid.



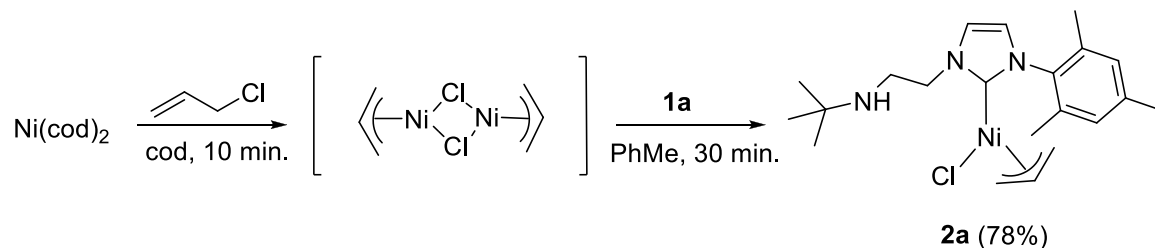
**Scheme 2.1** Multi-step synthesis of free NHC ligands **1a**, **1b**, and **1c**. Parenthetical numbers are isolated yields for the given step

The related NHC salt with a pendent mesityl amine,  $[HC\{(Mes)N(CH_2CH_2)N(CH_2CH_2NH(Mes))\}]Cl$ , was previously reported in the literature<sup>22</sup> and was synthesized by Doowon Joo in the Blacquiere group. This salt was deprotonated, following the same procedure employed for the *t*Bu amine derivative (Scheme 2.1, Step F), to afford the free NHC **1b** ( $R^1 = Mes, R^2 = Mes$ ) as a light brown solid. NHC **1c** ( $R^1 = tBu, R^2 = tBu$ ) was synthesized using similar procedures as outlined for the above carbenes, and was isolated as a dark brown oil. It should be noted that step D ( $R^1 = tBu$ ) in this synthesis proceeds with a very low isolated yield, acting as a barrier in the potential scale up of this derivative. At this moment, it is not apparent if the deprotonation was not complete, or if the low yield was due to an isolation issue. In the future a different procedure will have to be employed to give more favourable yields. In all cases,  $^1H$  NMR data matched to that reported in the literature, confirming the synthesis of NHC ligands **1a**, **1b**, and **1c**.<sup>1-3</sup>

## 2.2 Synthesis of NiCl(allyl/cinnamyl)(NHC) Complexes

### 2.2.1 Synthesis of Complex 2a

The initial target complex **2a** was prepared following a two-step, one-pot, procedure (Scheme 2.2) similar to reported methods for the synthesis of related NiCl(allyl)(NHC) complexes.<sup>4,5</sup>

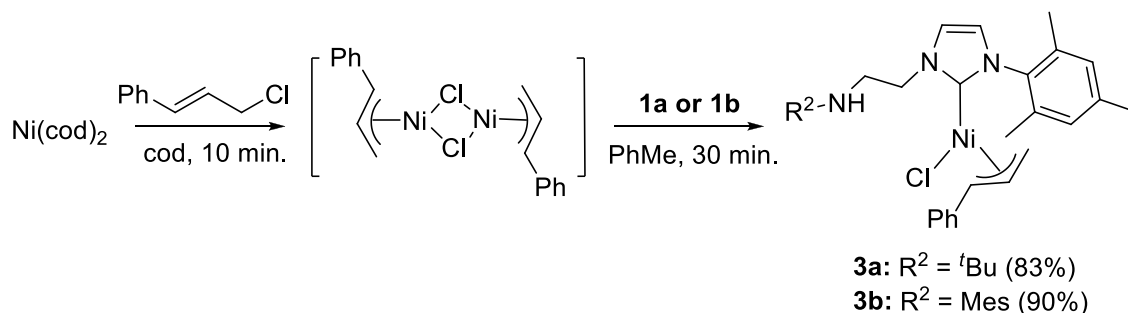


**Scheme 2.2** Two-step, one-pot synthesis of **2a**

From Ni(cod)<sub>2</sub>, the first step was the oxidative addition of allyl chloride to form the dark red allylnickel(II) chloride dimer. Analysis of a reaction aliquot by <sup>1</sup>H NMR spectroscopy revealed two doublets at 1.64 and 2.65 ppm and a multiplet at 4.83 ppm, consistent with literature values for the dimer.<sup>6</sup> This was followed by the *in situ* addition of **1a** to give the resultant complex **2a** isolated as a brown/orange solid in a 78% yield following solvent evaporation and washes with cold (−35 °C) hexanes.

### 2.2.2 Synthesis of Complexes **3a** and **3b**

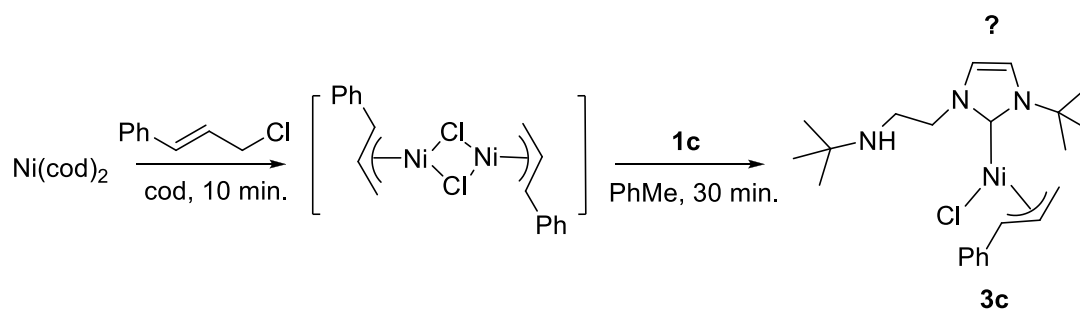
NiCl(cinnamyl)(NHC) complexes **3a** and **3b** were synthesized following a literature procedure from Sigman *et. al* for an analogous complex.<sup>4</sup> To Ni(cod)<sub>2</sub> was added cinnamyl chloride to form the dark red/purple cinnamylnickel(II) chloride dimer. This was followed by the *in situ* addition of ligand **1a** (R<sup>2</sup> = <sup>t</sup>Bu) to yield **3a** as an orange/brown solid in a 83% isolated yield. **3b** was synthesized in a similar fashion following reaction with mesityl amine containing ligand **1b**. This complex was isolated in a 90% yield as an orange/brown solid (Scheme 2.3).



**Scheme 2.3** Two-step, one-pot synthesis of **3a** and **3b**

### 2.2.3 Attempted Synthesis of Complex **3c**

The synthesis of complex **3c** was performed using an identical procedure to that above for **3a** and **3b**, with the exception of using NHC ligand **1c** in the second step (Scheme 2.4). Upon removal of the solvent under vacuum and washes with cold ( $-35^\circ\text{C}$ ) pentane, a red-orange solid was isolated. The resulting  $^1\text{H}$  NMR spectrum for the reaction product reveals the apparent presence of many different species, potentially including **3c** as well as unreacted cinnamylnickel(II) chloride dimer. Further investigation into this reaction will need to be made in the future.



**Scheme 2.4** Attempted two-step, one-pot synthesis of **3c**

## 2.3 Characterization of NiCl(allyl/cinnamyl)(NHC) Complexes

### 2.3.1 MALDI Mass Spectrometry Analysis of Complexes **2a**, **3a**, and **3b**

The Ni complex **2a** was analyzed by MALDI MS using pyrene or anthracene as the matrix. The resulting spectra, showed no evidence of a signal for  $[\mathbf{2a}]^{\bullet+}$  (Figure 2.1). A signal was

found that had an  $m/z$  value and isotope pattern that is consistent with a fragment of the molecular ion,  $[2\mathbf{a}-(\text{allyl})]^{•+}$  (Figure 2.1 inset). This confirmed that indeed the NHC is coordinated to the metal centre and that the chloride ligand is retained. No noticeable difference was observed in the mass spectra by changing the matrix from pyrene to anthracene.

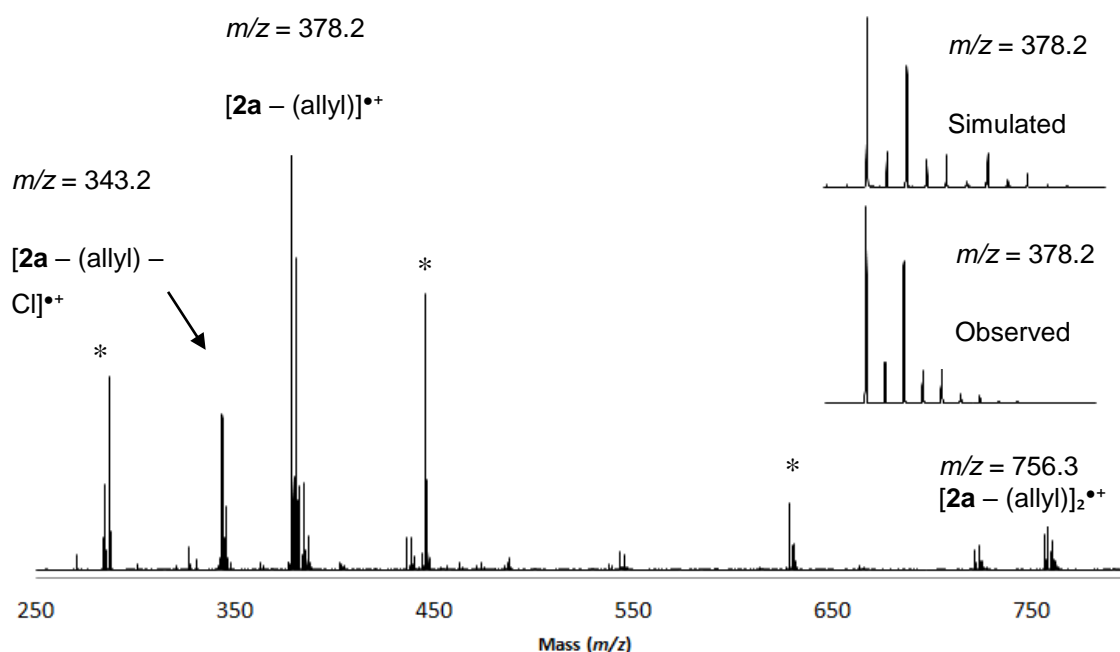


**Figure 2.1** MALDI MS of **2a** with pyrene as the matrix. The inset depicts the simulated<sup>7</sup> and observed isotope pattern for the most abundant signal. Signals that do not contain Ni or Cl (as judged by the isotope pattern) are labeled with an asterisk (\*).

A similar observation was noted in the analysis of the  $\text{NiCl}(\text{cinnamyl})(\text{NHC})$  complexes **3a** and **3b** by MALDI mass spectrometry, with anthracene as the matrix. The resulting spectra, showed no evidence of  $[3\mathbf{a/b}]^{•+}$  (Appendix 6.4, Figures 6.4 and 6.5), however a signal was found that has an  $m/z$  value and isotope pattern that is consistent with a fragment of the molecular ion,  $[3\mathbf{a}-(\text{cinnamyl})]^{•+}$  ( $m/z = 378.2$ ), and  $[3\mathbf{b} - \text{cinnamyl}]^{•+}$  ( $m/z = 440.1$ ). Once again, despite the lack of a signal for the molecular cation, the data obtained does confirm that the NHC is bound to the metal centre.

### 2.3.2 Solid-State Analysis of Complexes 2a, 3a, and 3b

An X-ray quality crystal of **2a** was obtained from slow vapour diffusion of pentane into a solution of **2a** in toluene at  $-35\text{ }^{\circ}\text{C}$ , which was analyzed by X-ray diffraction (Figure 2.2). The obtained data confirmed the structure of complex **2a** in the solid state, showing a monometallic Ni complex with the NHC bonded in a  $\kappa^1$ -coordination mode and the allyl ligand in a  $\eta^3$ -coordination mode. Comparison of the obtained bond parameters for the nickel-ligand bonds (Table 2.1) to related literature complexes of the type NiX(allyl)(NHC), show a close correlation.<sup>4,5,8</sup> Specifically, the Ni-NHC bond length of  $1.9052(10)\text{ \AA}$  is consistent with other  $\kappa^1$ -NHCs, with or without a pendent H-bonding group ( $1.902 - 1.929\text{ \AA}$ ).<sup>4,5,8</sup> The allyl group exhibited a disorder wherein the atom C2 was distributed over 2 sites, which is expected of this ligand type.<sup>8</sup> The disordered atom position C2' was omitted from Figure 3.2 for clarity, however is visualized in Appendix 6.1, Figure 6.1. Also, the Ni-C1 length is noticeably longer than Ni-C2 and Ni-C3 bond lengths (approximately  $0.09\text{ \AA}$  longer), a result of the strong influence of the NHC ligand weakening the bond trans to it (Ni-C1). Therefore the bond is elongated and by consequence the other Ni-allyl bonds are shortened. Additionally an interesting phenomena was observed in the solid-state, as there is an intermolecular hydrogen-bonding interaction between the N-H (N3) group of the pendent amine arm and the chloride ligand of another molecule in the unit cell. A  $\text{N3}\cdots\text{Cl1}$  bond length of  $3.7401(12)\text{ \AA}$  is consistent for a weak hydrogen bond ( $> 3.2\text{ \AA}$ ) for that type of functionality.<sup>9,10</sup> Excitingly, this shows that the pendent amine arm is active towards hydrogen-bonding, albeit a weak interaction, and could influence further chemistry.



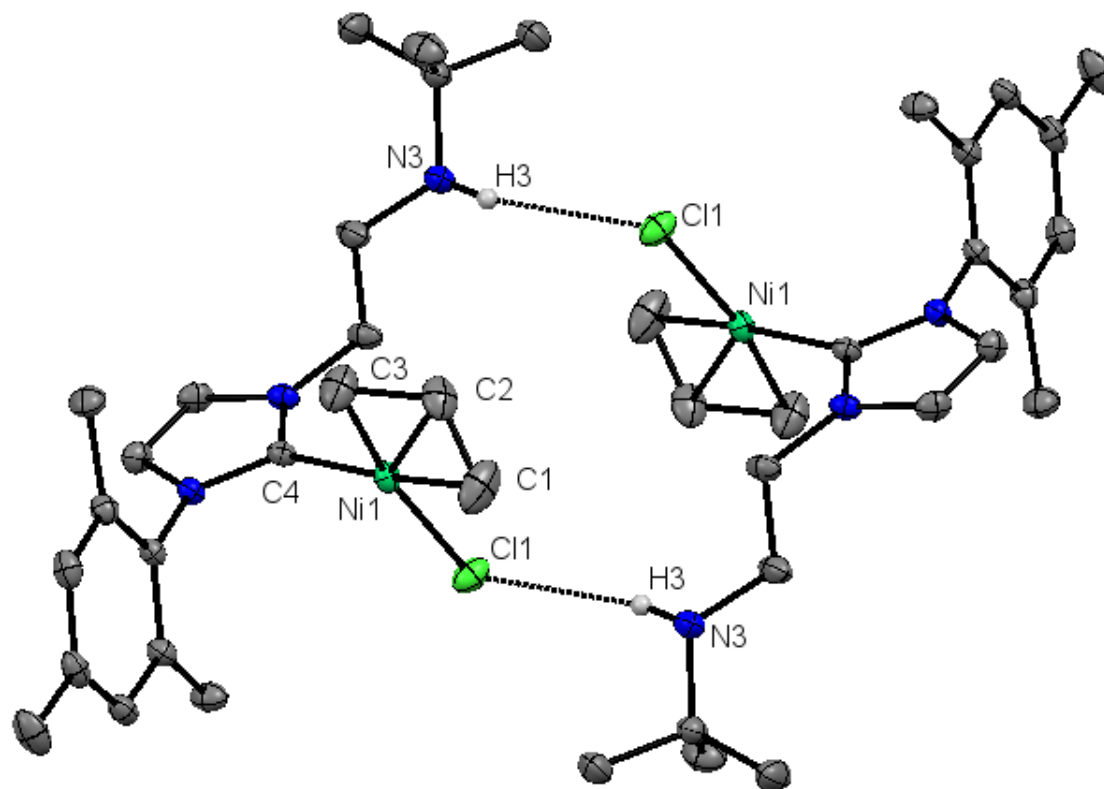


**Figure 2.2** ORTEP drawing of **2a** showing naming and numbering scheme for selected atoms of interest. Ellipsoids are at the 50% probability level and hydrogen atoms were omitted for clarity (with the exception of the hydrogen atom on N3). Disordered atom position C2' is omitted for clarity.

The structures of **3a** and **3b** in the solid-state were similarly confirmed by X-ray diffraction (Figures 2.3, 2.4). The obtained solid-state structures showed many of the same properties as those previously discussed for **2a**, with bond parameters (Table 2.1) matching closely with a reported NiCl(cinnamyl)(NHC) complex.<sup>11</sup> Unique for these structures is the phenyl substituted carbon (C1) of the cinnamyl group, is trans to the NHC ligand, as might be expected to avoid steric clash with the NHC ligand. The structure for **3b** crystallized with two molecules in the asymmetric unit cell, with both molecules exhibiting disorder in the cinnamyl groups. The disorder was slightly different in each molecule, and the molecules were designated molecule A and B. Shown below in Figure 2.3, is molecule A with the disordered atom positions omitted for clarity. The full structures for both molecules A and B with disordered atom positions can be found in Appendix 6.2, Figures 6.2 and 6.3.

Interestingly **3a** showed no evidence of disorder among the cinnamyl group. As was observed for **2a**, **3b** showed an intermolecular hydrogen-bond between N3-H3 and a chloride ligand of another molecule in the unit cell. The N3...C11 hydrogen-bond distance varies for molecule A (3.514(3) Å) and B (3.432(3) Å). Both distances, once again, fall in the range consistent for a weak hydrogen bond ( $> 3.2$  Å).<sup>9</sup>

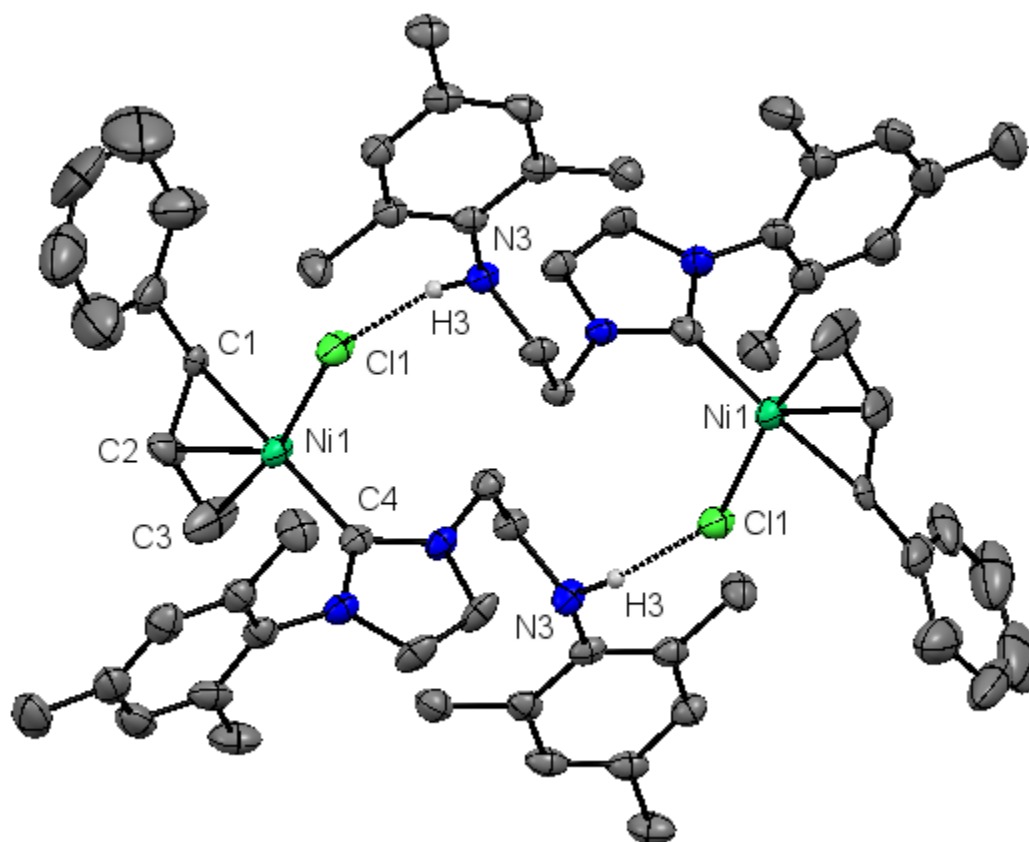


**Figure 2.3** ORTEP drawing of **3b** (Molecule A) showing naming and numbering scheme for selected atoms of interest. Ellipsoids are at the 50% probability level and hydrogen atoms were omitted for clarity (with the exception of the hydrogen atom on N3). Disordered atom positions omitted for clarity.

The solid state structure for **3a** (Figure 2.4) however showed no evidence for an intermolecular hydrogen bond, unlike the two other examples. The reason for this is not immediately obvious, however due to the fact that the previous examples only contain weak hydrogen bonds, the effect may not be enough to cause the molecule to crystallize in this fashion in all examples.

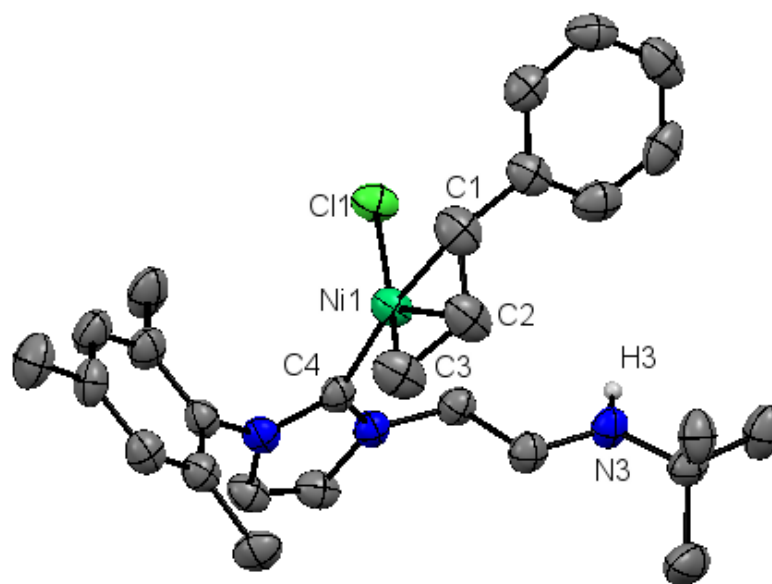


**Figure 2.4** ORTEP drawing of **3a** showing naming and numbering scheme for selected atoms of interest. Ellipsoids are at the 50% probability level and hydrogen atoms were omitted for clarity (with the exception of the hydrogen atom on N3)

**Table 2.1** Selected bond lengths (Å) and bond angles (deg) for solid-state structures of **2a**, **3a** and **3b**.

	<b>2a</b>	<b>3a</b>	<b>3b<sup>a</sup></b>
Ni(1)-C(4)	1.9052(10)	1.900(3)	1.907(3)
Ni(1)-C(3)	1.9852(12)	1.981(3)	1.985(3)
Ni(1)-C(2)	1.9873(16)	1.988(4)	1.96(2)
Ni(1)-C(1)	2.0710(13)	2.109(4)	2.131(6)
Ni(1)-Cl(1)	2.2112(6)	2.1994(10)	2.2024(10)
C(4)-Ni(1)-Cl(1)	97.93(3)	96.86(10)	97.09(9)
C(1)-C(2)-C(3)	120.11(16)	123.3(4)	127.0(15)
Hydrogen bonding (N3...Cl1)	3.7401(12)	N/A	3.514(3)

<sup>a</sup>Bond parameters for molecule A (parameters for molecule B located in Appendix 6.2, Table 6.3)

### 2.3.3 <sup>1</sup>H NMR Characterization and Dynamics of Complexes **2a**, **3a**, and **3b**

<sup>1</sup>H NMR analysis of **2a** in C<sub>6</sub>D<sub>6</sub> gave a complex spectrum in which there were a number of very broad peaks that precluded complete peak assignment at room temperature (Figure 2.5). Some peak assignments were made based on chemical shifts and integration values in comparison to that observed for the carbene ligand **1a**. A multiplet was observed at 4.86 ppm integrating to a value of approximately 1, relative to the signal for <sup>t</sup>Bu that was set to 9. This is a diagnostic signal for the internal proton of the allyl group (black dot in Figure 3.5), as seen in related NiX(allyl)(NHC) complexes.<sup>8</sup> Similar behaviour was observed in the resulting <sup>1</sup>H NMR spectra for complexes **3a** and **3b** (Appendix 6.5, Figures 6.7 and 6.8). Additionally in the spectra for **3a** and **3b**, there appeared to be a number of overlapping peaks, further adding to the complication of full peak assignment of the room temperature <sup>1</sup>H NMR spectra.

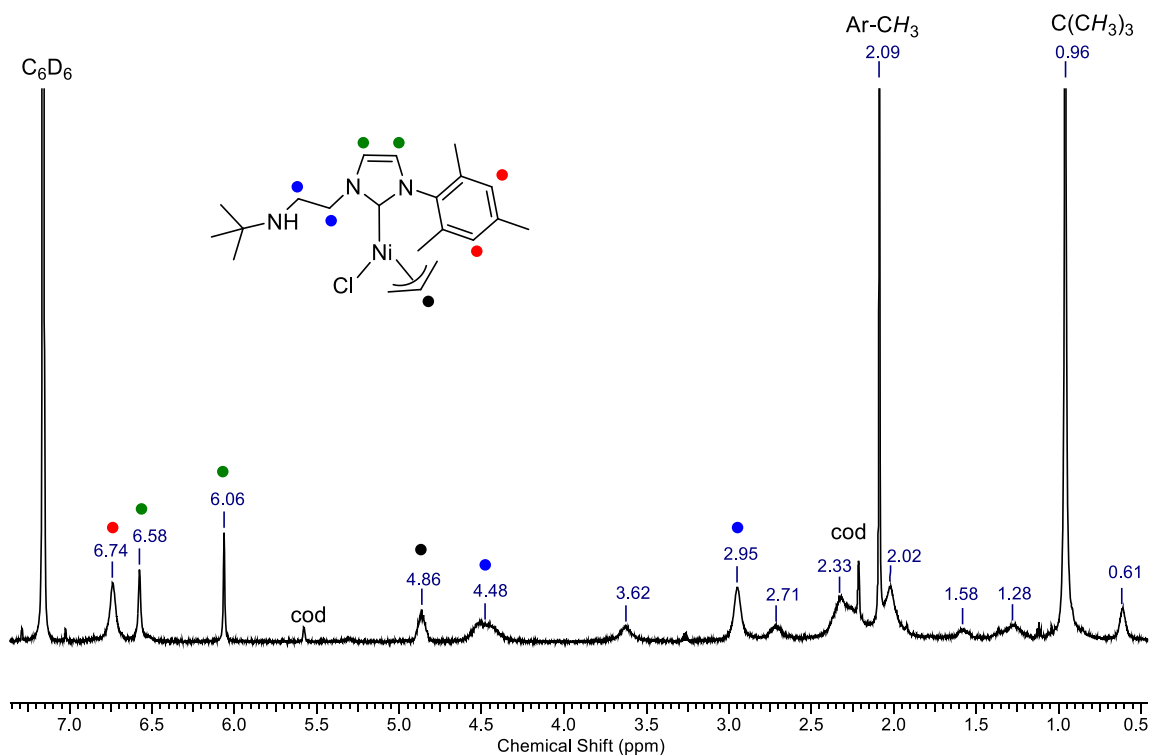


**Figure 2.5**  $^1\text{H}$  NMR spectrum of **2a** in  $\text{C}_6\text{D}_6$  at room temperature, 600 MHz

The broad nature of the peaks in the  $^1\text{H}$  NMR spectrum is likely due to the dynamic nature of the coordinated NHC and allyl ligands, which is not unprecedented and has been shown in some literature examples.<sup>8,12</sup> These literature  $\text{NiX}(\text{allyl})(\text{NHC})$  complexes display rapid interconversion on the NMR time scale between different conformations of the allyl ligand ( $\eta^3$  to  $\eta^1$ ) and NHC ligand rotations.<sup>5,8,12</sup> Additionally, our ligand with a pendent secondary amine, has the potential to coordinate to Ni through a  $\kappa^2\text{-C,N}$  mode. This postulation is supported by previous examples in the literature in which ligands **1a** and **1b** bond through a  $\kappa^2$ -mode in nickel or ruthenium organometallic complexes.<sup>13,14</sup> This process would likely occur following isomerisation of the allyl ligand from  $\eta^3$  to an  $\eta^1$ -mode. In addition the possibility exists for rotation among both the mesityl group of the ligand, as well as rotation of the pendent amine arm. These processes are illustrated below in Figure 2.6.

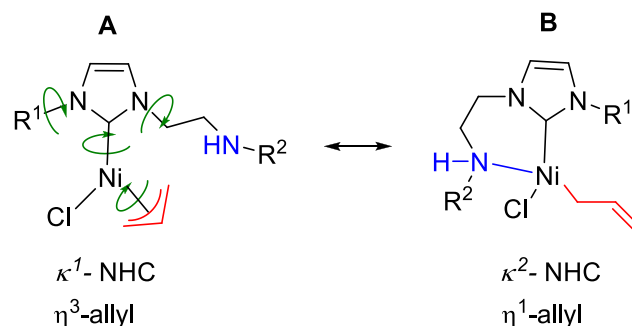


**Figure 2.6** Potential bonding modes and ligand rotations (green arrows) of Ni(allyl)(NHC) species. **A**: thermodynamically stable complex (based on X-ray crystallography) **B**: isomerisation of NHC and allyl ligands

Variable temperature (VT)  $^1\text{H}$  NMR studies were explored to characterize complex **2a**, since lowering the temperature should sufficiently slow the dynamic processes and decoalescence of the peaks should occur.<sup>8,12</sup> Since benzene has a relatively high melting point (5 °C), it has limited use in low temperature VT NMR studies. Deuterated toluene ( $\text{C}_7\text{D}_8$ ) was chosen as a solvent for the VT study as it has a low melting point of -95 °C, and has similar properties to that of benzene. Even upon cooling the NMR probe to a temperature of -65 °C, decoalescence of the peaks of **2a** in  $\text{C}_7\text{D}_8$  was not observed. However, in switching the NMR solvent to deuterated dichloromethane ( $\text{CD}_2\text{Cl}_2$ ), decoalescence appeared to be achieved starting at -70 °C (Figure 2.7). Some peaks however remained broad, making absolute peak assignment difficult. In addition, there appeared to be some overlapping signals (at 4.84, 2.28, and 1.12 ppm), based on integration values.  $^1\text{H}$ - $^1\text{H}$  COSY NMR data of the species at -75 °C was inconclusive, and more NMR experiments were needed for full peak assignment. The very low temperatures required for NMR analysis of this compound is undesirable, therefore a derivative of **2a** that may be analyzed at room temperature (or at least higher temperatures than -70 °C) for full NMR characterization will be beneficial.

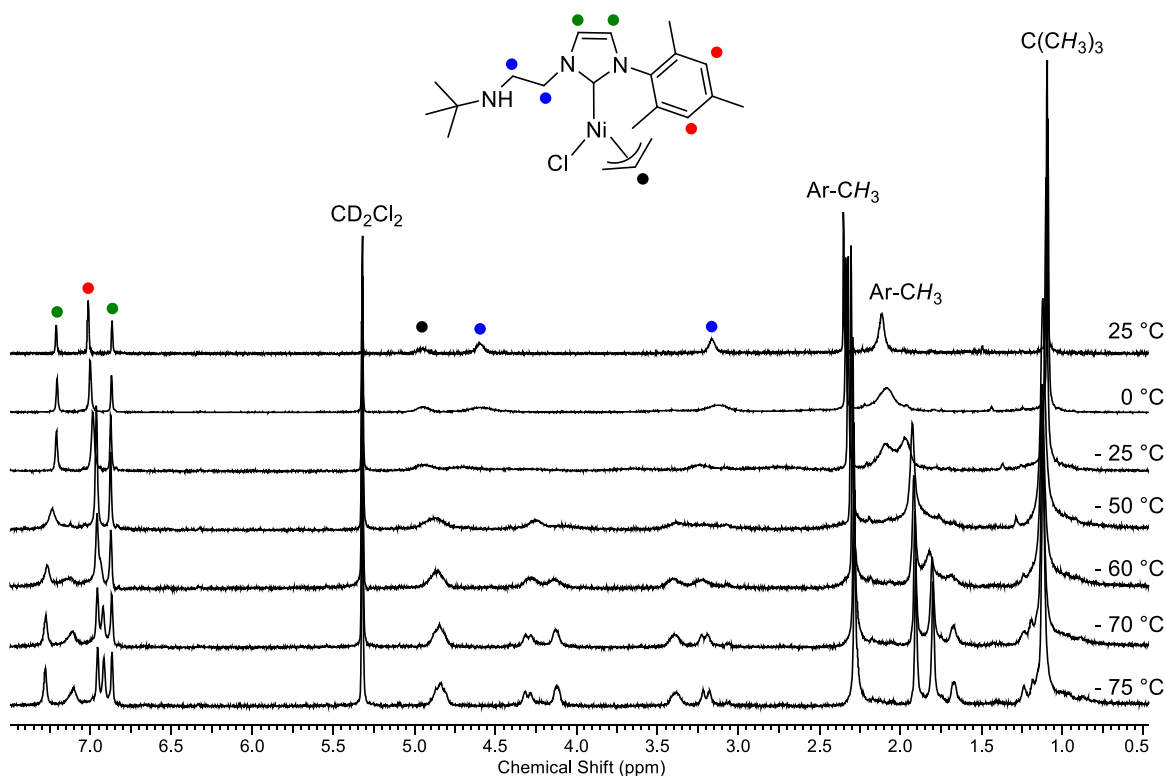


**Figure 2.7** Variable-Temperature  $^1\text{H}$  NMR experiment for complex **2a**, in  $\text{CD}_2\text{Cl}_2$ , 400 MHz

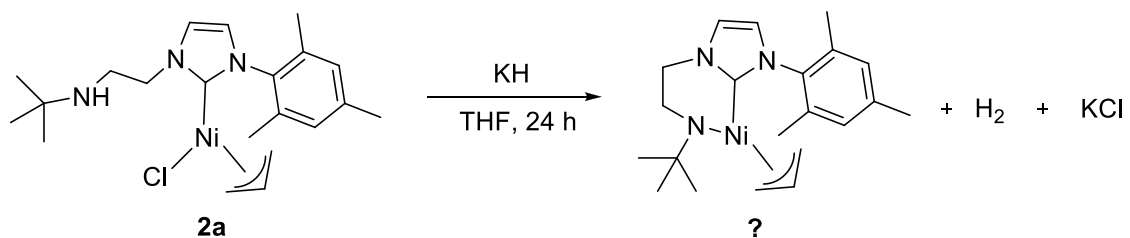
It should be noted that this dynamic behaviour, especially the rapid rotation of the NHC ligand, is very beneficial to oxygen reactivity. Sigman noted that complexes with lower barriers to M-NHC bond rotation react with  $\text{O}_2$ , whereas complexes with hindered Ni-NHC bond rotation showed no  $\text{O}_2$  reactivity at room temperature for a period of up to 2 days.<sup>5</sup> The dynamic behaviour observed for **2a**, as well as **3a** and **3b**, by  $^1\text{H}$  NMR spectroscopy is promising for the reactivity of our complexes with  $\text{O}_2$ .

## 2.4 Efforts Towards Reducing Dynamic Processes for $^1\text{H}$ NMR Characterization of **2a**

### 2.4.1 Attempted Deprotonation of **2a** with Base

We postulated that deprotonation of the pendent amine would result in formation of  $\text{H}_2$  and  $\text{KCl}$ . The resulting low coordinate Ni centre would be stabilized by coordination of the N centre to afford a  $\kappa^2$ -(*N,C*) NHC complex. Increasing the denticity would limit the potential

dynamic processes and may facilitate characterization. Complex **2a** was treated with a slight excess of KH in THF and allowed to stir for 24 hours (Scheme 2.5).



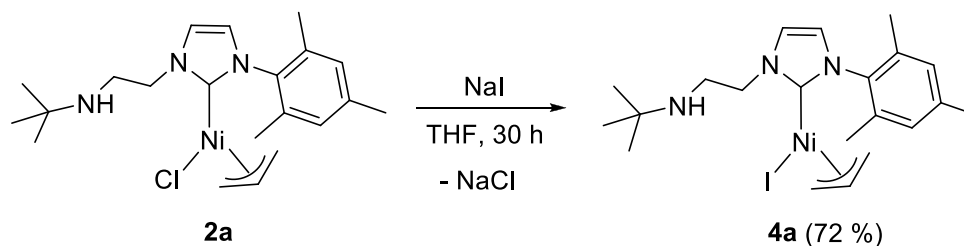
**Scheme 2.5** Attempted deprotonation of **2a** using KH

A lighter orange coloured solid (compared to **2a**) was isolated. A minimal change was observed in the  $^1\text{H}$  NMR spectrum ( $\text{C}_6\text{D}_6$ ) compared to that of the starting material (Appendix 6.5, Figure 6.9), with peaks remaining broad. Additionally, there was presence of metallic nickel being formed in the reaction, and the lack of evidence of  $\text{H}_2$  or  $\text{KCl}$  (no observed bubbles or white solid formed, respectively). The above evidence suggested that this reaction was not successful. A similar procedure was done using  $\text{K}_2\text{CO}_3$  in place of KH, with similar results obtained (Appendix 6.5, Figure 6.10).

#### 2.4.2 Synthesis and Characterization of a NiI(allyl)(NHC) Complex

Another proposed way to hinder the dynamic processes is through increasing the steric bulk by replacement of the chloride ligand for the larger iodide. Gomes *et. al.* have shown that by replacement of a bromide ligand for an iodide, a reduction in dynamic behaviour in their NiI(allyl)(NHC) complex was found.<sup>8</sup> An analogous iodide derivative was synthesized here by the addition of a slight excess of NaI to a solution of **2a**, and was allowed to stir for 30 hours (Scheme 2.6). A bright orange solid was isolated in good yields. Confirmation of halide substitution and assignment of **4a** was made through MALDI-MS, in which the resulting spectrum showed a peak corresponding to  $[\text{NiI}(\text{NHC})]^{+\bullet}$  ( $m/z = 470.1$ ) (Appendix 6.4, Figure 6.6).





**Scheme 2.6** Synthesis of **4a** through halide substitution of chloride for iodide

The  $^1\text{H}$  NMR spectrum of **4a** in  $\text{C}_6\text{D}_6$  at room temperature once again gave a spectrum in which there were a number of very broad peaks. VT  $^1\text{H}$  NMR studies were initially performed in  $\text{C}_7\text{D}_8$ , due to its large temperature window for VT studies ( $-95$  °C to  $111$  °C). However, at a temperature between  $-25$  and  $-50$  °C, there was precipitation of **4a** out of solution, evidenced by the absence of non-solvent signals in the  $^1\text{H}$  NMR at  $-50$  °C. Ultimately  $\text{CD}_2\text{Cl}_2$  was chosen as the NMR solvent of choice as **4a** remains dissolved in dichloromethane until temperatures of at least  $-80$  °C and due to the successful VT NMR experiment of **2a** in this solvent. Analysis of complex **4a** in  $\text{CD}_2\text{Cl}_2$  at room temperature by  $^1\text{H}$  NMR once again revealed a broad spectrum, with a number of expected signals missing. Excitingly however, decoalescence of the peaks was observed starting at  $-50$  °C and continued cooling to  $-70$  °C afforded sharp signals (Figure 2.8). In comparison to the VT NMR spectra for **2a**, decoalescence was achieved nearly  $20$  °C higher, which is evidence that the proposed slowing of dynamic processes has been achieved in **4a**. In the low-temperature static regime the observed peaks for **4a** are much sharper than for **2a**, showing better defined splitting which was helpful for peak assignment. A number of additional NMR experiments were performed to further characterize **4a**, including:  $^1\text{H}$ - $^1\text{H}$  COSY (collected at  $-70$  °C, Figure 2.9),  $^{13}\text{C}$  (collected at  $-50$  °C, Appendix 6.6, Figure 6.12), and  $^1\text{H}$ - $^{13}\text{C}$  HMBC (collected at  $-50$  °C).

At temperatures  $<-50$  °C, three peaks corresponding to the methyl groups of the mesityl group were observed at 2.29, 1.91, and 1.81 ppm. Additionally there were two singlets integrating to 1 proton each (6.96, 6.92 ppm), assigned to the mesityl aryl protons. This suggested the rotation of the mesityl group has been completely halted at temperatures of  $-50$  °C or below. A group of 5 signals at 4.90, 4.12, 3.28, 1.70, and 1.22 ppm integrating roughly to 1 proton each correlated to the inequivalent protons of the allyl group. The

chemical shifts and the splitting of the peaks matched closely to  $\eta^3$ -allyl species reported by Gomes *et. al.* for  $\text{NiX}(\eta^3\text{-allyl})(\text{NHC})$  ( $\text{X} = \text{I}, \text{Br}$ ) complexes.<sup>8</sup> Specifically, the allylic protons trans to the NHC ligand ( $\text{H}^4$  and  $\text{H}^5$ ) were shifted further downfield compared to the other allylic protons ( $\text{H}^1$  and  $\text{H}^2$ ), due to the trans-effect (as observed in the solid state structure of **2a**). Peak assignment was aided by  $^1\text{H}$ - $^1\text{H}$  COSY NMR spectrum showing the correlation of protons  $\text{H}^{1/2}$  and  $\text{H}^{4/5}$  among each other, in addition to correlation with the internal CH proton ( $\text{H}^3$ ) (Figure 2.9). This suggested that in the case of **4a**, the allyl group is likely the  $\eta^3$  isomer at low temperatures, however isomerization occurs at higher temperatures as the peaks in the room temperature spectrum are broadened into the baseline. If the allyl ligand was in a  $\eta^1$  bonding mode, there would be four signals present in the  $^1\text{H}$  NMR, versus the five observed for  $\eta^3$ , as observed for  $\text{Pd}(\eta^1\text{-allyl})$  complexes.<sup>15,16</sup>

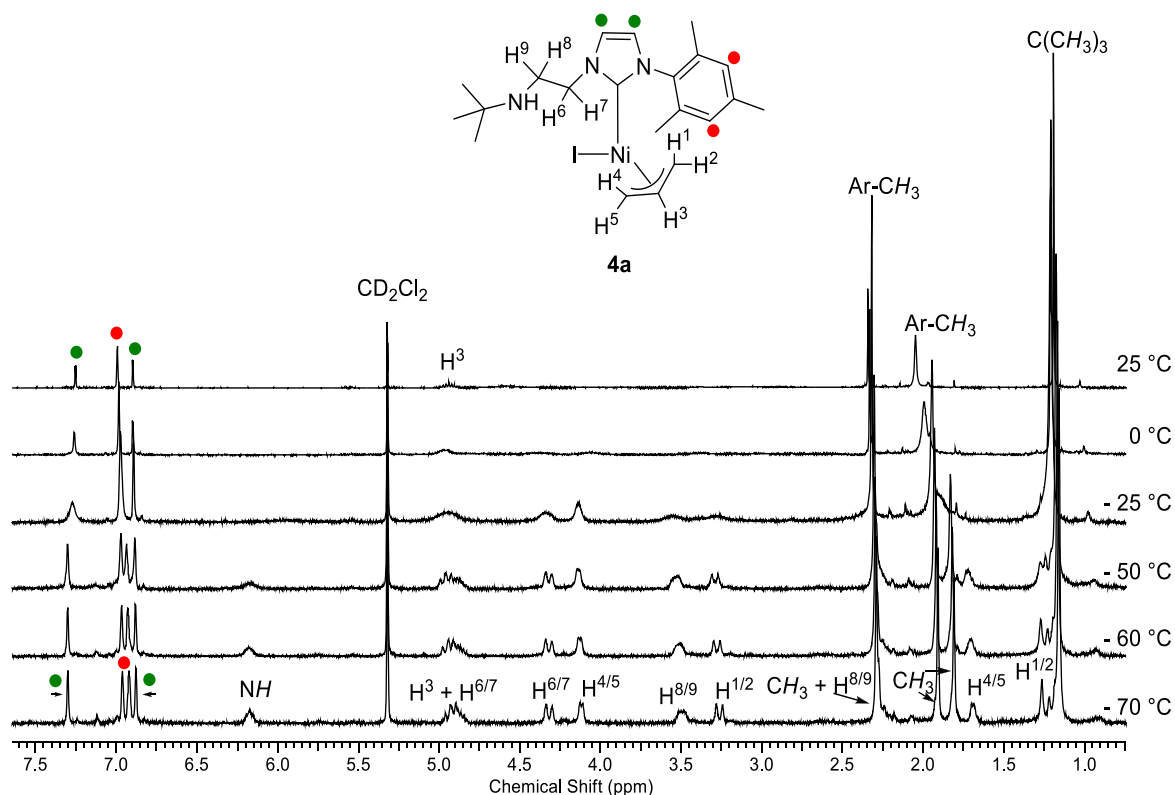


**Figure 2.8** Variable-Temperature  $^1\text{H}$  NMR experiment for complex **4a**, in  $\text{CD}_2\text{Cl}_2$ , 400 MHz

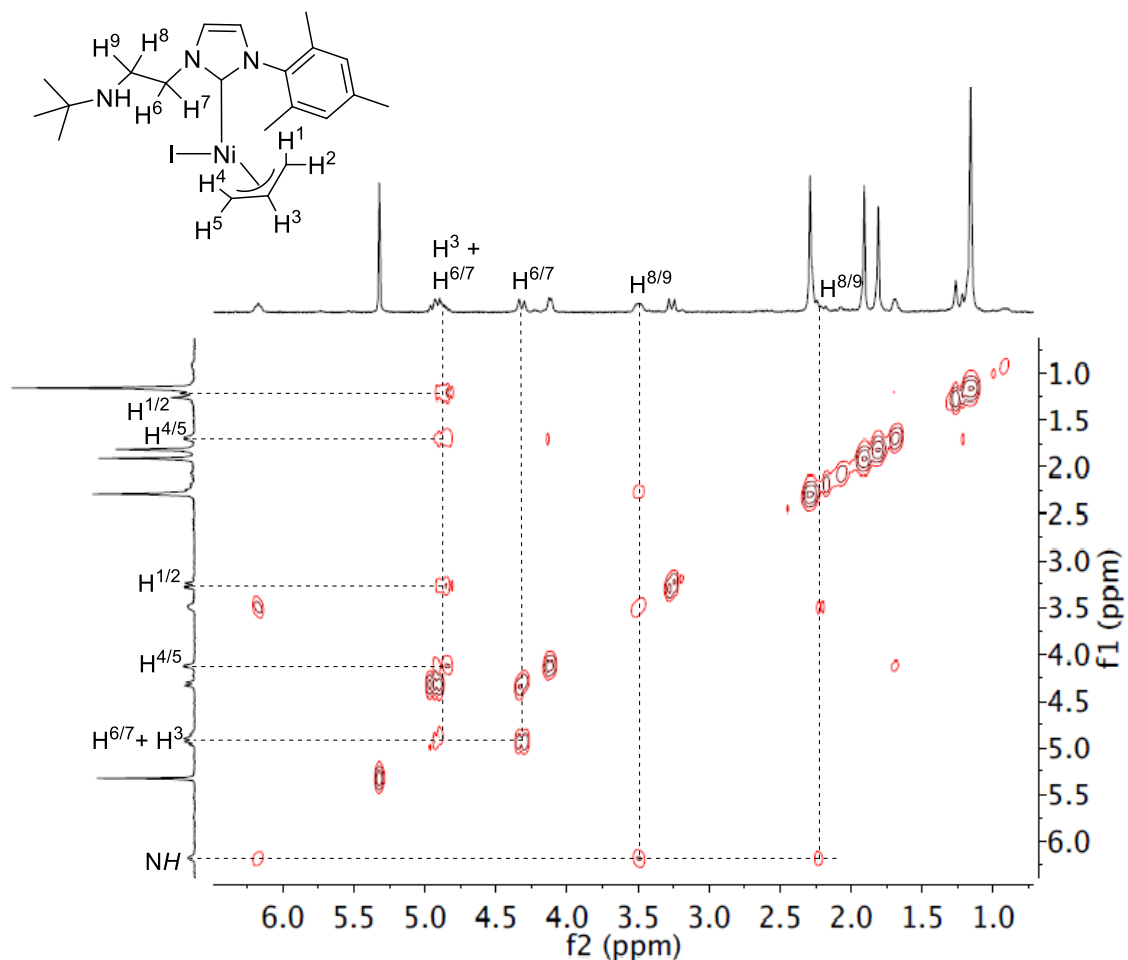
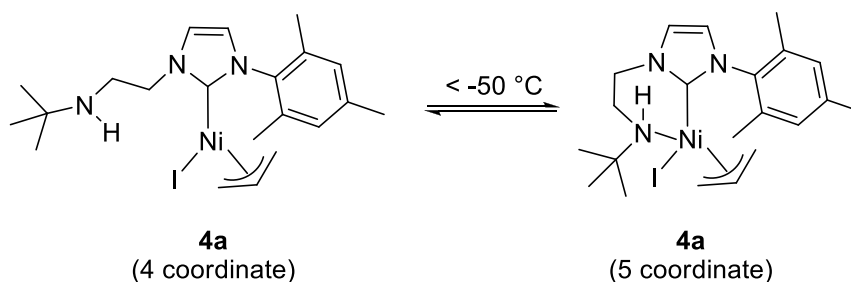


**Figure 2.9** Relevant portion of  $^1\text{H}$ - $^1\text{H}$  COSY NMR spectrum of **4a** (in  $\text{CD}_2\text{Cl}_2$ ) showing  $\text{H}^3$  of allyl group coupling to other allylic peaks, coupling of methylene protons, and coupling of NH to  $\text{H}^{8/9}$  of adjacent methylene group

There were overlapping peaks at 4.90 and 2.29 ppm, in addition to peaks at 4.32 and 3.50 ppm, all roughly integrating to 1. These signals were assigned to the methylene groups of the pendent amine arm. The  $^1\text{H}$ - $^1\text{H}$  COSY NMR spectrum showed a correlation between the peaks at 3.50 and 2.29 ppm (Figure 2.9), representing one of the methylene groups. The other methylene group consists of the peaks at 4.90 and 4.32 ppm, which also correlated to each other. The protons located adjacent to the N atom of the imidazole ring are likely  $\text{H}^6$  and  $\text{H}^7$  (4.90 and 4.32 ppm), and were located further downfield compared to those of the

other CH<sub>2</sub> group, H<sup>8</sup> and H<sup>9</sup> (3.50 and 2.29 ppm). Peak assignment was made based on the fact that in the case of free ligand **1a** (as well as all ligand precursors), the CH<sub>2</sub> group adjacent to the NH was further upfield in the <sup>1</sup>H NMR compared to the CH<sub>2</sub> group adjacent to imidazole ring (4.00 vs 2.83 ppm for **1a**). Exact peak assignment for these groups cannot be made at this time, and further NMR studies may be required. As these peaks are broadened into the baseline at room temperature, this suggests that the pendent amine arm is quite dynamic.

The remaining unassigned signal in the <sup>1</sup>H NMR at -70 °C was a triplet at 6.18 ppm integrating to 1. <sup>1</sup>H-<sup>1</sup>H COSY NMR data suggested that this peak corresponds to the amine proton, as it only correlates with H<sup>8</sup> and H<sup>9</sup> of the adjacent CH<sub>2</sub> group (see Figure 3.9). At a chemical shift of 6.18 ppm, this would represent a large shift downfield from a shift of 1.32 ppm in ligand **1a**. A logical suggestion for this behaviour is that there is coordination of the amine group to the metal centre, and at < -50 °C, this is the more favoured bonding mode at those temperatures. As previously mentioned, there has been literature reports of ligand **1a** (as well as **1b**) bonding in this sort of fashion, in which the authors observe a similar downfield shift of the amine proton in the <sup>1</sup>H NMR.<sup>13,14</sup> At higher temperatures, the rapid switch between  $\kappa^1$ -C and  $\kappa^2$ -C,N bonding modes is likely, with the NH signal being extremely broad at room temperature. Interestingly, the data from this NMR experiment suggested both a  $\kappa^2$ -NHC and an  $\eta^3$ -allyl bonding mode. This goes against the previous postulation that isomerization of the allyl ligand to  $\eta^1$  would occur upon coordination of the pendent amine arm to Ni. In the case of a  $\kappa^2$ -NHC and  $\eta^3$ -allyl species, the resulting structure would be an 18 electron five-coordinate Ni(II) species (Scheme 2.7). Five-coordinate Ni(II) species have been characterized in literature, however, none for a Ni(NHC)(allyl) complex.<sup>17,18</sup> Alternatively, the downfield shift could be a result of H-bonding of the NH to the halide ligand (as was observed in the solid state). At this moment, there is no evidence to distinguish between the two possibilities.



**Scheme 2.7** Potential formation of five-coordinate Ni(II) species at low temperatures

High temperature VT  $^1\text{H}$  NMR studies of **4a** were performed as well (up to  $100\text{ }^{\circ}\text{C}$ ), in attempt to achieve to fully coalesced spectrum. In the resulting  $^1\text{H}$  NMRs in  $\text{C}_7\text{D}_8$ , there was some peak sharpening starting to occur at  $75\text{ }^{\circ}\text{C}$ . However, even at  $100\text{ }^{\circ}\text{C}$ , the peaks remained broad and precluded complete peak assignment. Additionally, the solvent signal for toluene at 2.11 ppm appeared to overlap with the potential signals for the mesityl  $\text{CH}_3$  groups. The spectra for this experiment can be found in Appendix 6.4, Figure 6.11.

The NMR data obtained for **4a** can be used to retroactively assign the spectra for **2a** as the observed peaks match closely between the two spectra (Figure 2.10). One noted difference between the two spectra, was the disappearance of the NH signal at 6.18 ppm and the appearance of a signal integrating to 1 at 7.11 ppm in the spectrum for **2a** at  $-70\text{ }^{\circ}\text{C}$ . Logically the assignment of this proton would be the NH signal for **2a**, and the shift of about  $\sim 1$  ppm downfield for **2a** may be indicative of the change in electronics at the Ni centre in the switch from a Cl ligand to an I. Due to the success of this method in characterizing **2a**, similar methods may be employed for **3a** and **3b**.

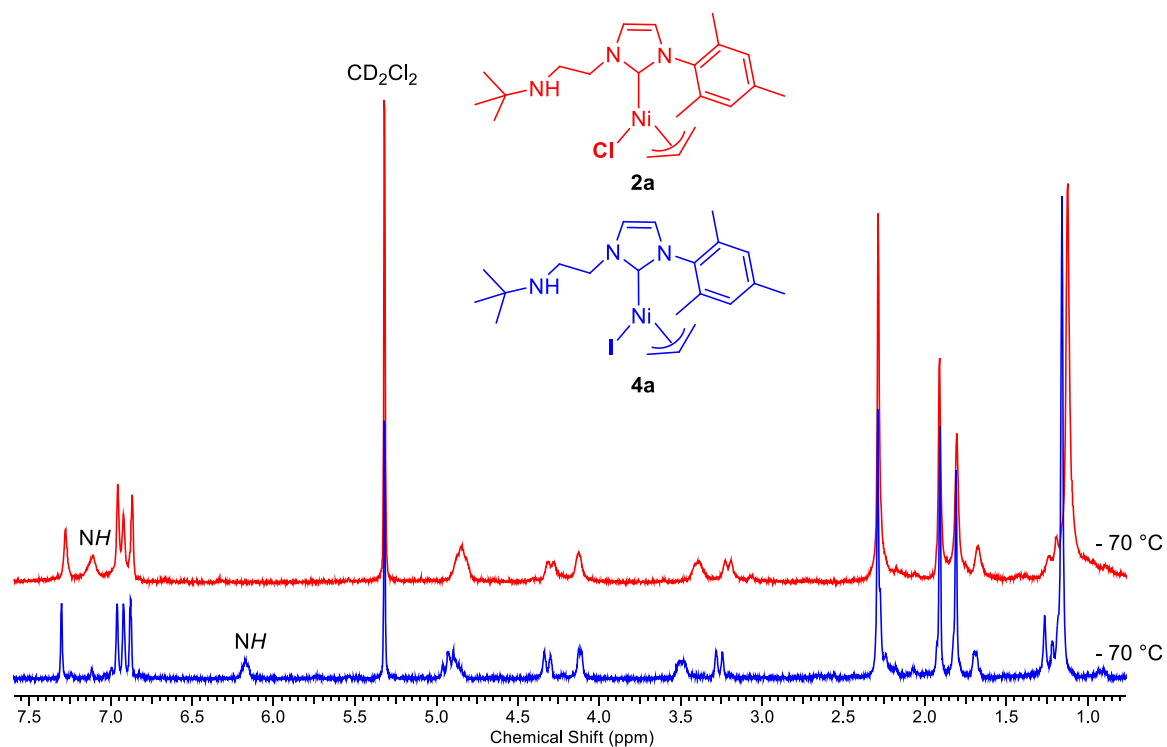


**Figure 2.10** Comparison of  $^1\text{H}$  NMR spectra for **2a** and **4a** at  $-70\text{ }^\circ\text{C}$ , 400 MHz

## 2.5 Conclusions

This chapter detailed the synthesis and characterization of four new  $\text{NiX}(\text{allyl}/\text{cinnamyl})(\text{NHC})$  ( $\text{X} = \text{Cl}, \text{I}$ ). Three asymmetric NHC ligands (**1a/b/c**) were targeted for this study. The NHC ligands chosen contained a unique feature in a pendent  $2^\circ$  amine arm, in which to act as a hydrogen-bond donor in the secondary coordination sphere or as a hemi-labile donor group. **1a-c** were successfully synthesized, and isolated as the free carbenes, following a multi-step literature procedure and/or modified literature reactions.  $^1\text{H}$  NMR spectroscopy was used to characterize the final products, and all intermediate products. The corresponding  $\text{NiCl}(\text{allyl}/\text{cinnamyl})(\text{NHC})$  complexes **2a**, and **3a-b** were synthesized following a two-step, one-pot literature procedure for related complexes. Characterization of the complexes was made using MALDI-MS,  $^1\text{H}$  and  $^{13}\text{C}$  NMR spectroscopy, and X-ray crystallography. Complex **3c** was synthesized in the same fashion, however confirmation of product formation has not been made.

MALDI-MS data showed evidence for coordination of the NHC to nickel, as in all cases there was observed signals corresponding to  $[\text{NiCl}(\text{NHC})]^{•+}$ , however none for the molecular ion. Solid-state structures for **2a**, and **3a-b** revealed a monometallic Ni complex with the NHC bonded in a  $\kappa^1$ -coordination mode and the allyl ligand in a  $\eta^3$ -coordination mode, confirming the structure of the complexes in the solid state. Interestingly for **2a** and **3b**, there was an observed hydrogen bonding interaction between the pendent amine arm of the NHC and the chloride ligand of another molecule in the unit cell. A  $\text{N}\cdots\text{Cl}$  bond length of 3.7401(12) Å was measured for **2a**, and 3.514(3) Å for **3b**. These values are consistent for a weak hydrogen bond ( $> 3.2$  Å) for that type of functionality. This phenomena is not observed for **3a**. The observed hydrogen bonding signals the potential for the pendent amine arm to act as a hydrogen-bond donor, in which to potential stabilize reactive Ni-OH intermediates.

$^1\text{H}$  NMR analysis at room temperature yielded complex spectra, with a number of very broad peaks, preventing full peak assignment. The breadth of the peaks in the  $^1\text{H}$  NMR was due to the dynamic nature of the coordinated NHC and allyl ligands. Low temperature VT  $^1\text{H}$  NMR studies on **2a** were undertaken, in order to slow the dynamic processes and achieve decoalescence of the peaks. Ultimately, a decoalesced  $^1\text{H}$  NMR spectrum for **2a** in  $\text{CD}_2\text{Cl}_2$  was obtained at  $-70$  °C, allowing for characterization of **2a** in the solution state. To further reduce the dynamic behaviour of the complexes, and obtain decoalesced  $^1\text{H}$  NMR spectra at higher temperatures, a derivative of **2a** was synthesized. The substitution of an iodide ligand for a chloride was postulated to reduce the dynamic processes, as observed in a related literature system.  $[\text{NiI}(\text{allyl})(\mathbf{1a})]$  (**4a**) was synthesized in a one-step procedure by reaction of **2a** with NaI. For **4a** in  $\text{CD}_2\text{Cl}_2$ , decoalescence of peaks starts at  $-50$  °C, evidence that the proposed slowing of dynamic processes has been achieved. Full NMR characterization of **4a** at low temperatures was done using  $^1\text{H}$ ,  $^{13}\text{C}$ ,  $^1\text{H}$ - $^1\text{H}$  COSY, and  $^1\text{H}$ - $^{13}\text{C}$  HMBC NMR techniques. Of note is the large downfield shift ( $\sim 5$  ppm) of the NH peak in comparison to the free ligand, possibly signifying either: coordination of the amine to the metal centre to form a five coordinate Ni(II) species; or a  $\text{N-H}\cdots\text{Cl}$  hydrogen bonding interaction similar to that observed in the solid state.

## 2.6 References

1. Jong, H.; Patrick, B. O.; Fryzuk, M. D. *Can. J. Chem.* **2008**, *86*, 803-810
2. Shih, W.-C.; Wang, C.-H.; Chang, Y.-T.; Yap, G. P. A.; Ong, T.-G. *Organometallics* **2009**, *28*, 1060-1067
3. Arnold, P. L.; Mungur, S. A.; Blake, A. J.; Wilson, C. *Angew. Chem.* **2003**, *115*, 6163 - 6166
4. Dible, B. R.; Sigman, M. S. *J. Am. Chem. Soc.* **2003**, *125*, 872-873
5. Dible, B. R.; Sigman, M. S. *Inorg. Chem.* **2006**, *45*, 8430-8441
6. Benson, S.; Payne, B.; Waymouth, R. M. *J. Polym. Sci. A1* **2007**, *45*, 3637-3647
7. ChemCalc: a building block for tomorrow's chemical infrastructure. Patiny, L.; Borel, A. *J. Chem. Inf. Model* **2013**. DOI: 10.1021/ci300563h
8. Silva, L. C.; Gomes, P. T.; Veiros, L. F.; Pascu, S. I.; Duarte, M. T.; Namorado, S.; Ascenso, J. R.; Dias, A. R. *Organometallics* **2006**, *25*, 4391- 4403
9. Steiner, T. *Angew. Chem. Int. Ed.* **2002**, *41*, 48-76
10. Gavette, J. V.; Klug, C. M.; Zakharov, L. N.; Shores, M. P.; Haley, M. M.; Johnson, D. W. *Chem. Commun.* **2014**, *50*, 7173-7175
11. Fernández-Salas, J. A.; Marelli, E.; Cordes, D. B.; Slawin, A. M. Z.; Nolan, S. P. *Chem. Eur. J.* **2015**, *21*, 3906-3909
12. Cámpora, J.; Ortiz de la Tabla, L.; Palma, P.; Álvarez, E.; Lahoz, F.; Mereiter, K. *Organometallics* **2006**, *25*, 3314-3316
13. Huang, Y.-P.; Tsai, C.-C.; Shih, W.-C.; Chang, Y.-C.; Lin, S.-T.; Yap, G. P. A.; Chao, I.; Ong, T.-G. *Organometallics* **2009**, *28*, 4316-4323
14. Jong, H.; Patrick, B. O.; Fryzuk, M. D. *Organometallics* **2011**, *30*, 2333-2341
15. Canovese, L.; Visentin, F.; Santo, C.; Chessa, G.; Bertolasi, V. *Organometallics* **2010**, *29*, 3027-3038
16. Crociani, B.; Antonaroli, S.; Paoli, P.; Rossi, P. *Dalton Trans.* **2012**, *41*, 12490-12500
17. Dolores Santana, M.; Abel Lozano, A.; García, G.; López, G.; Pérez, J. *Dalton Trans.* **2005**, 104-109
18. Zhang, C.-P.; Wang, H.; Klein, A.; Biewer, C.; Stirnat, K. Yamaguchi, Y.; Xu, L.; Gomez-Benitez, V.; Vicic, D. A. *J. Am. Chem. Soc.* **2013**, *135*, 8141-8144



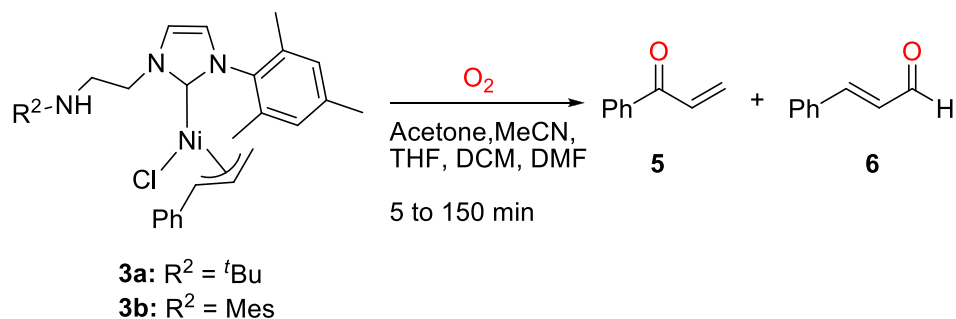
## Chapter 3

### 3 Dioxygen Reactivity Studies

#### 3.1 Reactivity of NiCl(allyl/cinnamyl)(NHC) complexes with O<sub>2</sub>

Following the synthesis of the three complexes NiCl(allyl/cinnamyl)(NHC) (**2a**, **3a**, and **3b**) described in the previous chapter, their reactivity toward O<sub>2</sub> was tested. It was proposed that the oxidation products formed would be the same to that observed by Sigman for related complexes that do not have a pendent H-bond donor on the NHC ligand.<sup>1</sup> The proposed oxidation products include 2-propenal in the oxidation of **2a**, and phenyl vinyl ketone (**5**) or cinnamaldehyde (**6**) in the oxidation of **3a** or **3b**. Selectivity however may differ between our system and that reported by Sigman due to the nature of the NHC ligands used, with the most notable feature being the secondary amine arm on our NHC.

Preliminary aerobic oxidation tests were conducted by simply opening a dark orange solution of **2a** in THF to air. Initial test reactions were performed with **2a** due to its accessibility, and the first question was simply whether these NHC ligands would allow for O<sub>2</sub> reactivity (as previously mentioned, some NHCs in the Sigman systems gave air stable complexes).<sup>2</sup> Within a period of ~ 2 minutes of exposure to air, a change in the colour of the solution from dark orange to a very pale orange was observed. An insoluble brown solid was also formed at the bottom of the vial. Similar observations were made in the exposure **3a** and **3b** to air in THF. Analysis of the reaction mixture of **3a** by GC-MS revealed the presence of **5** and **6**, signifying the successful oxidation of the allylic ligand by oxygen, along with minor amounts (ca. <5%) of other potential products from cinnamyl or NHC ligand oxidation. Therefore, reactivity of **2a**, **3a**, and **3b** with O<sub>2</sub> was successful. In order to optimize the reaction, a number of conditions were altered and tested such as reaction time, and solvent choice (Scheme 3.1). The focus moving forward was placed on **3a** and **3b** due to the ease of assessing selectivity. A complete table of data for all of these oxidation reactions can be found in Appendix 6.8, Table 6.5.



**Scheme 3.1** Reaction conditions tested in aerobic oxidation of **3a/b**

### 3.2 Time Scale of the Aerobic Oxidation of **3a**

The effect on reaction time in the oxidation reaction was studied with **3a** ( $\text{R}^2 = \text{tBu}$ ) as the model complex. In the glovebox, 10 mM samples of **3a** in THF were prepared, also containing an equivalent molar amount of tetradecane to act as an internal standard. Upon removal from the glovebox, the samples were exposed to dried  $\text{O}_2$  through our standard method of bubbling in  $\text{O}_2$  into the vial for a period of  $\sim 20$  seconds. Once again the colour change from dark orange to a very pale orange was observed. With the addition of  $\text{O}_2$  acting as the starting time point, each vial from the set reacted for a different time period (2, 15, 30, 60, and 150 minutes) prior to GC-FID analysis to quantify the reaction products (Figure 3.1).

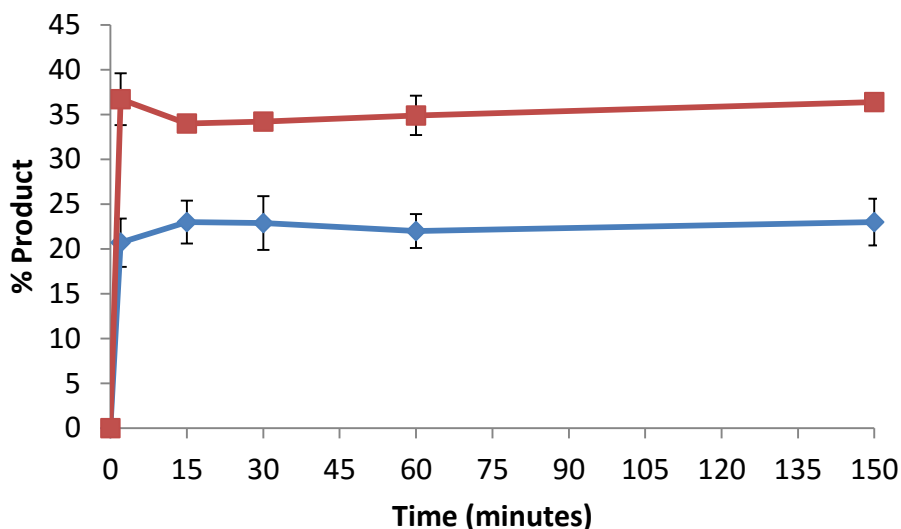


**Figure 3.1** Effect of reaction time on conversion in the oxidation of **3a** and O<sub>2</sub>. Points represent the average conversion to cinnamaldehyde (**6**, red) and phenyl vinyl ketone (**5**, blue) oxidation products. The experiments were performed in duplicate and the error bars represent the span of the duplicate runs

As evidenced from Figure 3.1, the reaction proves to be almost instantaneous, as further analysis of the reaction after the initial time point (2 minutes) showed no significant increase in products (within error). Taking into consideration all data points, an average overall yield of 63% (relative to internal standard) is observed with an average ratio of 1.3:1 (**6:5**). This represents a significant difference in selectivity in comparison to the results by Sigman, as he reported a ratio of 1.67:1 (**6:5**).<sup>1</sup> The results here suggests that the presence of the pendent amine arm has a notable effect in the oxidation reaction. Differences in selectivity may be steric in nature, where there is a less well-defined steric pocket due the flexibility of the amine arm. This may reduce the preference for the linear product (**6**). The exact role however will need to be investigated in the future to come to an accurate conclusion. It should be noted that Sigman used a different method for both exposure to oxygen and for analysis of the reaction (<sup>1</sup>H NMR). In order to achieve a better comparison between our results and that of Sigman's, NiCl(cinnamyl)(*i*Pr) was synthesized according to literature procedures. NiCl(cinnamyl)(*i*Pr) then underwent oxidation under our conditions and was analyzed using GC-FID. An average ratio of 1.68:1

(6:5) was achieved over 6 runs at a 15-minute reaction time, nearly identical to the literature value.

### 3.3 Effect of Solvent in the Aerobic Oxidation of 3a

To further probe the O<sub>2</sub> reactivity of our complexes, the effect of solvent on the performance of the oxidation of **3a** was tested in the following solvents: acetone, dichloromethane (DCM), acetonitrile (MeCN), and dimethylformamide (DMF). Samples were prepared identically as mentioned above with the exception of the replacement of THF with one of the aforementioned solvents, and were then exposed to oxygen. Initial qualitative assessment of the reactions after exposure to oxygen revealed a distinct colour change relative to reactions conducted in THF (with the exception of DCM). In the acetone, DMF, and MeCN samples, a colour change from dark orange to a light pinkish colour was observed after oxidation. In the acetone sample there was the formation of an insoluble beige precipitate, however, in the case of MeCN and DMF there was no formation of a precipitate. Each sample was analyzed by GC-FID at a set time point of 15 minutes after exposure of the vial to O<sub>2</sub>. The results for these experiments are shown below in Figure 3.2 (along with data for THF experiments for comparison).

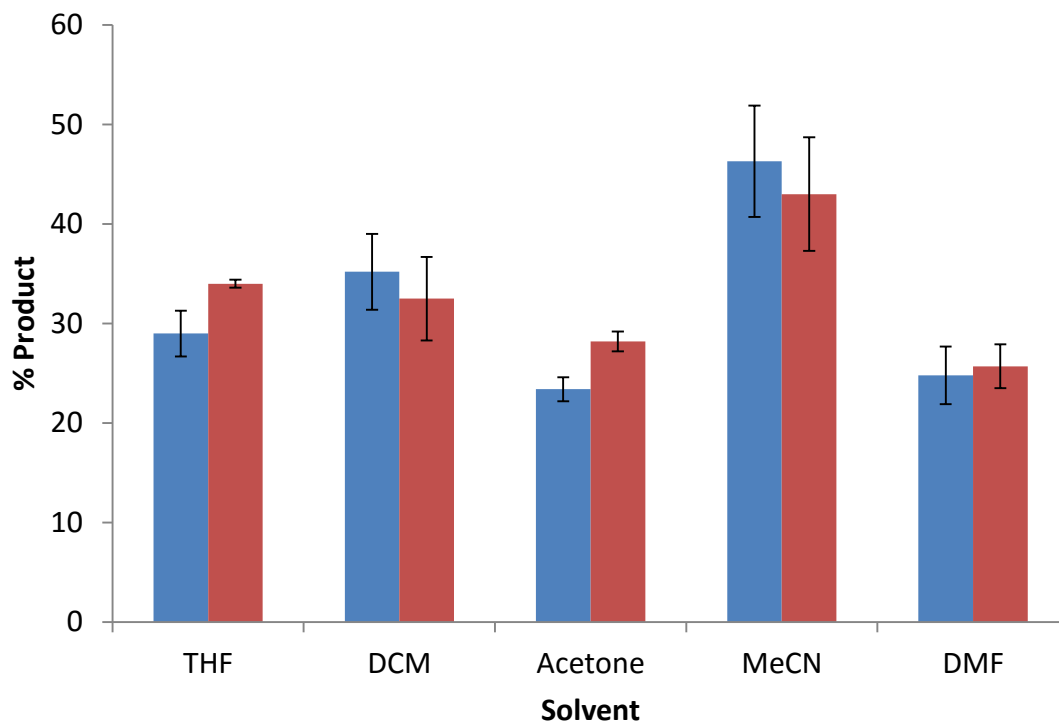


**Figure 3.2** Effect of solvent on conversion in the oxidation of **3a** and O<sub>2</sub>. Bars represent the average conversion to cinnamaldehyde (**6**, red) and phenyl vinyl ketone (**5**, blue) oxidation products. The experiments were performed in duplicate and the error bars represent the span of the duplicate runs

Apparent from the data in Figure 3.2 was that solvent appeared to affect the overall yield of the reaction. The highest yield was observed in MeCN (89%), with the yields for the other solvents being in the range of ~50-70 %. There was no evident trend based on yields observed and properties of the solvent, however future investigation into the oxidation reaction may yield a reasonable proposal. Product selectivity does not appear to be majorly affected by solvent choice, as there was an approximate 1:1 ratio (within error of each other) of products in DCM, MeCN, and DMF. There was a small preference for **6** for the reactions in acetone and THF. All examples react rapidly with O<sub>2</sub> within 15 minutes, and a second time point taken at 2 hours showed no significant change in conversion, therefore solvent choice appeared to play no role in elongating the reaction time. Interestingly Sigman reported that in the presence of chlorinated solvents, the reaction of O<sub>2</sub> with NiCl(cinnamyl)(NHC) complexes is inhibited due to competitive binding of solvent rather

than O<sub>2</sub>.<sup>2</sup> This appeared to not be the case in our system, although the immediate reason for this is not apparent.

### 3.4 Effect of Changing R<sup>2</sup> in Aerobic Oxidations

The effect of changing the R group of the pendent amine arm of the NHC on the oxidation chemistry was explored by the reaction of **3b** (R<sup>2</sup> = Mes) with O<sub>2</sub>. The standard conditions for **3a** were followed for **3b**. A similar colour change from dark orange to light orange was observed in addition to the formation of a brown insoluble solid. Data from GC-FID analysis is shown below in Figure 3.3.

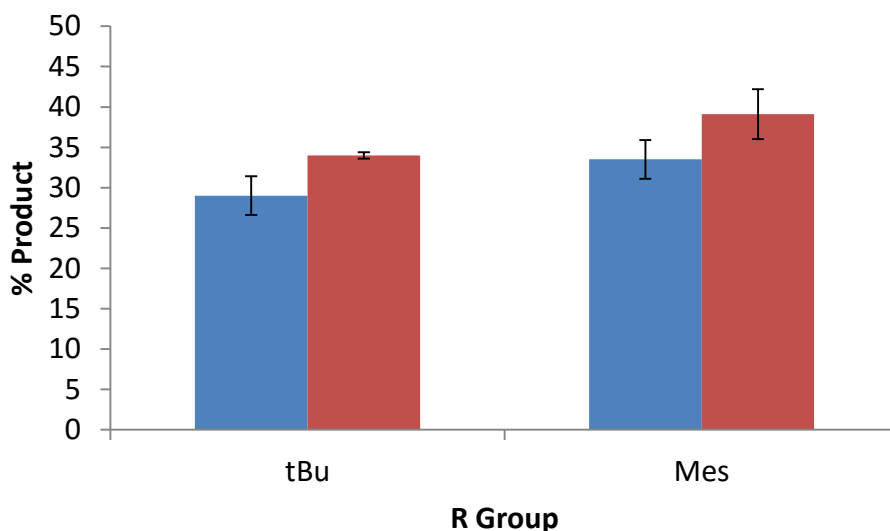


**Figure 3.3** Effect of changing R group in the reaction of **3a** (R<sup>2</sup> = *t*Bu), and **3b** (R<sup>2</sup> = Mes) with O<sub>2</sub>. Bars represent the average conversion to cinnamaldehyde (**6**, red) and phenyl vinyl ketone (**5**, blue) oxidation products. The experiments were performed in duplicate and the error bars represent the span of the duplicate runs. Solvent is THF

An average yield of approximately 72 %, with a product distribution of 1.16 (**6**:**5**), was observed for the oxidation of **3b**. This did not represent a large difference in performance in comparison to results achieved for **3a**, as the results are within error of each other. The lack of significant difference would suggest that altering the R<sup>2</sup> group does not play a role in product distribution.

### 3.5 Control Experiments

To ensure the observed oxidation products were due to the reaction of **3a** or **3b** with O<sub>2</sub>, a number of control experiments were performed. As expected, analysis of samples without exposure to O<sub>2</sub> showed no product formation (Table 3.1, entries 1-2). Samples of **3a** and **3b** were prepared and an excess of water was added, and analyzed without further exposure to O<sub>2</sub>. Once again, no evidence of cinnamaldehyde (**6**) or phenyl vinyl ketone products (**5**) was observed (Table 3.1, entries 3-4). There is the possibility that the observed oxidation products are due to dissociation of NHC ligands **1a** or **1b**, although this is highly unlikely. Solutions of the free NHC ligands showed no visible changes upon oxidation, and analysis by GC/MS revealed the absence of both **6** and **5** (Table 3.1, entries 5-6). Lastly to elucidate if the NHC itself is necessary to promote oxidation of the Ni centre, the cinnamylnickel(II) dimer [NiCl(cinnamyl)]<sub>2</sub> underwent aerobic oxidation. A solution of [NiCl(cinnamyl)]<sub>2</sub> in THF went from red to colourless instantly upon exposure to O<sub>2</sub>. Both **6** and **5** were observed by GC/MS, however in much smaller conversion values of 10% for **5**, and 7% for **6** (Table 3.1, entry 7), along with other potential oxidation products in relatively small amounts (ca. <5%). While the nickel(II) dimer can allow for product formation, complexes **3a** and **3b** give much higher conversion values, which opens the possibility for catalytic turnover.

**Table 3.1** Results of control experiments for aerobic oxidation reactions.<sup>a</sup>

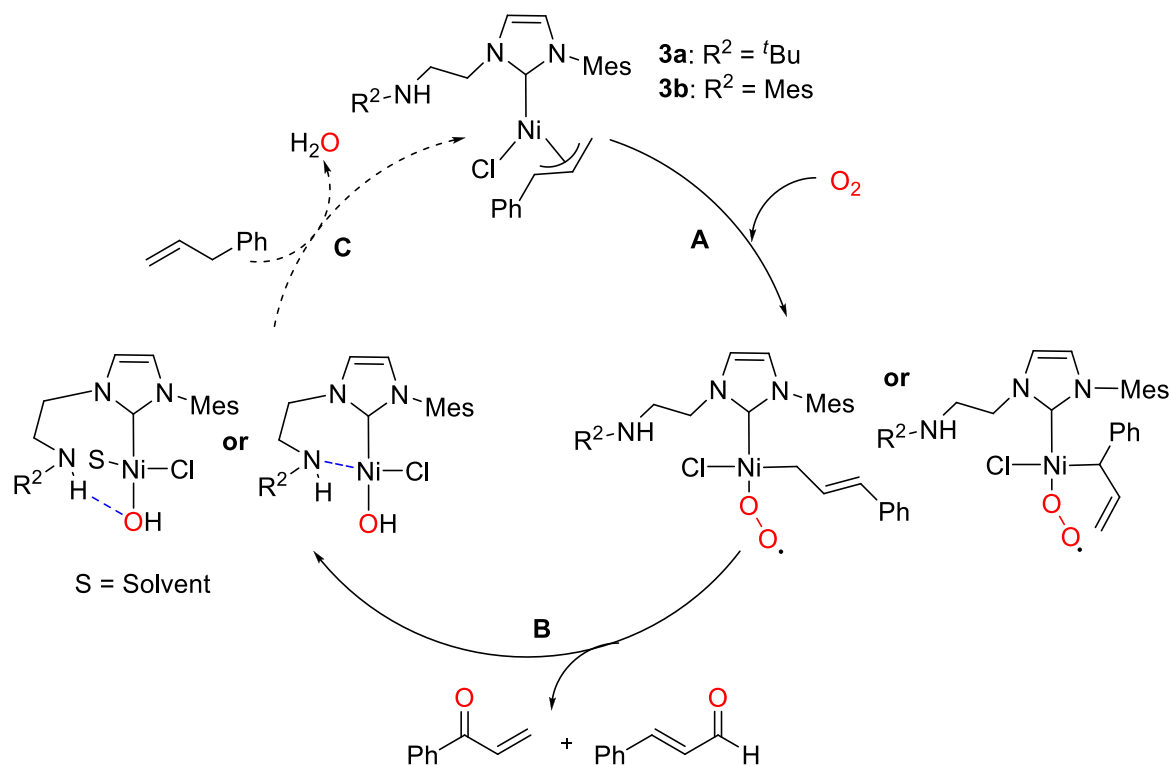
Entry	Ni Complex/ NHC ligand	Condition	% 5	% 6
1	<b>3a</b>	No O <sub>2</sub>	0	0
2	<b>3b</b>	No O <sub>2</sub>	0	0
3	<b>3a</b>	+ H <sub>2</sub> O, no O <sub>2</sub>	0	0
4	<b>3b</b>	+ H <sub>2</sub> O, no O <sub>2</sub>	0	0
5	<b>1a</b>	+ O <sub>2</sub>	0	0
6	<b>1b</b>	+ O <sub>2</sub>	0	0
7	[NiCl(cinnamyl)] <sub>2</sub>	+ O <sub>2</sub>	10	7

<sup>a</sup>Conditions: 5 mM [Ni] or ligand, 5 mM cyclodecane, reaction time of 15 minutes for oxidation reactions (where applicable), solvent = THF. Analyzed by GC/MS. Data calibrated via a single point calibration curve of 5 mM of cinnamaldehyde in THF.

### 3.6 Attempted Catalytic Aerobic Oxidations

The possibility of achieving catalytic turnover was investigated for complexes **3a** and **3b**. As mentioned previously, after the product release step (step **B**, Scheme 3.2) a Ni-OH intermediate would be formed. The hypothesis is that the pendent amine will then stabilize the reactive intermediate to avoid deactivation and promote step **C** (scheme 3.2). In this step, the Ni-OH intermediate would need to perform a C-H activation on another allylic substrate to regenerate **3a** or **3b**. The required substrate in this case is allyl benzene, and therefore a number of experiments were performed with this substrate (Scheme 3.2).





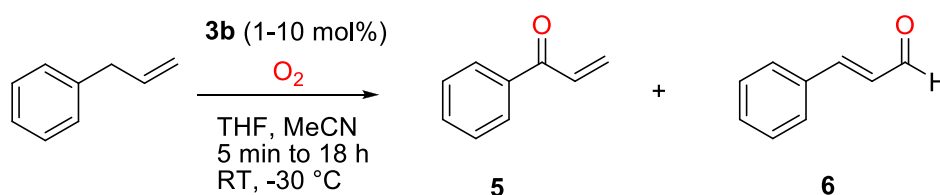
**Scheme 3.2** Postulated mechanism for catalytic oxidation of **3a** and **3b**

A 10 mM solution of **3b** in THF was prepared with a 10-fold excess of allyl benzene (substrate), in addition to tetradecane (internal standard). This orange solution was exposed to  $O_2$ , and a colour change similar to the previous examples in THF was observed (pale orange). The reaction mixture was then analyzed by GC-FID at the following time points: 5 minutes, 1, 4, and 18 hours. Data obtained from this experiment (shown below in Table 3.2, entries 1-4) suggested no catalytic activity, as the yields of **5** and **6** fall below 10 % conversion of substrate. Like the stoichiometric reactions, the attempted catalytic reactions were done within a period of ~5 minutes. In this case the pendent amine arm appeared to have no effect in stabilizing the reactive Ni-OH intermediate.

A number of reaction conditions were altered, aiming to increase the chances for catalytic turnover. The solvent was switched from THF to MeCN since observed yields in stoichiometric reactions were highest for MeCN. In addition there was no formation of an insoluble solid upon oxidation in MeCN. These results could be a result of a stabilization of a reactive intermediate due to the coordinating solvent. Secondly, the reaction

temperature was lowered from room temperature to  $-30\text{ }^{\circ}\text{C}$ . In addition to the aforementioned dimerization of the Ni-OH intermediate, a number of other decomposition products may exist due to oxidation of the NHC ligand. Upon lowering the temperature, these competitive decomposition products may become kinetically unfavourable. Lastly, the concentration of **3b** was lowered to 1 mM. This would theoretically reduce the favourability of dimerization (deactivation step found previously for NiCl(cinammyl)(*It*Pr)), as a reactive intermediate would be more likely to interact with the substrate than with each other.

A 1 mM sample of **3** in MeCN, with 100 mM of allyl benzene and 10 mM of tetradecane, was prepared and cooled at  $\sim -30\text{ }^{\circ}\text{C}$  for 15 minutes (Scheme 3.3).  $\text{O}_2$  was then bubbled into the solution for  $\sim 45$  seconds whilst being kept at  $-30\text{ }^{\circ}\text{C}$ . An immediate colour change from orange to a very pale pink (almost colourless) was observed, consistent with the stoichiometric reactions. The reaction remained stirring at  $-30\text{ }^{\circ}\text{C}$  for 15 minutes, before being warmed to room temperature. The warming step is essential to afford accurate results, as tetradecane has a melting point of approximately  $6\text{ }^{\circ}\text{C}$  and precipitates at low temperature. Analysis of the reaction mixture by GC-FID showed yields  $<1\%$  for **5** and **6**, consistent with non-catalytic reactivity (Table 3.2, entry 5). The reaction continued to stir at room temperature for 1.5 hours, and was once again analyzed by GC-FID. Similarly the results showed only stoichiometric reactivity (Table 3.2, entry 6).



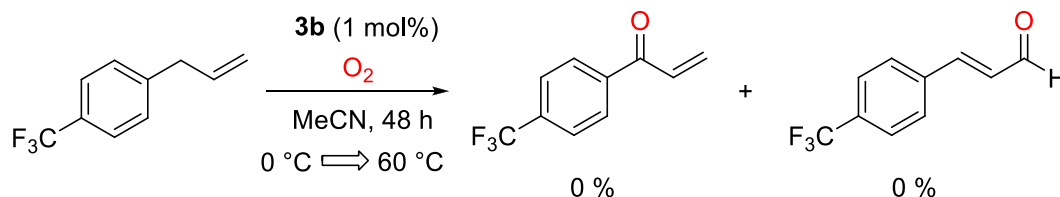
**Scheme 3.3** Attempted catalytic aerobic oxidation of allylbenzene with **3a/b**, with conditions tested

**Table 3.2** Data for attempted catalytic aerobic oxidations of **3b**.<sup>a</sup>

Entry	Time	Mol % <b>3b</b>	Solvent	Temp.	% <b>5</b>	% <b>6</b>	Yield <sup>b</sup> (%)
1	5 min	10	THF	RT	3	4	7
2	1 h	10	THF	RT	3	3	6
3	4 h	10	THF	RT	3	3	6
4	18 h	10	THF	RT	3	3	6
5	15 min	1	MeCN	−30 °C	1	1	0.7
6 <sup>c</sup>	105 min	1	MeCN	−30 °C	1	1	0.8

<sup>a</sup> Conditions: 100 mM allyl benzene, 10 mM tetradecane. Analyzed by GC-FID. <sup>b</sup> Combined yield of phenyl vinyl ketone (**5**) and cinnamaldehyde (**6**). <sup>c</sup> Data is average of two injections of entry 6

A potential issue preventing catalytic turnover could be the C-H activation of allyl benzene is not possible under our tested conditions. Switching to another substrate that may more readily undergo C-H activation may alleviate this problem. Adding a strong electron-withdrawing group on the para-position of the phenyl group may weaken the α-hydrogens, and allow for easier C-H activation. Therefore, 1-allyl-4-(trifluoromethyl)benzene was chosen as the new substrate, with a strongly deactivating CF<sub>3</sub> group. Additionally, the CF<sub>3</sub> group provides a nice NMR handle, in which the formation of new products can easily be monitored by <sup>19</sup>F NMR spectroscopy. The potential catalytic reaction starting from **3a** or **3b** would generate an equivalent of non-fluorinated products **5** and **6**, in addition to the CF<sub>3</sub> derivatives of these products (Scheme 3.4).

**Scheme 3.4** Attempted catalytic aerobic oxidation of 1-allyl-4-(trifluoromethyl)benzene with **3b**

Similar to above, two solutions containing 1-allyl-4-(trifluoromethyl)benzene and 1 mol% **3b** in MeCN were prepared. One sample was oxidized at room temperature (A), and the other was exposed to O<sub>2</sub> at ~ 0 °C (B). In both cases an instantaneous colour change from light orange to almost colourless was observed. Sample A was analyzed by <sup>19</sup>F NMR spectroscopy within a time period of 10 minutes after oxidation. The resulting <sup>19</sup>F NMR

showed only a singlet at  $-62.2$  ppm, which corresponds to unreacted 1-allyl-4-(trifluoromethyl)benzene. Sample B remained at  $0$  °C for 24 hours after oxidation, and subsequent analysis by  $^{19}\text{F}$  NMR showed only the same peak at  $-62.2$  ppm. Heating sample B at  $60$  °C for 24 hours, yielded no difference once analyzed by NMR spectroscopy. A representative  $^{19}\text{F}$  NMR spectrum for these experiments can be found in Appendix 6.8, Figure 6.16. Under the conditions tested catalytic turnover is not achieved, however continued alteration of reaction conditions and/or the substrate used may produce a catalytic system with current  $\text{NiCl}(\text{cinnamyl})(\text{NHC})$  complexes.

### 3.7 Determining the Fate of Nickel after Oxidation

In order to achieve catalytic turnover in the aerobic oxidation of our Ni complexes, better insight into the Ni product(s) after oxidation is required. Evidenced from the colour change of the reaction mixtures before and after oxidation, there is definitely a new species being formed. As noted above, aerobic oxidation of **3a/b** in MeCN and DMF did not afford a brown solid. This could be due to a stabilization effect as a result of the coordinating solvent, and may allow for analysis of a reactive Ni intermediate. Therefore, a NMR study was conducted in  $\text{CD}_3\text{CN}$  to observe the product directly without isolation (Figure 3.4). **2a** was chosen for the study as it has been previously characterized by  $^1\text{H}$  NMR spectroscopy, and there would only ideally be formation of one oxidation product (2-propenal), easing the analysis by NMR.

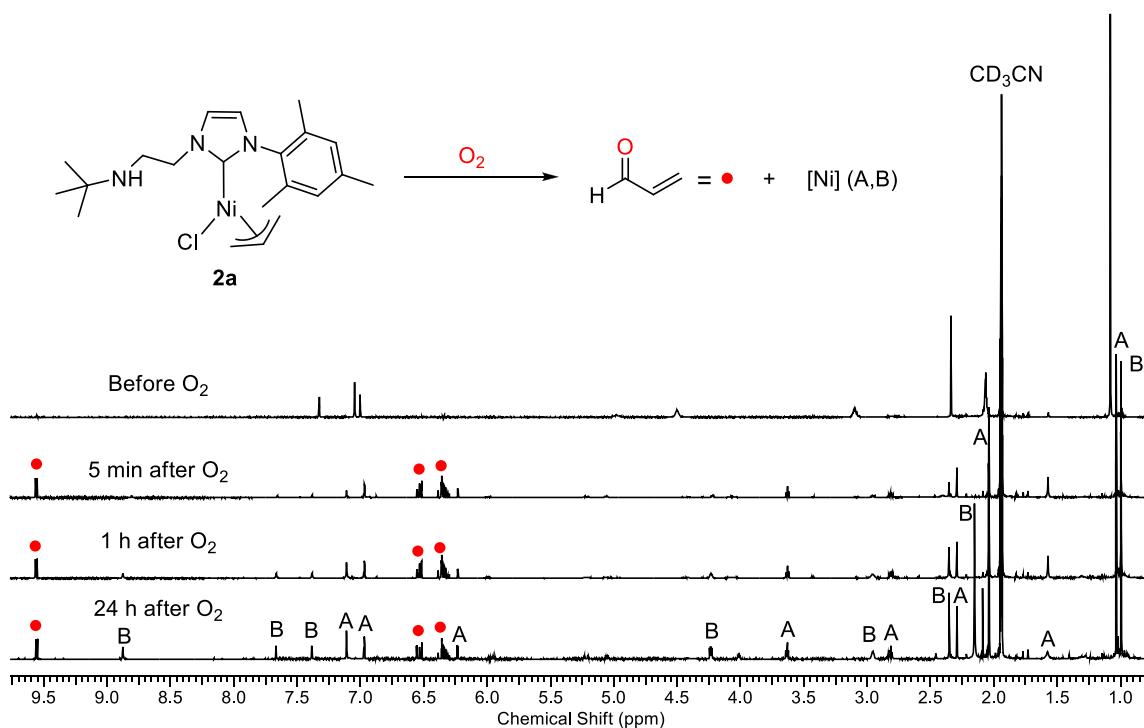


**Figure 3.4**  $^1\text{H}$  NMR spectroscopy study monitoring aerobic oxidation of **2a** in  $\text{CD}_3\text{CN}$  over time.

The initial orange solution of **2a** in  $\text{CD}_3\text{CN}$  underwent a rapid colour change to light pink/orange after exposure to  $\text{O}_2$ . Consistent with GC-FID data of the cinnamyl systems the oxidation product was observed within 5 min by  $^1\text{H}$  NMR (red dots, Figure 3.4). Also in this time period, there was complete disappearance of **2a** and formation of another species. At this time point, there was an initial major product (A), accompanied by a number of smaller peaks in the baseline (product B) in a 2:1 ratio (A:B). At the 1 hour time point, there was continued growth of product B relative to 2-propenal (acting as an internal standard of sorts), with relatively no increase in product A, giving a ratio of approximately 1:1. Analysis after 24 hours, no difference in product distribution was noted (still 1:1), however relative to 2-propenal the yields have doubled. This doubling of yield however may have been a result of evaporation of the 2-propenal. It should be noted at the 24 hour time point, brown solids in the NMR tube were observed (same as was observed in other solvents, as mentioned above), signaling some decomposition. The growth of products A and B over time would imply that there is another intermediate preceding the formation of

A/B, which is unobservable by NMR analysis. Identification of most peaks cannot be accurately made for either product A or B. However, for product A for example, there was a triplet and quartet at 3.63 and 2.82 ppm (respectively) that is most likely the methylene groups of the pendent amine arm. This along with the rough integration values (relative to the methylene groups) of the rest of the peaks for species A, suggests the NHC ligand is still intact and likely still bound to nickel (in either a  $\kappa^1$  or  $\kappa^2$  bonding mode), as the chemical shifts do not match for free ligand **1a**. It should be noted that the colour of the product after oxidation and the resulting  $^1\text{H}$  NMR spectra was not consistent with the formation of a Ni-OH dimer (dark purple), as reported by Sigman.<sup>1</sup> Most notably, there was no signal around  $-8$  ppm that would correlate to an OH signal in the Ni-OH dimer. Future investigation into the identity of the products being formed will be beneficial in order to move the chemistry forward.

### 3.8 Conclusions

In chapter 3 the aerobic oxidation of NiCl(allyl/cinnamyl) complexes was studied. Initial qualitative tests of **2a** and **3a/b** in THF revealed a change in colour, from dark orange to pale orange (with precipitation of a beige solid), within seconds ( $<30$  s) after exposure to  $\text{O}_2$ , suggesting successful oxidation. Analysis of the reaction mixture of **3a** by GC-MS revealed the presence of the expected oxidation products, phenyl vinyl ketone (**5**) and cinnamaldehyde (**6**), signifying successful oxidation of the cinnamyl ligand. Reaction optimization was performed by alteration of reaction time, and solvent. For the reaction of **3a** plus  $\text{O}_2$  (in THF), it was found after the initial time point (2 minutes after oxidation) there was no significant change in product yield, meaning the reaction is near instantaneous. An average overall yield of 63% (relative to internal standard) was observed with an average ratio of 1.3:1 (**6:5**) for this experiment. The 1.3:1 product ratio represents a notable change in selectivity for the reported values by Sigman (1.67:1 (**6:5**)). The oxidation of **3a** was also tested in the following solvents: acetone, DCM, DMF, and MeCN. Changing the reaction solvent was found to have an effect on product yield, with MeCN giving the highest yield of 89%, with the other solvents in the range of 50-70%. Product selectivity was not drastically affected by solvent. For the oxidation of **3b** in THF, nearly

identical results were observed, signifying changing the R group of the pendent amine has a negligible effect on product distribution.

Catalytic aerobic oxidation of allyl benzene was attempted, however no set of experiments showed any evidence of catalytic turnover. Switching the substrate to 1-allyl-4-(trifluoromethyl)benzene, which should be easier to activate, showed a similar lack of catalytic activity as analyzed by  $^{19}\text{F}$  NMR spectroscopy.

$^1\text{H}$  NMR analysis of complex **2a** in  $\text{CD}_3\text{CN}$  after exposure to  $\text{O}_2$  showed the formation of two new unidentified Ni-NHC products. Importantly, there was no signal correlating to a OH moiety in the  $^1\text{H}$  NMR spectrum, which should be located around  $-8$  ppm, suggesting the product is not a Ni-OH dimer (as observed by Sigman). This suggests a new final Ni product is formed.

### 3.9 References

1. Dible, B. R.; Sigman, M. S. *J. Am. Chem. Soc.* **2003**, *125*, 872-873
2. Dible, B. R.; Sigman, M. S. *Inorg. Chem.* **2006**, *45*, 8430-8441

## Chapter 4

### 4 General Conclusions and Future Work

#### 4.1 General Conclusions

In this report, the synthesis and characterization of novel NiX(allyl/cinnamyl)(NHC) (X= Cl, I) complexes, and their reactivity with dioxygen was discussed. The NHC ligands chosen for this study contain a pendent 2° amine arm, to act as a hydrogen-bond donor in the secondary coordination sphere or as a hemi-labile donor group. Three literature NHC compounds (**1a-c**), which have been isolated as the free carbenes, were targeted for this study. The synthesis was successfully achieved through multi-step literature, or modified literature, procedures and characterized using <sup>1</sup>H NMR spectroscopy. Three new NiCl(allyl/cinnamyl)(NHC) complexes, **2a** and **3a/b**, were synthesized in good yields following a two-step, one-pot, literature method developed for related complexes. Characterization of the new complexes was achieved using MALDI-MS, <sup>1</sup>H and <sup>13</sup>C NMR spectroscopy, and X-ray crystallography. Interestingly, for complexes **2a** and **3b** in the solid state there was an observed hydrogen-bonding interaction between the pendent amine arm of the NHC and the chloride ligand of another molecule in the unit cell (not observed for **3a**). The hydrogen bond distances were consistent for a weak hydrogen bond (> 3.2 Å) for that type of functionality. Excitingly, this showed that the pendent amine arm is active towards hydrogen-bonding, and could potentially have a stabilizing effect on reactive nickel intermediates present after aerobic oxidation.

<sup>1</sup>H NMR studies of the nickel complexes at room temperature yielded complex spectra, with a number of very broad peaks, indicative of dynamic processes for the coordinated NHC and allyl ligands. Variable Temperature (VT) <sup>1</sup>H NMR studies confirmed the dynamic behaviour of the attached ligands, as decoalescence of the broad peaks was observed at low temperatures (-70 °C for **2a**), allowing for full NMR characterization. The VT <sup>1</sup>H NMR studies suggested rapid allyl rotation/isomerization (as expected from literature examples), and dynamic or hemi-labile behaviour for the pendent amine arm. At low temperatures, there was a large downfield shift of the NH peak in comparison to the free ligand, providing further evidence towards the hemi-lability of the pendent amine. This



downfield shift signifies either: coordination of the amine to the metal centre to form a five coordinate Ni(II) species; or a N-H...Cl hydrogen bonding interaction similar to that observed in the solid state. In either case, the pendent amine showed the potential for the stabilization of reactive nickel intermediates in the solution state, allowing for catalytic aerobic oxidation. Additionally, the flexibility of the pendent amine arm is beneficial for O<sub>2</sub> reactivity, as the arm is able to move out of the way, as to not sterically block the O<sub>2</sub> from binding to the metal centre.

Slowing of the observed dynamic processes was made, in order to allow for NMR analysis at more favourable temperatures. [Ni(allyl)(**1a**)] (**4a**) was synthesized in a one-step procedure by reaction of **2a** with NaI. VT <sup>1</sup>H NMR studies confirms that by substitution of the chloride ligand for bulkier iodide, the dynamic processes were lessened. Decoalescence of the peaks was obtained at a higher temperature (-50 °C) in comparison to **2a**, and full NMR characterization of **4a** was done using <sup>1</sup>H, <sup>13</sup>C, <sup>1</sup>H-<sup>1</sup>H COSY, and <sup>1</sup>H-<sup>13</sup>C HMBC NMR techniques.

Qualitative tests of **2a** and **3a/b** in THF revealed a change in colour, from dark orange to pale orange (with precipitation of a beige solid), within seconds after exposure to O<sub>2</sub>. The rapid change in colour suggested successful oxidation. Confirmation of oxidation was made by analysis of the reaction mixture of cinnamyl derivative **3a** by GC-MS, revealing the presence of the expected oxidation products, phenyl vinyl ketone (**5**) and cinnamaldehyde (**6**). Furthermore, the rapid oxidation of **2a** and **3a/b** showed that the NHC ligands used are not sterically hindering, allowing for easy binding of oxygen to nickel.

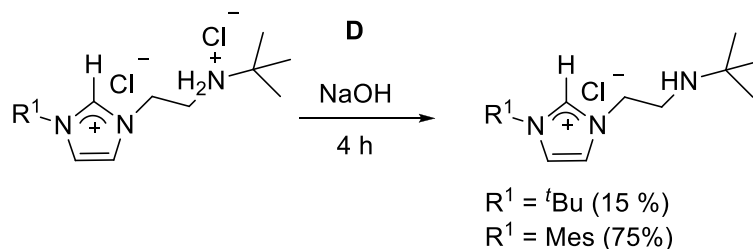
Aerobic oxidation reaction optimization was performed by alteration of reaction time, and solvent. For the reaction of **3a** plus O<sub>2</sub> (in THF), it was found after the initial time point (2 minutes after oxidation) there was no significant change in product yield, meaning the reaction was near instantaneous. A greater preference for the ketone product (**5**) was found for our complexes, in comparison to the literature complex with a symmetric *i*Pr NHC ligand. The change in product selectivity is most likely due to the change in sterics around the metal centre, due to the inclusion of the pendent amine arm on the NHC ligand. Changing the reaction solvent was found to have a minor effect on product yield, with

MeCN giving the highest yield of the solvents tested. Acetonitrile may be coordinating the metal centre to stabilize a reactive intermediate, therefore preventing competitive decomposition, and giving higher yields. For the oxidation of **3b** in THF, nearly identical results (to **3a**) were observed, signifying changing the R group of the pendent amine has a negligible effect on product distribution.

Catalytic aerobic oxidation was attempted, however no set of experiments showed any evidence of catalytic turnover. <sup>1</sup>H NMR analysis of **2a** in CD<sub>3</sub>CN after exposure to O<sub>2</sub> showed the formation of two new unidentified Ni-NHC products. The lack of a signal correlating to an OH moiety in the <sup>1</sup>H NMR, suggested the product is not a Ni-OH dimer (as observed by Sigman), but rather a new product(s). Identification of these products are critical to ultimately achieving catalytic turnover.

## 4.2 Future Work

Immediate work in the future will focus on finishing the characterization of complexes **2a**, **3a** and **3b**. Elemental analysis (EA) data is required for all complexes, as efforts thus far have not proved satisfactory. Presumably the poor data is due to decomposition of the very air-sensitive compounds prior to analysis. Additionally, <sup>1</sup>H NMR data in the static regime for the Ni(cinnamyl) complexes (**3a** and **3b**) is required. Similar methods to reduce dynamics, as employed for **2a**, can be used here with low temperature VT NMR studies and/or a halide ligand exchange. Isolation and full characterization of Ni(cinnamyl) complex **3c** (R<sup>1</sup>=R<sup>2</sup>= <sup>t</sup>Bu) is required as well. Prior to this the synthesis of ligand **3c**, particularly deprotonation of the ammonium-imidazolium intermediate, must be improved (Scheme 4.1). The reason for the current low yield of this step is not clear, especially when compared to the higher yield achieved for the very closely related compound where R<sup>1</sup> = Mes (Scheme 4.1). Optimization of reaction conditions or isolation techniques will be required.



**Scheme 4.1** NaOH deprotonation of ammonium-imidazolium intermediate

In terms of the aerobic oxidation of these nickel complexes, future work will be centered on achieving catalytic turnover. This may be achieved in a number of ways. First is the continued modification of the reaction conditions for our current complexes. This may include: the addition of a base; altering the reaction temperature; addition of sieves; and modifying the substrate used. Basic conditions are common in C-H activation reactions, as they are often required in the C-H bond cleavage step.<sup>1,2</sup> Due to the inertness of the C-H bond, elevated reaction temperatures (> room temperature) are typically required to promote C-H activation, and may be required in our case as well. In the proposed catalytic cycle water is released as a by-product, which may cause catalyst decomposition. Therefore, the addition of sieves can be beneficial to remove the water as it is formed in the reaction. Lastly, the use of a substrate that is more prone to C-H activation may allow for a reaction to take place under mild temperatures.

Secondly, and more importantly, is the determination of the nickel product(s) after aerobic oxidation. Preliminary NMR data suggests that after formation of the Ni-OH intermediate, there is quick decomposition to currently unknown Ni-NHC products. Due to the speed at which this occurs, the possibility of making a paramagnetic compound, and the fluxional behaviour of the NHC ligands, NMR is not the ideal method for analyzing the formation of the nickel by-products. Low temperature UV-Vis spectroscopy represents a more ideal analytical method. Cooling to very low temperatures (~ -80 °C) should sufficiently slow the reaction to observe the distinct Ni-OH species being formed as O<sub>2</sub> is being bubbled into the reaction mixture. Also, identification of the decomposition products will be beneficial into gaining insight to the reactivity following the aerobic oxidation step.

Lastly modifications to the nickel complexes themselves may be required, including the NHC ligand. One such modification could be to the pendent H-bonding group, changing either the electronics or sterics of the group. For example, switching to an amide group may be beneficial, as it is a stronger H-bonding group, and has already been shown to stabilize a monomeric Ni-OH complex.<sup>3</sup>

### 4.3 References

1. Wencel-Delord, J.; Dröge, T.; Liu, F.; Glorius, F. *Chem. Soc. Rev.* **2011**, *40*, 4740-4761
2. Rousseaux, S.; Gorelsky, S. I.; Chung, B. K. W.; Fagnou, K. *J. Am. Chem. Soc.* **2010**, *132*, 10692-10705
3. Samantaray, M. K.; Shaikh, M. M.; Ghosh, P. *Organometallics* **2009**, *28*, 2267-2275

## 5 Experimental

### General Considerations

Unless otherwise noted, all procedures were carried out under an inert nitrogen atmosphere using standard glovebox or Schlenk techniques. Dried solvents were obtained from an Innovative Technologies 400-5 Solvent Purification System and were stored over activated 4 Å molecular sieves. Acetonitrile was not stored over sieves. Reagents were purchased from Alfa Aesar or Sigma Aldrich and used without further purification unless otherwise stated. Cinnamyl chloride, allyl chloride, allyl benzene, and 1,5-cyclooctadiene were freeze-pump-thaw degassed prior to use.  $\text{CDCl}_3$  and  $\text{C}_6\text{D}_6$  were purchased from Cambridge Isotope Laboratories and were sparged with nitrogen and stored over 4 Å molecular sieves before use. Ampules of  $\text{CD}_2\text{Cl}_2$ ,  $\text{CD}_3\text{CN}$ , and  $\text{C}_7\text{D}_8$  were purchased from Cambridge Isotope Laboratories and used as received. Water was deoxygenated by sparging with nitrogen before use.  $\text{O}_2$  was purchased from Praxair, and passed through a drying tube containing calcium sulfate prior to use.  $[\text{Ni}(\text{cod})_2]$ ,<sup>1</sup> *N*-mesitylimidazole,<sup>2</sup>  $[\text{C}\{(\text{Mes})\text{N}(\text{CHCH})\text{N}(\text{CH}_2\text{CH}_2\text{NH}(\text{Mes}))\}]$  (**1b**),<sup>3</sup> 1,3-bis(2,6-diisopropylphenyl)imidazol-2-ylidene (*i*Pr),<sup>4</sup>  $[\text{NiCl}(\text{cinnamyl})(\text{iPr})]$ ,<sup>5</sup> and phenyl vinyl ketone<sup>6</sup> were synthesized according to literature procedures. NMR spectra were acquired at 25 °C (unless otherwise noted) on Varian INOVA 400 or 600, or Varian Mercury 400 spectrometers.  $^1\text{H}$  and  $^{13}\text{C}$  spectra were referenced using residual solvent signals to tetramethylsilane at 0 ppm.  $^{19}\text{F}$  spectra were referenced externally to trifluorotoluene at -63.9 ppm. Variable temperature NMR experiments performed by cooling an external heat exchanger on the spectrometer with liquid  $\text{N}_2$ , and managing the probe temperature through the spectrometer software (VnmrJ 3.2A). Peak multiplicities are designated as: s = singlet, d = doublet, t = triplet, m = multiplet, br = broad, ov = overlapping. Oxidation reactions were analyzed using a Shimadzu GCMS-QP2010 Ultra GC with a DB-5 column or a calibrated Agilent 7890A GC-FID with an HP-5 column. MALDI-TOF mass spectra were collected using an AB Sciex 5800 TOF/TOF mass spectrometer using either pyrene or anthracene as the matrix in a 20:1 matrix:substrate molar ratio in dichloromethane. Infrared spectra were collected

on solid samples using a PerkinElmer UATR TWO FT-IR spectrometer. Experimental details for x-ray diffraction experiments are located in Appendix 6.1, 6.2, and 6.3.

### Synthesis of 2-(*tert*-butylamino)ethyl chloride hydrochloride

In air, a 100 mL round bottom flask was equipped with 2-(*tert*-butylamino)ethanol (3.033 g, 25.88 mmol) and a stir bar. Thionyl chloride (20 mL, 0.3 mol) was added dropwise to the reaction flask, and the mixture was refluxed while stirring for 7 hours. Upon removal of the excess thionyl chloride under vacuum, a white solid formed, which was washed with hexanes (3 × 10 mL) and dried *in vacuo*, to give a pure product (3.822 g, 22.21 mmol, 86%). <sup>1</sup>H NMR data is consistent with literature values.<sup>7</sup>

### Synthesis of [HC{(Mes)N(CHCH)N(CH<sub>2</sub>CH<sub>2</sub>NH<sup>t</sup>Bu)}]Cl·HCl

In air, [HC{(Mes)N(CHCH)N(CH<sub>2</sub>CH<sub>2</sub>NH<sup>t</sup>Bu)}]Cl · HCl was prepared according to a modified procedure for a related compound reported by Fryzuk *et al.*<sup>3</sup> *N*-Mesitylimidazole (3.100 g, 16.65 mmol) was combined with 2-(*tert*-butylamino)ethyl chloride hydrochloride (2.851 g, 16.57 mmol) in a 50 mL pressure tube. The reaction mixture was heated at 155 °C for 12 hours. The resulting tough brown solid was suspended in THF, and was collected by filtration and washed with THF (3 × 10 mL), to produce a light brown solid (4.617 g, 12.89 mmol, 78%). <sup>1</sup>H NMR (CDCl<sub>3</sub>, 400 MHz): δ 10.19 (br s, NH<sub>2</sub>, 2H), 10.10 (s, NCHN, 1H), 8.45 (s, NCHCHN, 1H), 7.19 (s, NCHCHN, 1H), 6.97 (s, Ar-*H*, 2H), 5.25 (t, <sup>3</sup>J<sub>H-H</sub> = 6.0 Hz, HNCH<sub>2</sub>CH<sub>2</sub>N, 2H), 3.67 (t, <sup>3</sup>J<sub>H-H</sub> = 6.0 Hz, HNCH<sub>2</sub>CH<sub>2</sub>N, 2H), 2.33 (s, *p*-CH<sub>3</sub>(Ar), 3H), 2.15 (s, *o*-CH<sub>3</sub>(Ar), 6H), 1.49 (s, C(CH<sub>3</sub>)<sub>3</sub>, 9H). <sup>13</sup>C NMR (CDCl<sub>3</sub>, 100 MHz): δ 141.2 (NCHN), 138.3 (Ar), 134.4 (Ar), 130.6 (Ar), 129.8 (Ar), 124.5 (NCH), 123.4 (NCH), 58.1 (NCMe<sub>3</sub>), 46.4 (NCH<sub>2</sub>), 40.8 (NCH<sub>2</sub>), 25.6 (*t*Bu), 21.0 (Ar-*Me*), 18.0 (Ar-*Me*).

### Synthesis of [HC{(Mes)N(CHCH)N(CH<sub>2</sub>CH<sub>2</sub>NH<sup>t</sup>Bu)}]Cl

In air, [HC{(Mes)N(CHCH)N(CH<sub>2</sub>CH<sub>2</sub>NH<sup>t</sup>Bu)}]Cl was synthesized using a modified procedure for a related compound reported by Ong *et al.*<sup>8</sup> A 100 mL round bottom was charged with a stir bar, and [HC{(Mes)N(CHCH)N(CH<sub>2</sub>CH<sub>2</sub>NH<sup>t</sup>Bu)}]Cl · HCl (4.617 g,

12.89 mmol). An aqueous sodium hydroxide solution (1.0 M, 15 mL) was added to the round bottom, and the reaction was stirred for 4 hours. The product was extracted using dichloromethane (3 × 50 mL), and the combined organic layers were dried over sodium sulfate. The sample was filtered and the solvent of the filtrate was removed under vacuum. The residue was washed with hexanes (3 × 10 mL) to give a light brown solid (3.119 g, 9.694 mmol, 75%). <sup>1</sup>H NMR (CDCl<sub>3</sub>, 600 MHz): δ 10.19 (s, NCHN, 1H), 7.93 (s, NCHCHN, 1H), 7.08 (s, NCHCHN, 1H), 6.96 (s, Ar-H, 2H), 4.76 (t, <sup>3</sup>J<sub>H-H</sub> = 5.0 Hz, HNCH<sub>2</sub>CH<sub>2</sub>N, 2H), 2.97 (t, <sup>3</sup>J<sub>H-H</sub> = 5.0 Hz, HNCH<sub>2</sub>CH<sub>2</sub>N, 2H), 2.31 (s, *p*-CH<sub>3</sub>(Ar), 3H), 2.03 (s, *o*-CH<sub>3</sub>(Ar), 6H), 0.96 (s, C(CH<sub>3</sub>)<sub>3</sub>, 9H). <sup>13</sup>C NMR (CDCl<sub>3</sub>, 100 MHz): δ 141.4 (NCHN), 139.5 (Ar), 134.6 (Ar), 131.1 (Ar), 130.0 (Ar), 123.3 (NCH), 122.3 (NCH), 51.1 (NCH<sub>2</sub>), 50.4 (NCMe<sub>3</sub>), 42.6 (NCH<sub>2</sub>), 29.3 (*t*Bu), 21.4 (Ar- Me), 17.8 (Ar- Me).

### Synthesis of [C{(Mes)N(CHCH)N(CH<sub>2</sub>CH<sub>2</sub>NH'Bu)}] (1a)

[C{(Mes)N(CHCH)N(CH<sub>2</sub>CH<sub>2</sub>NH'Bu)}] was synthesized according to a modified procedure for a related compound by Fryzuk *et al.*<sup>3</sup> In a 20 mL vial with a stir bar, a solution of KN(SiMe<sub>3</sub>)<sub>2</sub> (280 mg, 1.40 mmol) dissolved in THF (5 mL) was added dropwise to a stirring suspension of [HC{(Mes)N(CHCH)N(CH<sub>2</sub>CH<sub>2</sub>NH'Bu)}]Cl (378 mg, 1.17 mmol) in THF (5 mL). The reaction mixture was allowed to stir for 45 minutes. The resulting solution was filtered through a medium filter frit to remove the KCl byproduct, and the solvent of the filtrate was removed under vacuum to yield a brown solid (301 mg, 1.06 mmol, 90%). <sup>1</sup>H NMR data matched the literature values.<sup>7</sup>

### Synthesis of *N*-*tert*-Butylimidazole

In air, *N*-*tert*-butylimidazole was prepared according to a modified procedure for the synthesis for the related *N*-mesitylimidazole.<sup>2</sup> A 100 mL two-neck round bottom flask was equipped with a stir bar, reflux condenser, and addition funnel. A solution containing aqueous formaldehyde (3.0 mL, 40 mmol), aqueous glyoxal (4.6 mL, 40 mmol), and glacial acetic acid was transferred to the round bottom flask and heated to 70 °C. Another solution with glacial acetic acid (10 mL), ammonium acetate in water (3.10 g, 3 mL), and *tert*-butylamine (4.2 mL, 40 mmol) was transferred to the addition funnel, and added dropwise over a period of 30 minutes. Upon stirring and heating at 70 °C for 20 hours a dark red

solution formed. The reaction mixture was neutralized by the slow addition to a solution of sodium bicarbonate in water (29 g, 300 mL). The product was extracted using dichloromethane (3 × 150 mL), and the combined organic layers were dried over sodium sulfate. Removal of the solvent under vacuum afforded a brown oil (1.360 g, 11.00 mmol, 28%). <sup>1</sup>H NMR data matched the literature values.<sup>9</sup>

### Synthesis of [HC{(tBu)N(CHCH)N(CH<sub>2</sub>CH<sub>2</sub>NHtBu)}]Cl·HCl

In air, [HC{(tBu)N(CHCH)N(CH<sub>2</sub>CH<sub>2</sub>NHtBu)}]Cl·HCl was prepared according to a modified procedure for a related compound by Fryzuk *et al.*<sup>3</sup> 1.1 equivalents of *N-tert-butylimidazole* (1.331 g, 10.74 mmol) was combined with 2-(*tert*-butylamino)ethyl chloride hydrochloride (1.635 g, 9.501 mmol) in a 50 mL pressure tube. The reaction mixture was heated at 160 °C for 18 hours. The resulting tough brown solid was suspended in THF, and was collected by filtration and washed with THF (3 × 10 mL) to give a dark brown solid (2.554 g, 8.594 mmol, 90%). <sup>1</sup>H NMR (CDCl<sub>3</sub>, 600 MHz): δ 10.20 (br, NH<sub>2</sub>, 2H), 10.12 (s, NCHN, 1H), 8.03 (s, NCHCHN, 1H), 7.49 (s, NCHCHN, 1H), 5.10 (t, <sup>3</sup>J<sub>H-H</sub> = 5.9 Hz, HNCH<sub>2</sub>CH<sub>2</sub>N, 2H), 3.52 (t, <sup>3</sup>J<sub>H-H</sub> = 5.9 Hz, HNCH<sub>2</sub>CH<sub>2</sub>N, 2H), 1.71 (s, C(CH<sub>3</sub>)<sub>3</sub>, 9H), 1.49 (s, C(CH<sub>3</sub>)<sub>3</sub>, 9H). <sup>13</sup>C NMR (CDCl<sub>3</sub>, 100 MHz): δ = 135.7 (NCHN), 123.6 (NCH), 119.8 (NCH), 60.4 (NCMe<sub>3</sub>), 58.1 (NCMe<sub>3</sub>), 45.9 (NCH<sub>2</sub>), 41.0 (NCH<sub>2</sub>), 29.8 (*t*Bu), 25.6 (*t*Bu).

### Synthesis of [HC{(tBu)N(CHCH)N(CH<sub>2</sub>CH<sub>2</sub>NHtBu)}]Cl

In air, [HC{(tBu)N(CHCH)N(CH<sub>2</sub>CH<sub>2</sub>NHtBu)}]Cl was synthesized using a modified procedure for a related compound by Ong *et al.*<sup>8</sup> A 25 mL round bottom was charged with a stir bar, and [HC{(tBu)N(CHCH)N(CH<sub>2</sub>CH<sub>2</sub>NHtBu)}]Cl·HCl (0.749 g, 2.52 mmol). An aqueous sodium hydroxide solution (1.0 M, 3 mL) was added to the round bottom, and the reaction was stirred for 4 hours. The product was extracted using dichloromethane (3 × 30 mL), and the combined organic layers were dried over sodium sulfate. Upon filtration, removal of the solvent under vacuum yields the product as a dark brown oil (0.100 g, 0.383 mmol, 15%). <sup>1</sup>H NMR (CDCl<sub>3</sub>, 600 MHz): δ 10.85 (s, NCHN, 1H), 7.53 (s, NCHCHN, 1H), 7.23 (s, NCHCHN, 1H), 4.57 (t, <sup>3</sup>J<sub>H-H</sub> = 5.6 Hz, HNCH<sub>2</sub>CH<sub>2</sub>N, 2H), 3.03 (t, <sup>3</sup>J<sub>H-H</sub> = 5.6 Hz, HNCH<sub>2</sub>CH<sub>2</sub>N, 2H), 1.73 (s, C(CH<sub>3</sub>)<sub>3</sub>, 9H), 1.04 (s, C(CH<sub>3</sub>)<sub>3</sub>, 9H). <sup>13</sup>C NMR



(CDCl<sub>3</sub>, 100 MHz):  $\delta$  135.5 (NCHN), 122.4 (NCH), 117.6 (NCH), 60.0 (NCMe<sub>3</sub>), 50.8 (NCH<sub>2</sub>), 50.5 (NCMe<sub>3</sub>), 42.2 (NCH<sub>2</sub>), 30.1 (*t*Bu), 28.9 (*t*Bu).

### Synthesis of [C{(<sup>t</sup>Bu)N(CHCH)N(CH<sub>2</sub>CH<sub>2</sub>NH<sup>t</sup>Bu)}] (1c)

[C{(<sup>t</sup>Bu)N(CHCH)N(CH<sub>2</sub>CH<sub>2</sub>NH<sup>t</sup>Bu)}] was synthesized according to a modified procedure for a related compound from Fryzuk *et al.*<sup>3</sup> In a 20 mL vial with a stir bar, a solution of KN(SiMe<sub>3</sub>)<sub>2</sub> (92.1 mg, 0.462 mmol) dissolved in THF (2 mL) was added dropwise to a stirring suspension of [HC{(<sup>t</sup>Bu)N(CHCH)N(CH<sub>2</sub>CH<sub>2</sub>NH<sup>t</sup>Bu)}]Cl (100 mg, 0.383 mmol) in THF (4 mL). The reaction mixture was allowed to stir for 45 minutes. The resulting solution was filtered through a filter frit to remove the KCl byproduct, and the solvent removed under vacuum to yield a brown solid (60.0 mg, 0.269 mmol, 70%). <sup>1</sup>H NMR data matched the literature values from a report by Arnold *et al.*<sup>10</sup>

### General Synthesis of Complexes 2a, 3a, and 3b

The synthesis of **2a**, **3a**, **3b**, and **3c** all followed a modified procedure for related complexes reported by Sigman *et al.*<sup>11,12</sup>

### Synthesis of 2a

In a 20 mL vial with a stir bar, a suspension of Ni(cod)<sub>2</sub> (208 mg, 0.757 mmol) in 1,5-cyclooctadiene (1 mL) was prepared. Allyl chloride (57.9 mg, 0.757 mmol) was added dropwise to the stirring suspension and the mixture was stirred for 5 minutes. By this time the suspension changed colour from yellow to dark red, consistent with formation of [NiCl(CH<sub>2</sub>CHCH<sub>2</sub>)<sub>2</sub>]. Toluene (4 mL) was added to dissolve all the solids and a solution of **1a** (216 mg, 0.757 mmol) in toluene (4 mL) was added dropwise. The mixture was allowed to stir for 15 minutes, during which time a colour change from dark red to dark orange-brown was observed. The resulting solution was filtered through a glass-microfiber pipette filter to remove metallic nickel, and the solvent from the filtrate was removed under vacuum to yield a dark brown-orange oil. The oil was then washed with cold hexanes (–35°C, 5 × 1 mL), and subsequently dried under vacuum to yield **2a** as a brown-orange solid (248 mg, 0.588 mmol, 78%). Dark orange crystals suitable for x-ray crystallography were grown from the slow vapour diffusion of pentane into a solution of **2a** dissolved in a

minimal amount of toluene at  $-35\text{ }^{\circ}\text{C}$ .  $^1\text{H}$  NMR (benzene- $d_6$ , 600 MHz):  $\delta$  6.74 (s, Ar- $H$ , 2H), 6.58 (s, NCHCHN, 1H), 6.06 (s, NCHCHN, 1H), 4.86 (m,  $\text{CH}_2\text{CHCH}_2$ , 1H), 4.48 (br,  $\text{HNCH}_2\text{CH}_2\text{N}$ , 2H), 3.62 (br, 1H), 2.95 (br,  $\text{HNCH}_2\text{CH}_2\text{N}$ , 2H), 2.71 (br, 1H), 2.33 (br,  $p\text{-CH}_3(\text{Ar})$ , 3H) 2.09-2.02 (br m,  $o\text{-CH}_3(\text{Ar})$ , 6H), 1.57 (br, 1H), 1.27 (br, 2H), 0.96 (s,  $\text{C}(\text{CH}_3)_3$ , 9H), 0.61 (br, 1H).  $^1\text{H}$  NMR ( $\text{CD}_2\text{Cl}_2$ , 400 MHz):  $\delta$  7.21 (s, NCHCHN, 1H), 7.01 (s, Ar- $H$ , 2H), 6.87 (s, NCHCHN, 1H), 4.94 (m,  $\text{H}^3$ , 1H), 4.59 (br,  $\text{HNCH}_2\text{CH}_2\text{N}$ , 2H), 3.17 (br,  $\text{HNCH}_2\text{CH}_2\text{N}$ , 2H), 2.35 (s,  $p\text{-CH}_3(\text{Ar})$ , 3H), 2.11 (s,  $o\text{-CH}_3(\text{Ar})$ , 6H), 1.09 (s,  $\text{C}(\text{CH}_3)_3$ , 9H).  $^1\text{H}$  NMR ( $\text{CD}_2\text{Cl}_2$ , 400 MHz,  $-75\text{ }^{\circ}\text{C}$ ):  $\delta$  7.28 (s, NCHCHN, 1H), 7.11 (br, NH, 1H), 6.96 (s, Ar- $H$ , 1H), 6.92 (s, Ar- $H$ , 1H), 6.87 (s, NCHCHN, 1H), 4.84 (ov,  $\text{H}^3$  and  $\text{H}^{6/7}$ , 2H), 4.30 (d,  $^2J_{\text{H-H}} = 14.5\text{ Hz}$ ,  $\text{H}^{6/7}$ , 1H), 4.12 (br,  $\text{H}^{4/5}$ , 1H), 3.38 (br,  $\text{H}^{8/9}$ , 1H), 3.20 (d,  $^3J_{\text{H-H}} = 14.2\text{ Hz}$ ,  $\text{H}^{1/2}$ , 1H), 2.28 (ov,  $\text{CH}_3(\text{Ar})$  and  $\text{H}^{8/9}$ , 4H), 1.91 (s,  $\text{CH}_3(\text{Ar})$ , 3H), 1.80 (s,  $\text{CH}_3(\text{Ar})$ , 3H), 1.66 (br,  $\text{H}^{4/5}$ , 1H), 1.24-1.12 (ovm,  $\text{C}(\text{CH}_3)_3$  and  $\text{H}^{1/2}$ , 10H). MALDI-MS: found [**2a** – allyl] $^{*+}$   $m/z = 378.2$ ; calcd. for [**2a** – allyl] $^{*+}$   $m/z = 378.2$ . IR (ATR,  $\text{cm}^{-1}$ ):  $\nu(\text{NH})$  3294

### Synthesis of Complex **3a**

In a 20 mL vial with a stir bar, a suspension of  $\text{Ni}(\text{cod})_2$  (177 mg, 0.644 mmol) in 1,5-cyclooctadiene (1 mL) was prepared. Cinnamyl chloride (92.9  $\mu\text{L}$ , 0.644 mmol) was added dropwise to the stirring suspension and the mixture was stirred for 5 minutes. By this time the suspension changed colour from yellow to dark red/purple, consistent with formation of  $[\text{NiCl}(\text{CH}_2\text{CHCH}_2\text{C}_6\text{H}_5)]_2$ . Toluene (4 mL) was added to dissolve all the solids and a solution of **1a** (190 mg, 0.644 mmol) in toluene (4 mL) was added dropwise. The mixture was allowed to stir for 15 minutes, during which time a colour change from dark red to dark orange-brown was observed. The resulting solution was filtered through a glass microfiber pipette filter to remove metallic nickel, and the solvent from the filtrate was removed under vacuum to yield a dark brown-orange oil. The oil was then washed with cold hexanes ( $-35\text{ }^{\circ}\text{C}$ ,  $5 \times 1\text{ mL}$ ), and subsequently dried under vacuum to yield **3a** as a brown-orange solid (263 mg, 0.532 mmol, 83%). Dark orange crystals suitable for x-ray crystallography were grown from the slow vapour diffusion of hexanes into a solution of **3a** dissolved in a minimal amount of toluene at  $-35\text{ }^{\circ}\text{C}$ .  $^1\text{H}$  NMR (benzene- $d_6$ , 600 MHz):  $\delta$  7.47 (d,  $J_{\text{H-H}} = 6.9\text{ Hz}$ , 2H), 6.79 (d,  $J_{\text{H-H}} = 13.9\text{ Hz}$ , Ar- $H$ , 2H), 6.57 (s, NCHCHN, 1H),

6.07 (s, NCHCHN, 1H), 5.33 (br, 1H), 4.47-4.30 (brovm, 3H), 3.98 (d,  $J_{\text{H-H}} = 12.6$  Hz, 1H), 2.90 (br, 2H), 2.34 (br, 3H), 2.13-2.01 (brovm, 6H), 1.53 (br, 1H), 0.95 (s,  $\text{C}(\text{CH}_3)_3$ , 9H), 0.60 (br, 1H), 0.54 (s, 1H). MALDI-MS: found [**3a** – cinnamyl]<sup>++</sup>  $m/z = 378.2$ ; calcd. for [**3a** – cinnamyl]<sup>++</sup>  $m/z = 378.2$ . IR (ATR,  $\text{cm}^{-1}$ ):  $\nu(\text{NH})$  3250.

### Synthesis of Complex **3b**

In a 20 mL vial with a stir bar, a suspension of  $\text{Ni}(\text{cod})_2$  (131 mg, 0.478 mmol) in 1,5-cyclooctadiene (1 mL) was prepared. Cinnamyl chloride (67.0  $\mu\text{L}$ , 0.478 mmol) was added dropwise to the stirring suspension and the mixture was stirred for 5 minutes. By this time the suspension changed colour from yellow to dark red/purple, consistent with formation of  $[\text{NiCl}(\text{CH}_2\text{CHCH}_2\text{C}_6\text{H}_5)]_2$ . Toluene (4 mL) was added to dissolve all the solids and a solution of **1b** (166 mg, 0.478 mmol) in toluene (4 mL) was added dropwise. The mixture was allowed to stir for 15 minutes, during which time a colour change from dark red to dark orange-brown was observed. The resulting solution was filtered through a glass microfiber pipette filter to remove metallic nickel, and the solvent from the filtrate was removed under vacuum to yield a dark brown-orange oil. The oil was then washed with cold hexanes ( $-35$  °C,  $5 \times 1$  mL), and subsequently dried under vacuum to yield **3b** as a brown-orange solid (238 mg, 0.428 mmol, 90%). Dark red/orange crystals suitable for x-ray crystallography were grown from the slow vapour diffusion of pentane into a solution of **3b** dissolved in a minimal amount of toluene at  $-35$  °C.  $^1\text{H}$  NMR (benzene- $d_6$ , 600 MHz):  $\delta$  7.42 (br, 2H), 6.79 (s, Ar-*H*, 4H), 6.34 (s, NCHCHN, 1H), 6.06 (s, NCHCHN, 1H), 5.25 (br, 1H), 4.59-4.28 (brovm, 3H), 3.92 (br, 1H), 3.33 (br, 3H), 2.34-1.88 (brovm, 18H), 1.45 (br, 2H). MALDI-MS: found [**3b** – cinnamyl]<sup>++</sup>  $m/z = 440.1$ ; calcd. for [**3b** – cinnamyl]<sup>++</sup>  $m/z = 440.1$  IR (ATR,  $\text{cm}^{-1}$ ):  $\nu(\text{NH})$  3340.

### Attempted Synthesis of **3c**

In a 20 mL vial with a stir bar, a suspension of  $\text{Ni}(\text{cod})_2$  (73.0 mg, 0.265 mmol) in 1,5-cyclooctadiene (0.5 mL) was prepared. Cinnamyl chloride (36.6  $\mu\text{L}$ , 0.265 mmol) was added dropwise to the stirring suspension and the mixture was stirred for 5 minutes. By this time the suspension changed colour from yellow to dark red/purple, consistent with formation of  $[\text{NiCl}(\text{CH}_2\text{CHCH}_2\text{C}_6\text{H}_5)]_2$ . Toluene (2 mL) was added to dissolve all the

solids and a solution of **1c** (60.0 mg, 0.644 mmol) in toluene (2 mL) was added dropwise. The mixture was allowed to stir for 15 minutes, during which time a colour change from dark red to dark orange-brown was observed. The resulting solution was filtered through a glass microfiber pipette filter to remove metallic nickel, and the solvent from the filtrate was removed under vacuum to yield a dark red-orange oil. The oil was then washed with cold pentane ( $-35\text{ }^{\circ}\text{C}$ ,  $5 \times 1\text{ mL}$ ), and subsequently dried under vacuum to yield a red-orange solid.  $^1\text{H}$  NMR data suggests the presence of many species and **3c** could not be identified.

### Synthesis of **4a**

**4a** was synthesized according to a modified procedure for a related compound by Gomes *et al.*<sup>13</sup>. In a 20 mL vial with a stir bar, a solution of NaI (26.3 mg, 0.175 mmol) in THF (1 mL) was added to a solution of **2a** (50.4 mg, 0.120 mmol), and allowed to stir for 30 hours. Removal of the solvent under vacuum yields a brown-orange solid. Diethyl ether was added to the reaction flask, and the resulting suspension was passed through a glass-microfiber filter pipette to remove the NaCl by-product. The filtrate was then concentrated to dryness under vacuum to yield **4a** as a bright orange solid (44.0 mg, 0.0859 mmol, 72%).  $^1\text{H}$  NMR ( $\text{CD}_2\text{Cl}_2$ , 400 MHz):  $\delta$  7.25 (d,  $^3J_{\text{H-H}} = 1.8\text{ Hz}$ , NCHCHN, 1H), 6.99 (s, Ar-H, 2H), 6.90 (d,  $^3J_{\text{H-H}} = 1.8\text{ Hz}$ , NCHCHN, 1H), 4.94 (m,  $\text{H}^3$ , 1H), 2.34 (s, *p*- $\text{CH}_3(\text{Ar})$ , 3H), 2.05 (s, *o*- $\text{CH}_3(\text{Ar})$ , 6H), 1.19 (s,  $\text{C}(\text{CH}_3)_3$ , 9H).  $^1\text{H}$  NMR ( $\text{CD}_2\text{Cl}_2$ , 400 MHz,  $-70\text{ }^{\circ}\text{C}$ ):  $\delta$  7.30 (s, NCHCHN, 1H), 6.96 (s, Ar-H, 1H), 6.92 (s, Ar-H, 1H), 6.88 (s, NCHCHN, 1H), 6.18 (t,  $^3J_{\text{H-H}} = 8.0\text{ Hz}$ , NH, 1H), 4.90 (ov,  $\text{H}^3$  and  $\text{H}^{6/7}$ , 2H), 4.32 (d,  $^2J_{\text{H-H}} = 14.0\text{ Hz}$ ,  $\text{H}^{6/7}$ , 1H), 4.12 (d,  $^3J_{\text{H-H}} = 5.0\text{ Hz}$ ,  $\text{H}^4$ , 1H), 3.50 (br,  $\text{H}^{8/9}$ , 1H), 3.26 (d,  $^3J_{\text{H-H}} = 15.0\text{ Hz}$ ,  $\text{H}^{1/2}$ , 1H), 2.29 (ov,  $\text{CH}_3(\text{Ar})$  and  $\text{H}^{8/9}$ , 4H), 1.91 (s,  $\text{CH}_3(\text{Ar})$ , 3H), 1.81 (s,  $\text{CH}_3(\text{Ar})$ , 3H), 1.70 (br,  $\text{H}^{4/5}$ , 1H), 1.16 (ov,  $\text{C}(\text{CH}_3)_3$  and  $\text{H}^{1/2}$ , 10H).  $^{13}\text{C}$  NMR ( $\text{CD}_2\text{Cl}_2$ , 100 MHz,  $-50\text{ }^{\circ}\text{C}$ ):  $\delta$  174.9 (NCN), 139.1 (Ar), 135.6 (Ar), 135.4 (Ar), 134.7 (Ar), 129.0 (Ar), 128.7 (Ar), 123.1 (NCH), 122.3 (NCH), 111.0 (C2), 74.2 (C3), 57.1 (NCMe<sub>3</sub>), 50.0 (C1), 43.1 (NCH<sub>2</sub>), 40.9 (NCH<sub>2</sub>), 29.4 (*t*Bu), 21.0 (Ar- Me), 18.0 (Ar- Me), 17.7 (Ar- Me). MALDI-MS: found  $m/z = 470.1$  [**4a** – allyl]<sup>++</sup>; calcd. for [**4a** – allyl]<sup>++</sup>  $m/z = 470.1$

### Attempted in-situ Deprotonation of **2a** with $\text{K}_2\text{CO}_3$

A 20 mL vial was equipped with a stir bar, and  $K_2CO_3$  (6.60 mg, 0.0480 mmol). To the vial was added a solution of **2a** (20.0 mg, 0.0478 mol) in  $C_6D_6$  (1 mL). The reaction mixture was allowed to stir for 3 days, and over this time the solution changed colour from dark orange to light orange.  $^1H$  NMR (benzene- $d_6$ , 600 MHz):  $\delta$  6.74 (br, 4H), 6.06 (br, 2H), 4.88 (br, 2H), 3.64 (br, 2H), 2.74 (br, 1H), 2.31-2.09 (br, 14H), 1.36-0.88 (br, 12H).

#### **Attempted in-situ Deprotonation of 2a with KH**

A similar method to above was employed, substituting  $K_2CO_3$  with KH (2.60 mg, 0.0648 mmol). A solution of **2a** (20.6 mg, 0.0490 mol) in 1 mL THF was added to the vial and allowed to stir for 24 hours. No change in colour was observed, however there was presence of metallic nickel in the reaction mixture. Solvent was removed under reduced pressure to give an orange solid.  $^1H$  NMR (benzene- $d_6$ , 400 MHz):  $\delta$  6.73-6.57 (br, 4H), 6.05 (br, 1H), 4.85 (br, 1H), 4.49 (br, 1H), 3.57 (br, 2H), 2.97 (br, 2H), 2.70 (br, 1H), 2.27-2.08 (br, 15 H), 1.41 (br, 1H), 0.97 (br, 12 H), 0.29 (br 1H).

#### **General procedure for the Semi-Quantification of GC-MS Data**

Reaction products were quantified relative to the internal standard cyclodecane, which was present in 1 molar equivalent to the nickel starting material. The response factor of the reaction product cinnamaldehyde relative to cyclodecane was determined to be 0.8 from a single point calibration. It is assumed that the response of both major oxidation products, cinnamaldehyde and phenyl vinyl ketone, have the same response factor. The area count for maximum product formation was thus set to 80% of the internal standard signal. The percentage conversion of the oxidation products was calculated as (area count of oxidation product / (area count of internal standard\* 0.80)) \* 100. It should be noted that a single point calibration is not sufficient for accurate data, however only the control reactions were analyzed by this method, and in this case only the presence (or lack thereof) of the oxidation products is of interest.

#### **General procedure for the Quantification of GC-FID Data**

Reaction products were quantified relative to the internal standard tetradecane, which was added in a 1 molar equivalent to the nickel starting material. The response factors for the

major oxidation products compared to tetradecane were determined by multi-point calibration curves performed in duplicate (Appendix 6.7). The response factor determined for authentic cinnamaldehyde relative to tetradecane was determined to be 0.58. A response factor of 0.46 was determined for phenyl vinyl ketone. The percentage conversion and selectivity of the oxidation products was calculated as shown below.

$$\% \text{ Aldehyde} = \left( \frac{\text{aldehyde area count} / 0.58}{\text{tetradecane area count}} \right) \times 100$$

$$\% \text{ Ketone} = \left( \frac{\text{ketone area count} / 0.46}{\text{tetradecane area count}} \right) \times 100$$

$$\% \text{ Yield} = \% \text{ Aldehyde} + \% \text{ Ketone}$$

$$\text{Selectivity} = \frac{\text{aldehyde area count} / 0.58}{\text{ketone area count} / 0.46}$$

In the case of the attempted catalytic reactions, 10 equivalents of tetradecane was present relative to the nickel starting material. The same formulas as above were used with the exception of dividing the area count of tetradecane by 10.

### **General Procedure for Analysis of Aerobic Oxidation of NiCl(cinnamyl)(NHC) over Time**

In a 20 mL vial, a solution was prepared containing either **3a**, **3b**, or [NiCl(cinnamyl)(LiPr)] (10 mM) and tetradecane (10 mM) as an internal standard, dissolved in the solvent of choice (THF, DCM, acetone, MeCN or DMF). The solution was daughtered into 2 mL GC vials in 1 mL portions. The vials were sealed with a screw cap fitted with a PTFE septum. These samples were then removed from the glovebox. Dry O<sub>2</sub> gas was bubbled through a stainless steel needle into each vial through the septum, fitted with a bleed needle, for ~20 seconds. An immediate colour change from dark orange to a very pale orange was observed, for the samples in THF and DCM. For the samples in acetone, DMF, and MeCN a colour change from dark orange to a very pale pink. The vials were left sealed under the O<sub>2</sub> atmosphere for a given wait time (5 minutes to 150 minutes) prior to analysis by GC-FID. The experiments were performed in duplicate. Data for these experiments can be found in Appendix 6.8, Table 6.5.

### Attempted Catalytic Aerobic Oxidation of 3b

In a 4 mL vial, **3b** (11.1 mg, 0.0199 mmol) was dissolved in 2 mL of THF to give a 10 mM solution. To this was added tetradecane (5.6  $\mu$ L, 0.020 mmol) as an internal standard, and 10 equivalents of allylbenzene (26.5  $\mu$ L, 0.200 mmol) as the substrate. Portions (1 mL) of the resulting solution were daughtered into two separate 2 mL GC vials, and removed from the glovebox. The samples then underwent reaction with dioxygen following a procedure identical to that described above (section 2.16). The samples were then analyzed by GC-FID at the following time periods after initial oxidation: 5 minutes, 1 hour, 4 hours, and 18 hours. Data for these experiments can be found in Table 3.2.

### Attempted Catalytic Aerobic Oxidation of 3b at Low Temperature

In a 25 mL round bottom flask equipped with a stir bar, **3b** (2.80 mg, 0.00503 mmol) was dissolved in 5 mL of MeCN to give a light orange 1 mM solution. 10 equivalents of the internal standard tetradecane (13.0  $\mu$ L, 0.0500 mmol), and 100 equivalents of the substrate allylbenzene (66.4  $\mu$ L, 0.500 mmol) were added to the solution. The flask was sealed with a septum and removed from the glovebox, and transferred to a dry ice-MeCN cold bath ( $\sim -30$  °C). The reaction mixture was allowed to sit at  $-30$  °C for 15 minutes. Dry dioxygen was bubbled into the reaction mixture for  $\sim 45$  seconds, whilst stirring at  $-30$ °C. An immediate colour change from orange to a very pale pink (almost colourless) was observed. The reaction remained stirring at  $-30$ °C for 15 minutes, before being brought back up to room temperature to ensure thawing of all reaction components. A 1.0 mL aliquot was transferred from the round bottom via syringe to a 2 mL GC vial, and analyzed by GC-FID. The reaction continued to stir at room temperature for 1.5 hours, and was once again analyzed by GC-FID. Data for these experiments can be found in Table 3.2.

### Attempted Catalytic Aerobic Oxidation of 3b with 1-Allyl-4-(trifluoromethyl)benzene



In a 25 mL round bottom flask equipped with a stir bar, a solution in MeCN similar to section 2.18 was prepared with the exception of 1-Allyl-4-(trifluoromethyl)benzene (83.8  $\mu$ L, 0.500 mmol) is now the substrate. A 1.0 mL portion of this solution was transferred to a NMR tube equipped with a septum cap. The round bottom flask and NMR tube were removed from the glovebox. The solution in the NMR tube was exposed to O<sub>2</sub> using the above oxidation method, resulting in a colour change from light orange to almost colourless. This sample was then analyzed by <sup>19</sup>F NMR within a time period of 10 minutes after oxidation. The solution in the round bottom was cooled to ~ 0 °C for 15 minutes, and reacted with dioxygen using above method. The reaction was kept at 0 °C for ~ 24 hours, and an aliquot was transferred to an NMR tube via a syringe, and analyzed by <sup>19</sup>F NMR spectroscopy. The solution remaining in the round bottom flask was then heated to 60 °C and allowed to stir for ~ 24 hours. An aliquot was transferred to an NMR tube via a syringe, and analyzed by <sup>19</sup>F NMR spectroscopy (Appendix 6.8, Figure 6.16)

### General Procedure for Control Reactions

In a 20 mL vial, **3a** (49.5 mg, 0.0999 mmol) was dissolved in 10 mL of THF to give a 10 mM stock solution. To this stock solution was added one equivalent of the internal standard cyclodecane (14.0 mg, 0.100 mmol). The stock solution was daughtered (0.5 mL portions) into four GC vials (A-D) and the solutions were further diluted with THF (0.5 mL) to give a 5 mM dark orange solution. To vials A and B an excess of degassed H<sub>2</sub>O (1.0  $\mu$ L, 0.056 mmol) was added, while no further changes were made to C and D. The samples were then analyzed by GC/MS without exposure to O<sub>2</sub>. A solution of **1a** (1.40 mg, 0.00499 mmol) in THF (1.0 mL) was prepared with one equivalent of the internal standard cyclodecane (0.70 mg, 0.0050 mmol). This sample then underwent the previously mentioned oxidation procedure, in which no change in colour (brown) was observed. [NiCl(CH<sub>2</sub>CHCH<sub>2</sub>C<sub>6</sub>H<sub>5</sub>)<sub>2</sub>] (2.10 mg, 0.00501 mmol) and cyclodecane (as an internal standard) were combined in a GC vial, and was filled up to a total volume of 1.0 mL with THF. The red solution underwent the previously described oxidation method, in which a change of colour to a colourless solution was observed. The nickel(II) dimer sample was then analyzed by GC/MS 15 minutes after oxidation. The experiments were performed in duplicate. Data for these experiments can be found in Table 3.1.



## References

1. Krysan, D. J.; Mackenzie, P. B. *J. Org. Chem.* **1990**, *55*, 4229-4230
2. He, Y.; Lv, M.-F.; Cai, C. *Dalton Trans.* **2012**, *41*, 12428-12433
3. Jong, H.; Patrick, B. O.; Fryzuk, M. D. *Can. J. Chem.* **2008**, *86*, 803-810
4. Jafarpour, L.; Stevens, E. D.; Nolan, S. P. *J. Organomet. Chem.* **2000**, *606*, 49-54
5. Dible, B. R.; Sigman, M. S. *J. Am. Chem. Soc.* **2003**, *125*, 872-873
6. Slagbrand, T.; Lundberg, H.; Adolfsson, H. *Chem. Eur. J.* **2014**, *49*, 16102-16106
7. Foster, P.; Chien, J. C. W.; Rausch, M. D.; *J. Organomet. Chem.* **1997**, 35-38
8. Shih, W.-C.; Wang, C.-H.; Chang, Y.-T.; Yap, G. P. A.; Ong, T.-G. *Organometallics* **2009**, *28*, 1060-1067
9. Howson, S. E.; Allan, L. E. N.; Chmel, N. P.; Clarkson, G. J.; Deeth, R. J.; Faulkner, A. D.; Simpson, D. H.; Scott, P. *Dalton Trans.* **2011**, *40*, 10416-10433
10. Arnold, P. L.; Mungur, S. A.; Blake, A. J.; Wilson, C. *Angew. Chem.* **2003**, *115*, 6163-6166
11. Dible, B. R.; Sigman, M. S. *J. Am. Chem. Soc.* **2003**, *125*, 872-873
12. Dible, B. R.; Sigman, M. S. *Inorg. Chem.* **2006**, *45*, 8430-8441
13. Silva, L. C.; Gomes, P. T.; Veiros, L. F.; Pascu, S. I.; Duarte, M. T.; Namorado, S.; Ascenso, J. R.; Dias, A. R. *Organometallics* **2006**, *25*, 4391-4403



## 6 Appendix

### 6.1 Crystallographic Data for 2a

#### Experimental for C<sub>21</sub>H<sub>32</sub>ClN<sub>3</sub>Ni (2a)

Data collection and structure solution performed by myself (Richard Hazlehurst) and Dr. Paul Boyle.

*Data Collection and Processing.* The sample was mounted on a Mitegen polyimide micromount with a small amount of Paratone N oil. All X-ray measurements were made on a Bruker Kappa Axis Apex2 diffractometer at a temperature of 110 K. The unit cell dimensions were determined from a symmetry constrained fit of 9707 reflections with  $5.2^\circ < 2\theta < 74.7^\circ$ . The data collection strategy was a number of  $\omega$  and  $\phi$  scans which collected data up to  $81.184^\circ$  ( $2\theta$ ). The frame integration was performed using SAINT.<sup>1</sup> The resulting raw data was scaled and absorption corrected using a multi-scan averaging of symmetry equivalent data using SADABS.<sup>2</sup>

*Structure Solution and Refinement.* The structure was solved by using a dual space methodology using the SHELXT program.<sup>3</sup> All non-hydrogen atoms were obtained from the initial solution. The allyl group exhibited a disorder wherein the atom C2 was distributed over 2 sites. The normalized occupancy for the predominant conformer refined to a value of 0.708(4). The carbon bound hydrogen atoms were introduced at idealized positions and were allowed to ride on the parent atom. The position of the hydrogen atom bound to N3 was recovered from a difference Fourier map and was allowed to refine isotropically. The structural model was fit to the data using full matrix least-squares based on  $F^2$ . The calculated structure factors included corrections for anomalous dispersion from the usual tabulation. The structure was refined using the SHELXL program from the SHELX suite of crystallographic software.<sup>4</sup> Graphic plots were produced using the NRCVAX program suite.<sup>5</sup>

**Table 6.1** Summary of crystal data for **2a**

Formula	C <sub>21</sub> H <sub>32</sub> ClN <sub>3</sub> Ni
Formula Weight ( <i>g/mol</i> )	420.65
Crystal Dimensions ( <i>mm</i> )	0.343 × 0.232 × 0.196
Crystal System	triclinic
Space Group	P -1
Temperature, K	110
<i>a</i> , Å	9.402(3)
<i>b</i> , Å	11.543(3)
<i>c</i> , Å	12.100(3)
α, °	63.047(8)
β, °	70.271(7)
γ, °	78.117(9)
<i>V</i> , Å <sup>3</sup>	1099.6(5)
<i>Z</i>	2
ρ ( <i>g/cm</i> )	1.270
λ, Å, (MoKα)	0.71073
μ, ( <i>cm</i> <sup>-1</sup> )	1.013
Measured fraction of data	0.992
R <sub>1</sub>	0.0389
wR <sub>2</sub>	0.0989
R <sub>1</sub> (all data)	0.0585
wR <sub>2</sub> (all data)	0.1068
GOF	1.045

Where:

$$R_1 = \sum (|F_o| - |F_c|) / \sum F_o$$

$$wR_2 = [ \sum (w(F_o^2 - F_c^2)^2) / \sum (w F_o^4) ]^{1/2}$$

$$GOF = [ \sum (w(F_o^2 - F_c^2)^2) / (\text{No. of reflns.} - \text{No. of params.}) ]^{1/2}$$

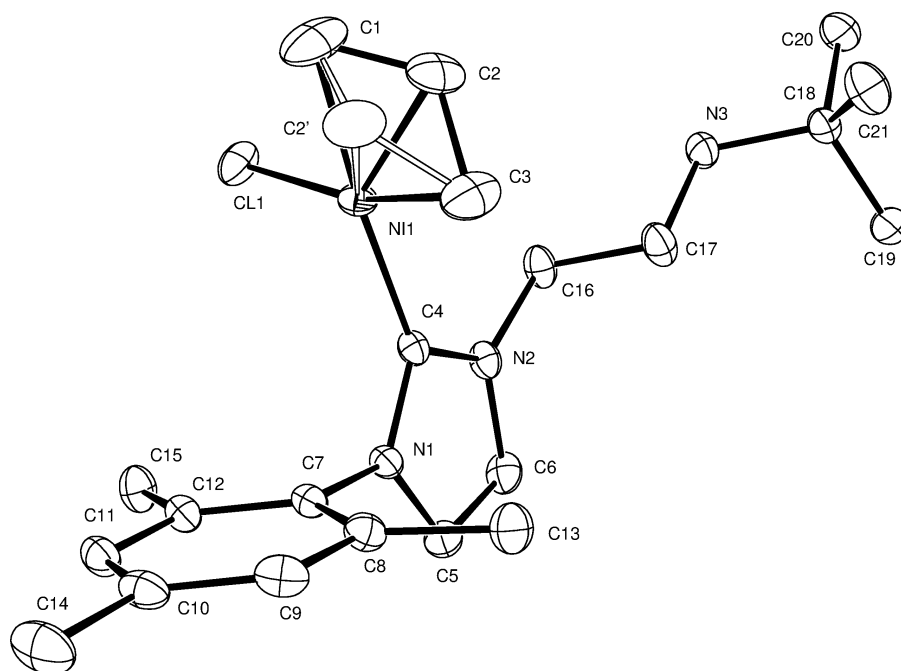


**Figure 6.1** ORTEP drawing of **2a** showing naming and numbering scheme. Ellipsoids are at the 50% probability level and hydrogen atoms were omitted for clarity. Disordered atom position is depicted using “hollow” ellipsoids and bonds

## 6.2 Crystallographic Data for 3b

### Experimental for $C_{32}H_{38}ClN_3Ni$ (**3b**)

Data collection and structure solution performed by myself (Richard Hazlehurst) and Dr. Paul Boyle.

*Data Collection and Processing.* The sample was mounted on a Mitegen polyimide micromount with a small amount of Paratone N oil. All X-ray measurements were made on a Bruker Kappa Axis Apex2 diffractometer at a temperature of 110 K. The unit cell dimensions were determined from a symmetry constrained fit of 9916 reflections with  $5.7^\circ$

$< 2\theta < 50.4^\circ$ . The data collection strategy was a number of  $\omega$  and  $\varphi$  scans which collected data up to  $56.688^\circ$  ( $2\theta$ ). The frame integration was performed using SAINT.<sup>1</sup> The resulting raw data was scaled and absorption corrected using a multi-scan averaging of symmetry equivalent data using SADABS.<sup>2</sup>

*Structure Solution and Refinement.* The structure was solved by using a dual space methodology using the SHELXT program.<sup>3</sup> Most non-hydrogen atoms were obtained from the initial solution. The remaining atomic positions were obtained from subsequent difference Fourier maps. The structure crystallized with 2 molecules in the asymmetric unit designated molecules A and B. Both molecules exhibited disorders in the cinnamyl groups. The disorder was slightly different in each molecule and is described below.

*Disorder in Molecule A.* Within molecule A, the cinnamyl was disordered over 2 orientations. The orientations were differentiated by an “A”/”C” naming scheme. The normalized occupancy refined to a value of 0.421(6) for orientation A. There was a number of common atoms sites shared between the two orientations. These shared sites were: C31A/C30C, C30A/C29C, C27A/C27B, and C3A/C3C.

*Disorder in Molecule B.* Within molecule B, the cinnamyl was disordered over 2 orientations. The orientations were differentiated by an “B”/”D” naming scheme. The normalized occupancy refined to a value of 0.564(5) for orientation B. There was a number of common atoms sites shared between the two orientations. These shared sites were: C29B/C31D, C27B/C27D, C2B/C2D, and C3B/C3D. The difference in disorders between molecules A and B was the presence of 2 independent sites for C2(A/C) in molecule A, separated by a distance of 0.49 Å whereas in molecule B, the C2 site for the B and D conformers was a common site.

The carbon bound hydrogen atoms were introduced at idealized positions and were allowed to ride on the parent atom. The positions of the hydrogen atoms bound to N3{A,B} were obtained from a difference Fourier map and were idealized so the N—H bond was 0.86 Å and then were allowed ride on the parent nitrogen atom. The structural model was fit to

the data using full matrix least-squares based on  $F^2$ . The calculated structure factors included corrections for anomalous dispersion from the usual tabulation. The structure was refined using the SHELXL program from the SHELX suite of crystallographic software.<sup>4</sup> Graphic plots were produced using the NRCVAX program suite.<sup>5</sup>

**Table 6.2** Summary of crystal data for **3b**

Formula	$C_{32}H_{38}ClN_3Ni$
Formula Weight ( <i>g/mol</i> )	558.81
Crystal Dimensions ( <i>mm</i> )	$0.239 \times 0.141 \times 0.057$
Crystal System	triclinic
Space Group	P -1
Temperature, K	110
<i>a</i> , Å	10.548(5)
<i>b</i> , Å	15.072(7)
<i>c</i> , Å	19.440(6)
$\alpha$ , °	88.549(8)
$\beta$ , °	82.640(9)
$\gamma$ , °	71.483(12)
<i>V</i> , Å <sup>3</sup>	2906(2)
<i>Z</i>	4
$\rho$ ( <i>g/cm</i> )	1.277
$\lambda$ , Å, (MoK $\alpha$ )	0.71073
$\mu$ , ( <i>cm</i> <sup>-1</sup> )	0.784
Measured fraction of data	0.988
<i>R</i> <sub>1</sub>	0.0518
<i>wR</i> <sub>2</sub>	0.1162
<i>R</i> <sub>1</sub> (all data)	0.1082
<i>wR</i> <sub>2</sub> (all data)	0.1369
GOF	1.027

Where:

$$R_1 = \frac{\sum (|F_o| - |F_c|)}{\sum F_o}$$

$$wR_2 = \left[ \frac{\sum (w(F_o^2 - F_c^2)^2)}{\sum (w F_o^4)} \right]^{1/2}$$

$$\text{GOF} = [ \sum w( F_o^2 - F_c^2 )^2 / (\text{No. of reflns.} - \text{No. of params.} ) ]^{1/2}$$

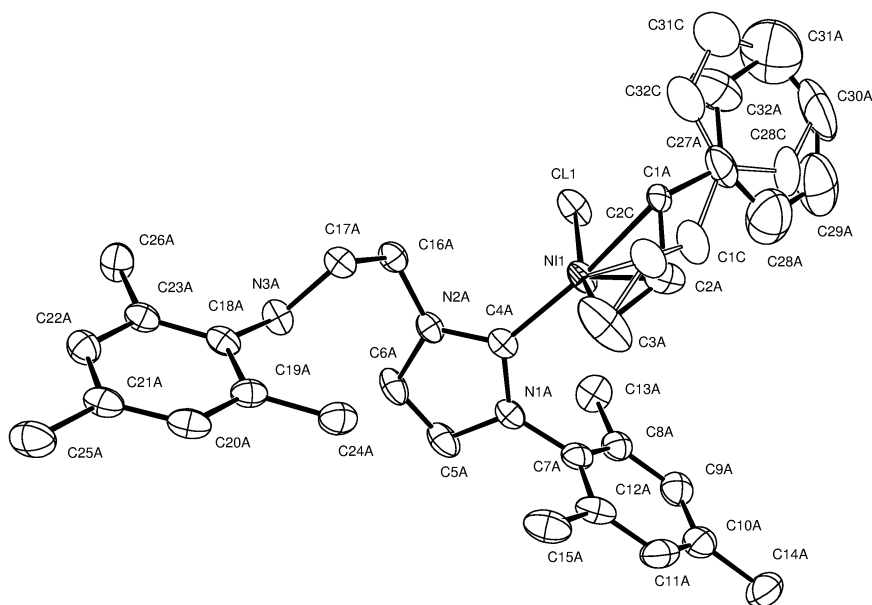


**Figure 6.2** ORTEP drawing of molecule A (**3b**) showing naming and numbering scheme. Ellipsoids are at the 50% probability level and hydrogen atoms were omitted for clarity. Disordered part of the structures is depicted by “hollow” atoms and bonds



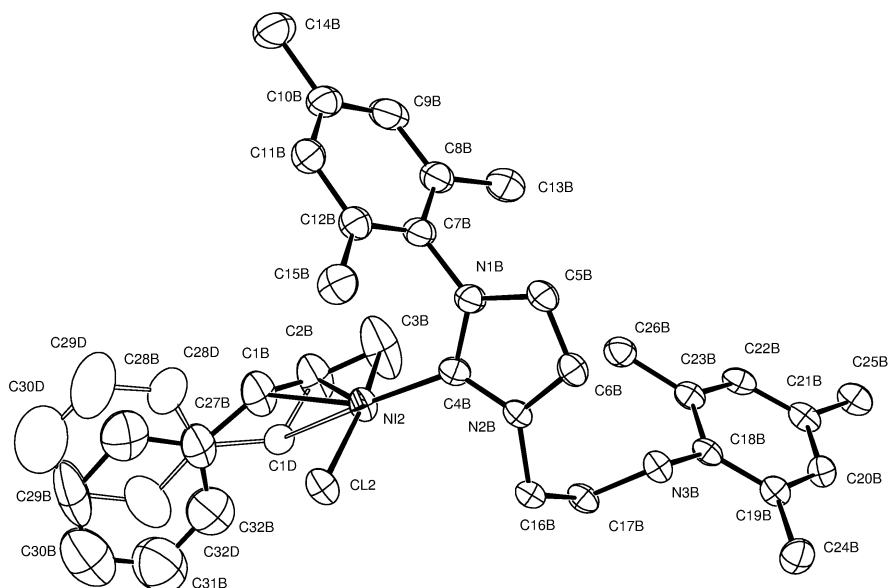


**Figure 6.3** ORTEP drawing of molecule B (**3b**) showing naming and numbering scheme. Ellipsoids are at the 50% probability level and hydrogen atoms were omitted for clarity. Disordered part of the structures is depicted by “hollow” atoms and bonds

**Table 6.3** Selected bond lengths (Å) and bond angles (deg) for molecule B (**3b**)

<b>3b</b>	
Ni(1)-C(4)	1.899(3)
Ni(1)-C(3)	1.989(4)
Ni(1)-C(2)	1.957(3)
Ni(1)-C(1)	2.136(6)
Ni(1)-Cl(1)	2.2088(10)
C(4)-Ni(1)-Cl(1)	97.08(9)
C(1)-C(2)-C(3)	145.3(5)
Hydrogen bonding (N3...Cl1)	3.432(3)

### 6.3 Crystallographic Data for 3a

#### Experimental for C<sub>34</sub>H<sub>44</sub>ClN<sub>3</sub>Ni (**3a**)

Data collection and structure solution performed by Dr. Paul Boyle.

*Data Collection and Processing.* The sample was mounted on a Mitegen polyimide micromount with a small amount of Paratone N oil. All X-ray measurements were made on a Bruker-Nonius KappaCCD Apex2 diffractometer at a temperature of 110 K. The unit cell dimensions were determined from a symmetry constrained fit of 5108 reflections with  $8.82^\circ < 2\theta < 131.58^\circ$ . The data collection strategy was a number of  $\omega$  and  $\phi$  scans which collected data up to  $135.112^\circ$  ( $2\theta$ ). The frame integration was performed using SAINT.<sup>1</sup> The resulting raw data was scaled and absorption corrected using a multi-scan averaging of symmetry equivalent data using SADABS.<sup>2</sup>

*Structure Solution and Refinement.* The structure was solved by using a dual space methodology using the SHELXT program.<sup>3</sup> All non-hydrogen atoms were obtained from the initial solution. The hydrogen atoms were introduced at idealized positions and were

allowed to ride on the parent atom. The structural model was fit to the data using full matrix least-squares based on  $F^2$ . The calculated structure factors included corrections for anomalous dispersion from the usual tabulation. The structure was refined using the SHELXL-2014 program from the SHELX suite of crystallographic software.<sup>4</sup> Graphic plots were produced using the NRCVAX program suite.<sup>5</sup>

**Table 6.4** Summary of crystal data for **3a**

Formula	$C_{34}H_{44}ClN_3Ni$
Formula Weight ( <i>g/mol</i> )	588.88
Crystal Dimensions ( <i>mm</i> )	$0.190 \times 0.100 \times 0.056$
Crystal System	monoclinic
Space Group	P 2 <sub>1</sub> /c
Temperature, K	110
<i>a</i> , Å	11.365(2)
<i>b</i> , Å	10.896(3)
<i>c</i> , Å	25.833(4)
$\alpha$ , °	90
$\beta$ , °	97.961(15)
$\gamma$ , °	90
<i>V</i> , Å <sup>3</sup>	3168.1(12)
<i>Z</i>	4
$\rho$ ( <i>g/cm</i> )	1.235
$\lambda$ , Å, (CuK $\alpha$ )	1.54178
$\mu$ , ( <i>cm</i> <sup>-1</sup> )	1.844
Measured fraction of data	0.967
R <sub>1</sub>	0.0529
wR <sub>2</sub>	0.1311
R <sub>1</sub> (all data)	0.0896
wR <sub>2</sub> (all data)	0.1509
GOF	1.020

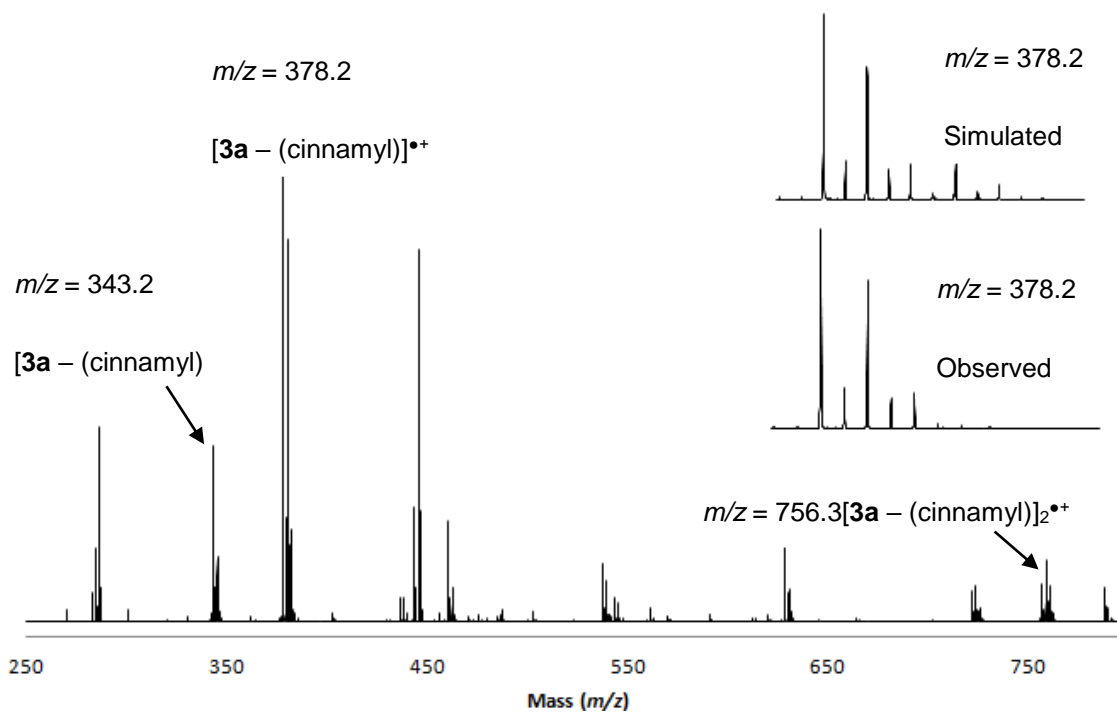
Where:

$$R_1 = \frac{\sum (|F_o| - |F_c|)}{\sum F_o}$$

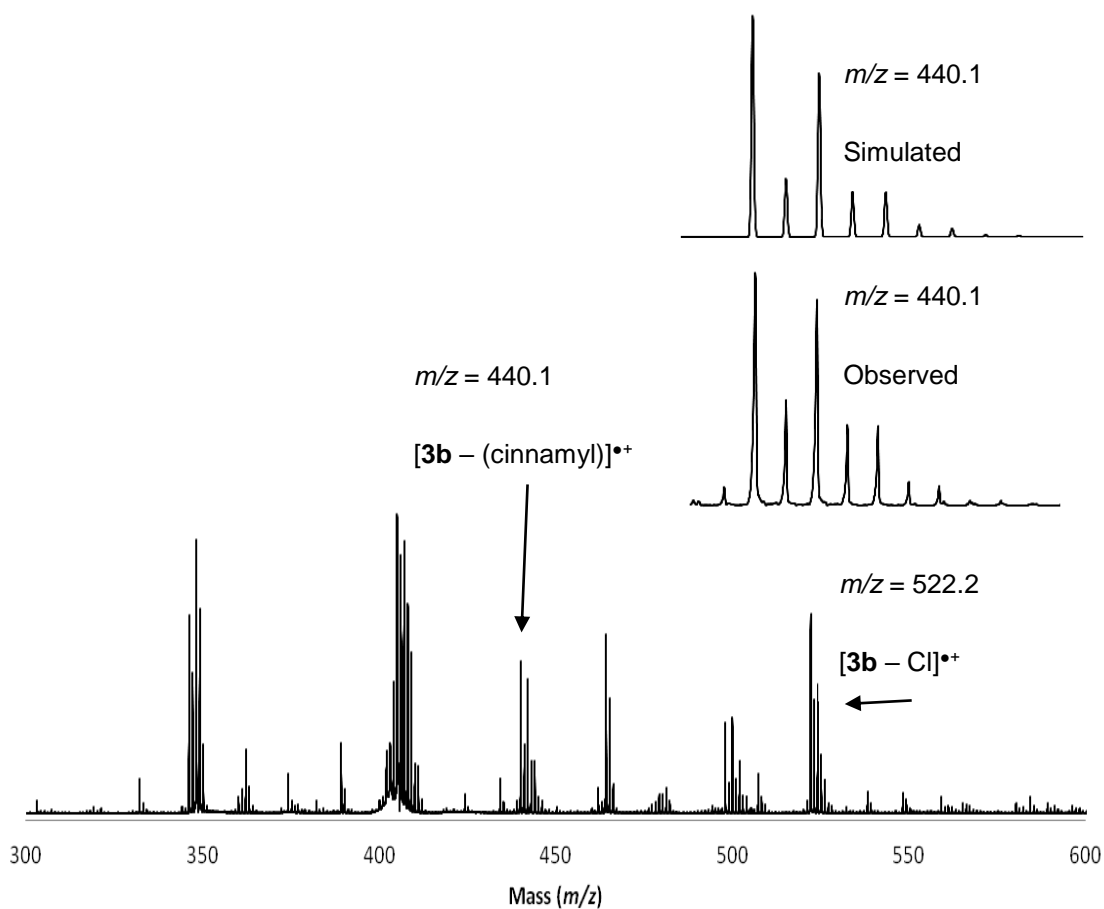
$$wR_2 = \left[ \frac{\sum w (F_o^2 - F_c^2)^2}{\sum w F_o^4} \right]^{1/2}$$

$$GOF = \left[ \frac{\sum w (F_o^2 - F_c^2)^2}{(\text{No. of reflns.} - \text{No. of params.})} \right]^{1/2}$$

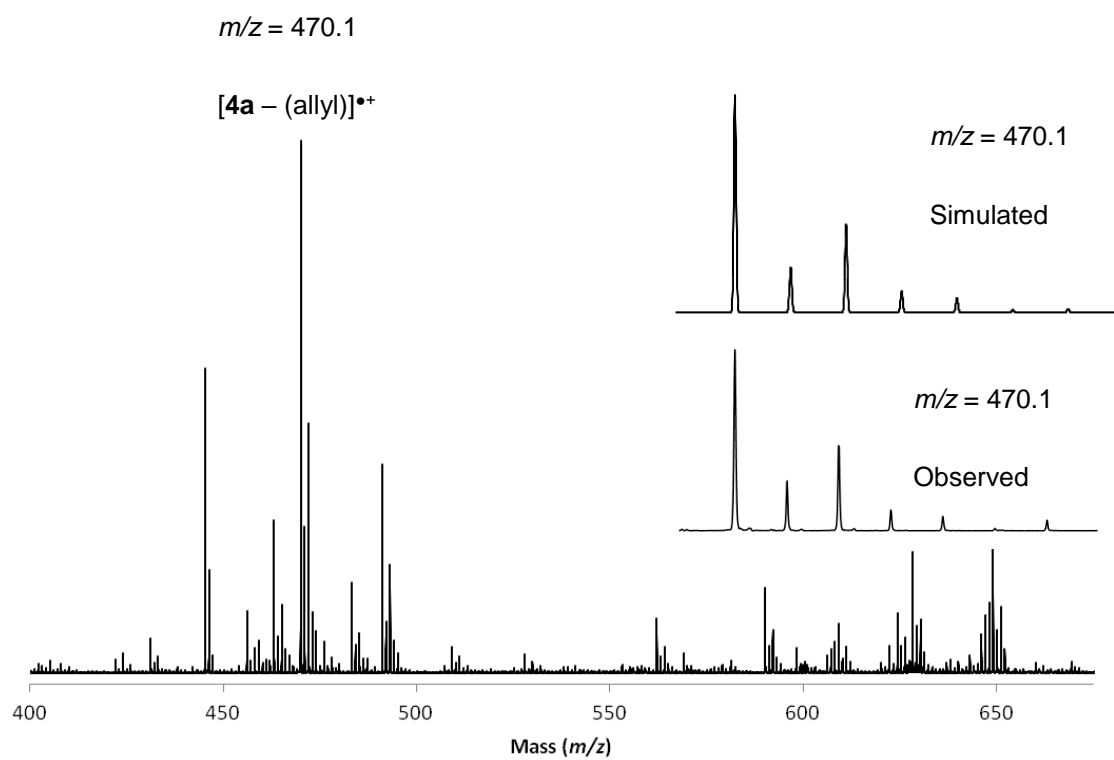
## 6.4 MALDI-MS Data



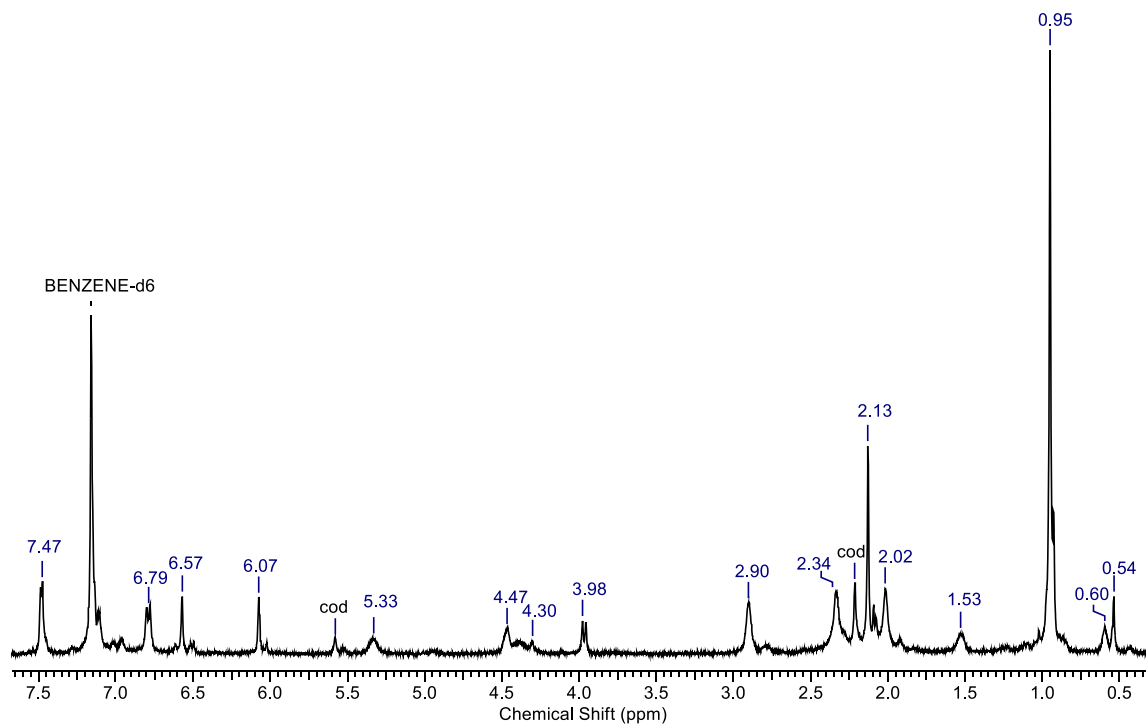
**Figure 6.4** MALDI-MS of **3a** with anthracene as the matrix. The inset depicts the simulated and observed isotope pattern for the most abundant signal



**Figure 6.5** MALDI-MS of **3b** with anthracene as the matrix. The inset depicts the simulated and observed isotope pattern for the signal at  $m/z = 440.1$

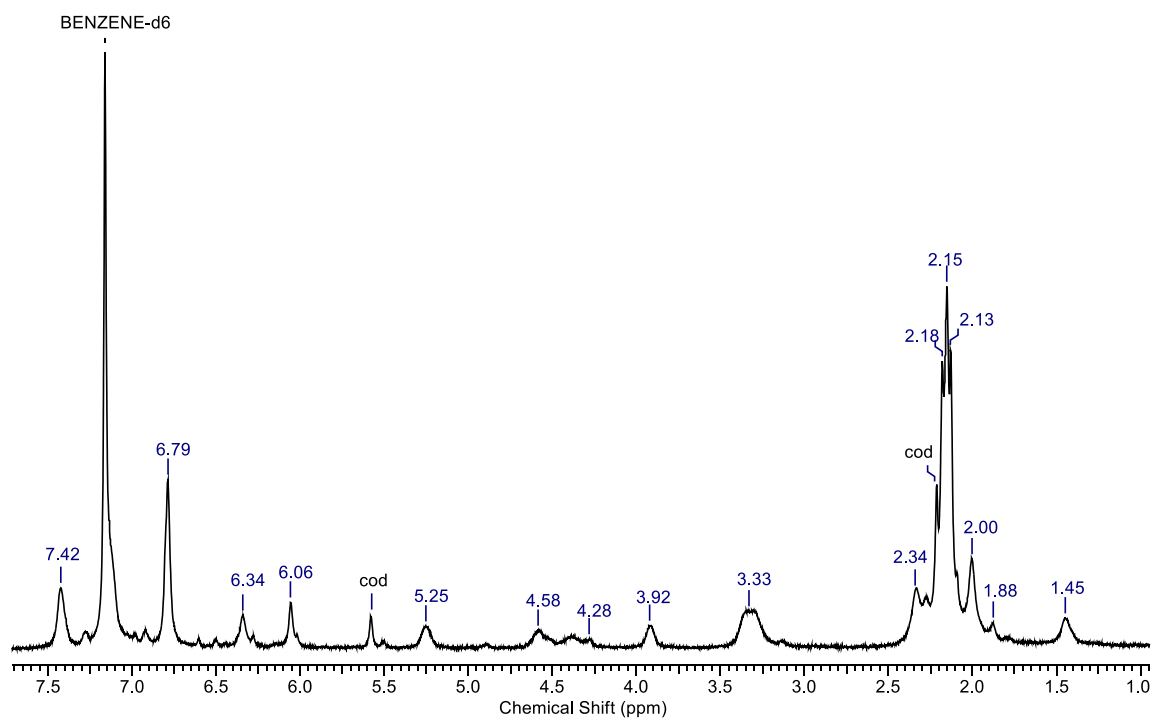


**Figure 6.6** MALDI MS of **4a** with pyrene as the matrix. The inset depicts the simulated and observed isotope pattern for the most abundant signal

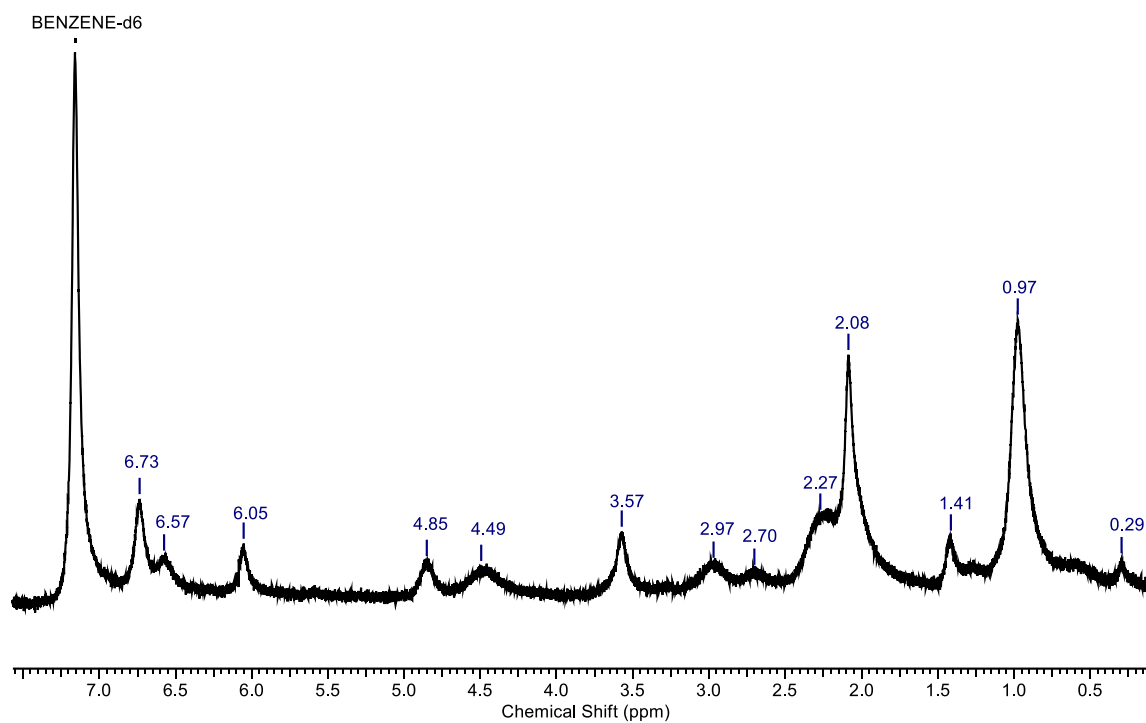
6.5  $^1\text{H}$  NMR Spectra

**Figure 6.7**  $^1\text{H}$  NMR spectrum (in  $\text{C}_6\text{D}_6$ ) of **3a**, 600 MHz

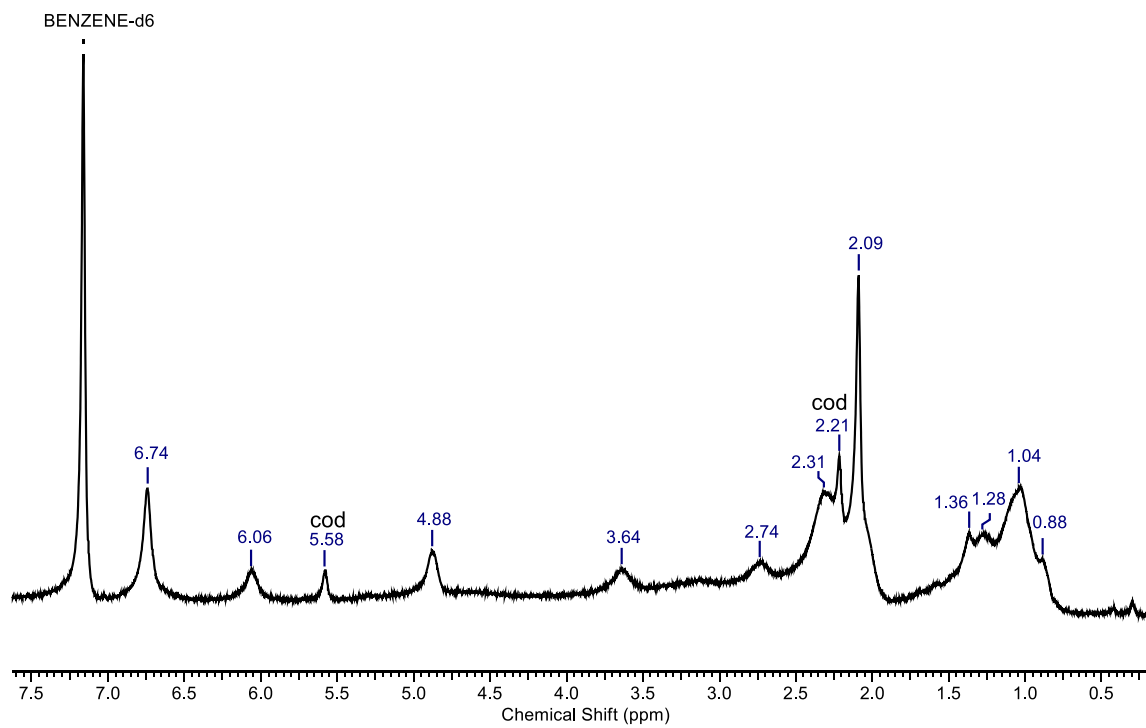




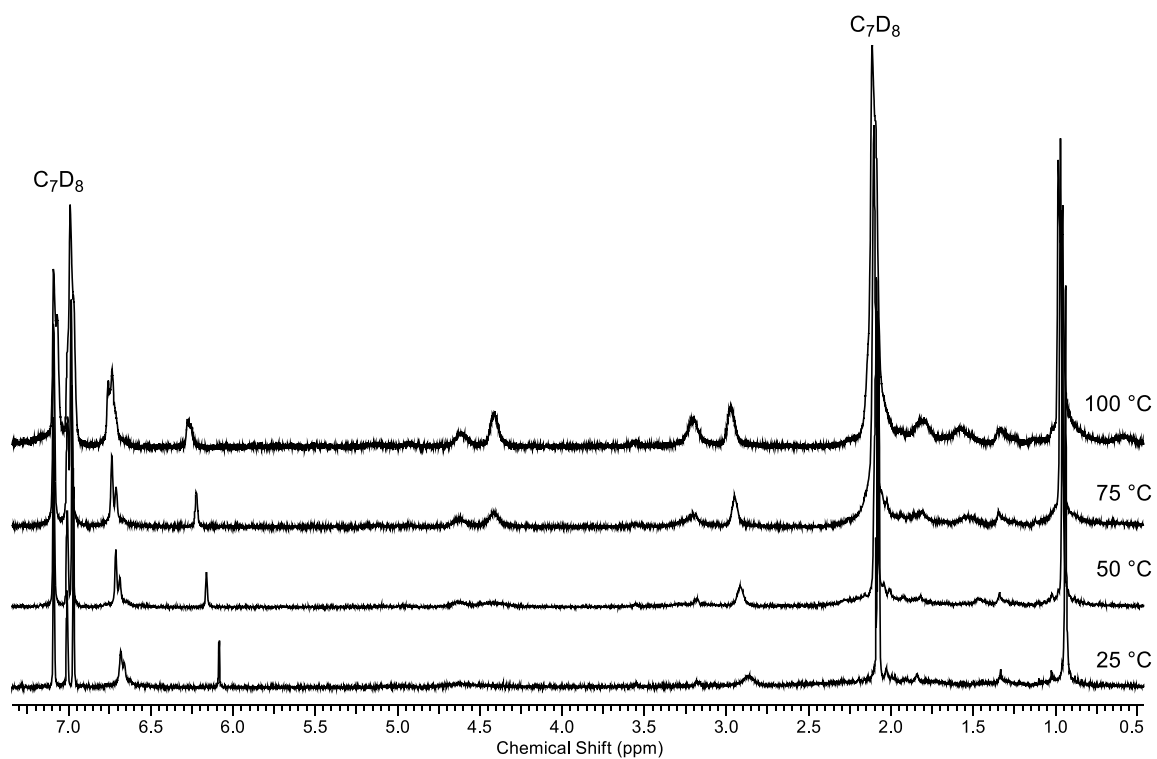
**Figure 6.8**  $^1\text{H}$  NMR Spectrum (in  $\text{C}_6\text{D}_6$ ) for Complex **3b**, 600 MHz



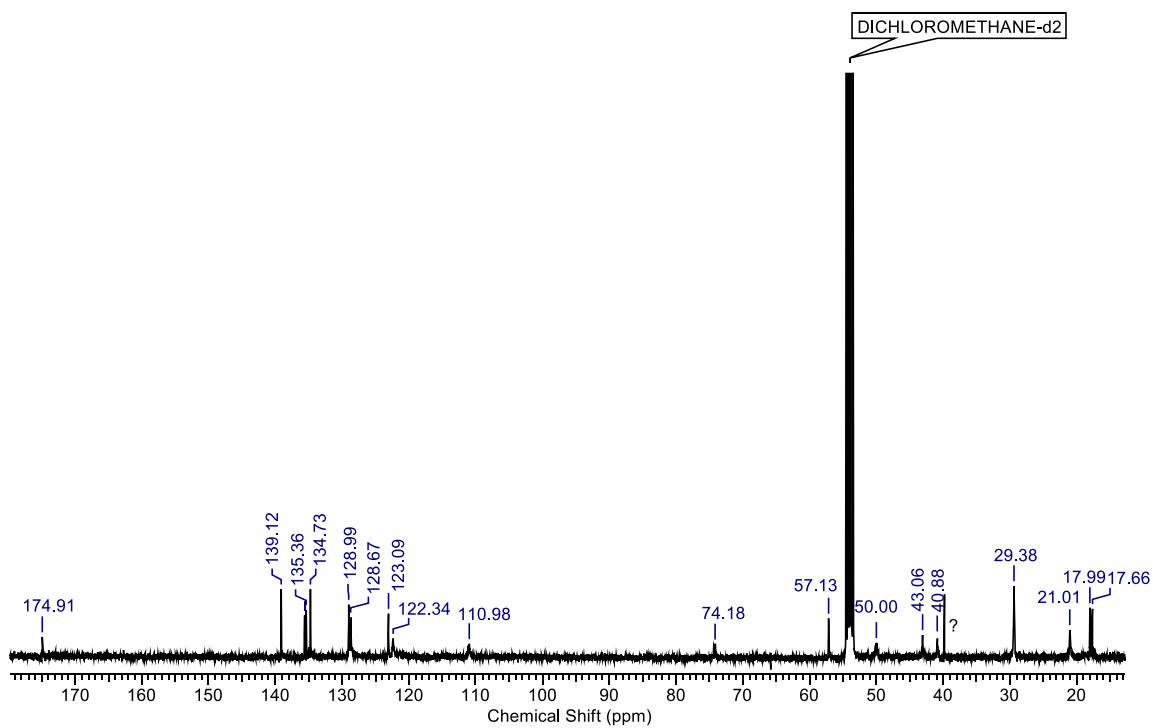
**Figure 6.9**  $^1\text{H}$  NMR Spectrum (in  $\text{C}_6\text{D}_6$ ) for reaction of **2a** with KH, 400 MHz



**Figure 6.10**  $^1\text{H}$  NMR Spectrum (in  $\text{C}_6\text{D}_6$ ) for reaction of **2a** with  $\text{K}_2\text{CO}_3$ , 600 MHz



**Figure 6.11** High Temperature Variable-Temperature  $^1\text{H}$  NMR Spectra for **4a** in  $\text{C}_7\text{D}_8$ , 400 MHz

6.6  $^{13}\text{C}$  NMR Spectrum for Complex 4a

**Figure 6.12**  $^{13}\text{C}$  NMR Spectrum (in  $\text{CD}_2\text{Cl}_2$ ) for Complex **4a** at  $-50\text{ }^\circ\text{C}$

## 6.7 GC-FID Calibration Data for Aerobic Oxidation Reactions

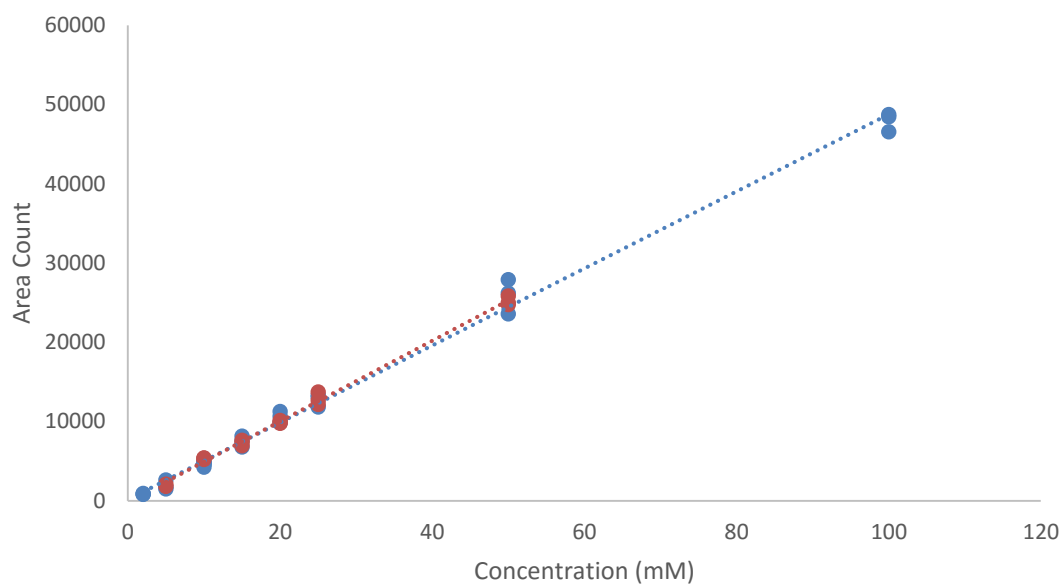


**Figure 6.13** Plot of tetradecane area count vs concentration. Red and blue dots represent data from two separate runs. Triple injections of each concentration were made. Acetone was the solvent. Dotted coloured lines represent linear trend line for respective run

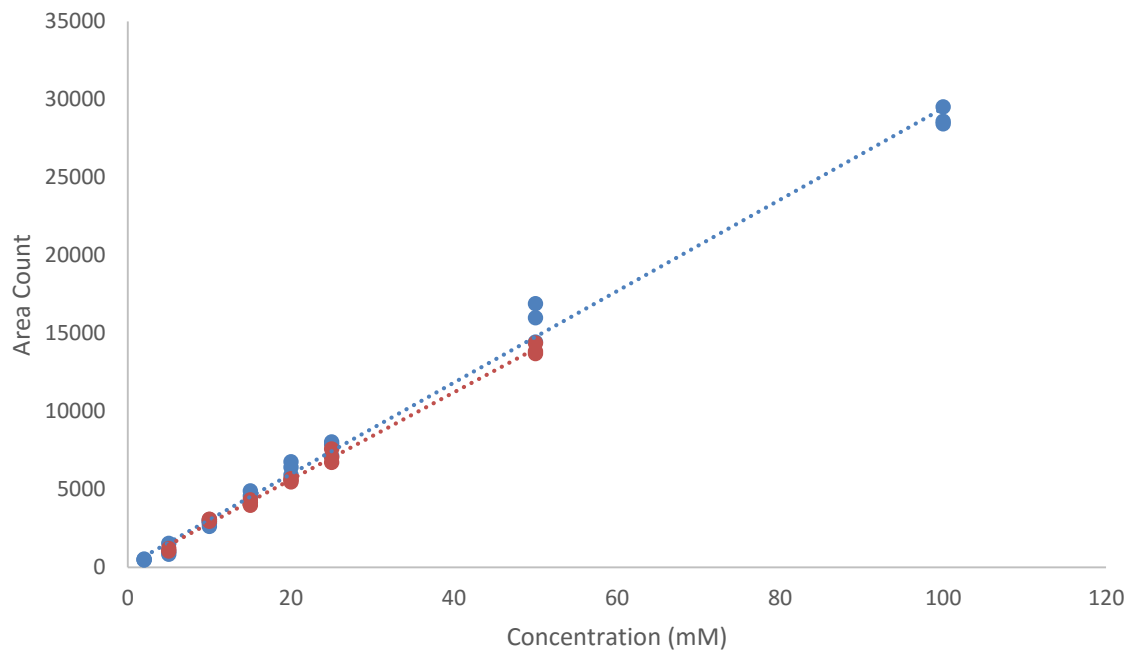


**Figure 6.14** Plot of cinnamaldehyde (**6**) area count vs concentration. Red and blue dots represent data from two separate runs. Triple injections of each concentration were made. Acetone was the solvent. Dotted coloured lines represent linear trend line for respective run

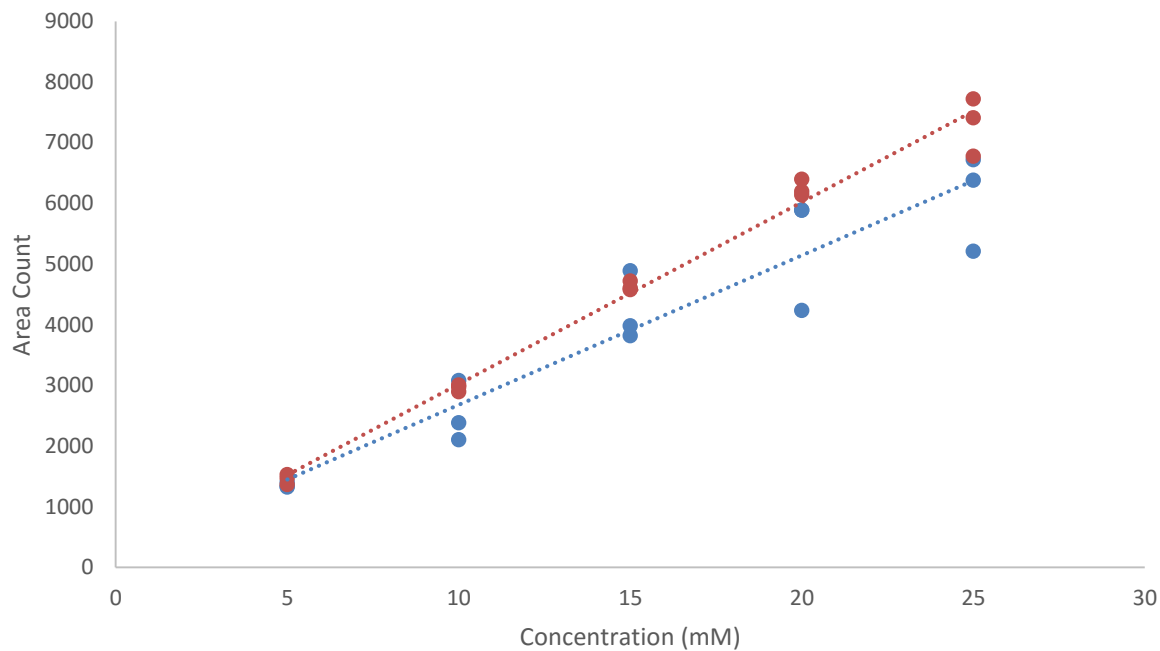


**Figure 6.15** Plot of phenyl vinyl ketone (**5**) area count vs. concentration. Red and blue dots represent data from two separate runs. Triple injections of each concentration were made. Acetone was the solvent. Dotted coloured lines represent linear trend line for respective run



## 6.8 Data for Aerobic Oxidation Reactions

**Table 6.5** Data for aerobic oxidation reactions of complexes **3a** and **3b**.<sup>a</sup>

Entry	Time (min.)	Complex	Solvent	%Ketone (5)	%Aldehyde (6)	Yield <sup>b</sup>	A:K <sup>c</sup>
1	5 min	3a	THF	26	37	63	1.42:1
2	15 min	3a	THF	29	34	63	1.18:1
3	30 min	3a	THF	29	34	63	1.20:1
4	60 min	3a	THF	28	35	63	1.26:1
5	150 min	3a	THF	27	36	63	1.29:1
6	15min	3a	DCM	35	33	68	0.92:1
7	15min	3a	Acetone	24	28	52	1.20:1
8	15min	3a	MeCN	46	43	89	0.93:1
9	15min	3a	DMF	25	26	51	1.04:1
10	15min	3b	THF	33	39	72	1.16:1
11	30 min	3b	THF	32	35	67	1.09:1

<sup>a</sup> Conditions: 10 mM [Ni], 10 mM tetradecane, room temperature. Analyzed by GC-FID. <sup>b</sup> Combined yield of phenyl vinyl ketone (5) and cinnamaldehyde (6). <sup>c</sup>Yield of 6 divided by yield of 5

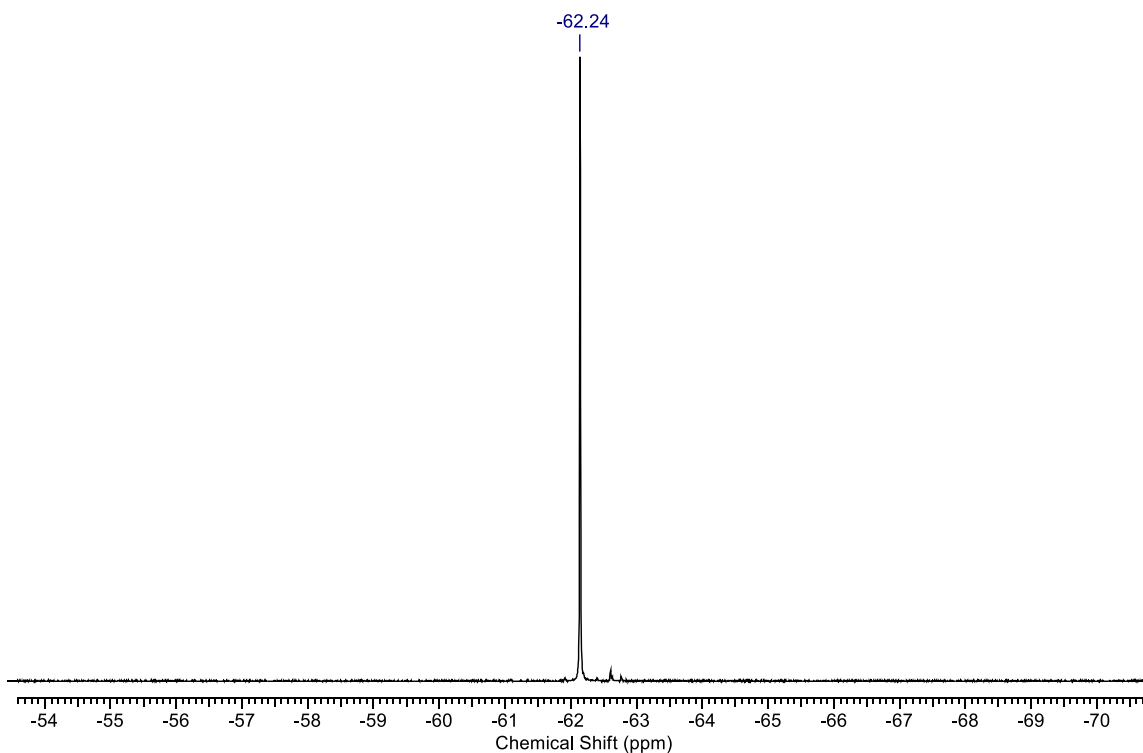


**Figure 6.16** Representative  $^{19}\text{F}$  NMR Spectrum for Attempted Catalytic Aerobic Oxidation of 1-allyl-4-(trifluoromethyl)benzene with **3b**

## 6.9 References

1. Bruker-AXS, SAINT version 2013.8, **2013**, Bruker-AXS, Madison, WI 53711, USA
2. Bruker-AXS, SADABS version 2012.1, **2012**, Bruker-AXS, Madison, WI 53711, USA
3. Sheldrick, G. M., *Acta Cryst.* **2015**, A71, 3-8
4. Sheldrick, G. M., *Acta Cryst.* **2015**, C71, 3-8
5. Gabe, E. J.; Le Page, Y.; Charland, J. P.; Lee, F. L. and White, P. S. *J. Appl. Cryst.* **1989**, 22, 384-387

# Curriculum Vitae

**Richard J. Hazlehurst**

## Education

**Master of Science in Chemistry (in progress) 2014 - Present**

*The University of Western Ontario* London, Ontario

- Thesis supervisor: Dr. Johanna M. Blacquiere. Thesis title: Aerobic Oxidations Mediated by NiCl(allyl)(NHC) Complexes: Investigating the Role of a Pendent H-Bonding Group

**Bachelor of Science, Honors Specialization in Chemistry  
2009 - 2013**

*The University of Western Ontario* London, Ontario

- Thesis supervisor: Dr. Richard J. Puddephatt. Thesis title: Oxidative Addition of Cyclobutane Malonoyl Peroxide to Dimethylplatinum(II) Complexes

## Other Research Experience

**Research Assistant – Dr. Paul J. Ragona Research Group  
Summer 2012**

*The University of Western Ontario* London, Ontario

- Creation of ultrathin polymer films by the photo-polymerization of phosphonium salts

## Teaching Assistant Experience

- Chemistry 1301: Discovering Chemical Structure **Fall 2014, Summer 2015**
- Chemistry 2281: Inorganic Chemistry of the Main Group Elements **Winter 2015**
- Chemistry 1302: Discovering Chemical Energetics **Winter 2014, Summer 2015**

---

### Publications and Conferences (FP = Full Paper, PP = Poster Presentation)

**FP1.** Hazlehurst, R. J.; Pellarin, K. R.; McCready, M. S.; Puddephatt, R. J. "Oxidation of dimethylplatinum(II) complexes with malonyl peroxide derivatives", *Can. J. Chem.* **2015**, 93, 74

**PP1.** Hazlehurst, R. J.; Blacquiere, J. M. "Aerobic Oxidations Mediated by Ni(NHC) Complexes: Investigating the Role of a Pendent H-Bonding Group", *98<sup>th</sup> Canadian Chemistry Conference and Exhibition*, **June 2015**, Ottawa, Ontario

---

### Summary of Course Work

- Crystallography I, Chem 9541, 0.5 credits, Grade achieved: 94
- Molecular Energy Conversion, Chem 9531, 0.25 credits, Grade achieved: 89
- Organometallic Chemistry for Bond Activation, Chem 9651, 0.25 credits, Grade achieved: 90
- Seminar, Chem 9658, 0.5 credits, Grade achieved: 84

---

### Volunteer Experiences

#### Student Volunteer

**July 2014**

*19th International Symposium on Homogeneous Catalysis*

Ottawa, Ontario

---

### Certifications

- First Aid (Level C)
- WHMIS
- Laboratory - Environmental Waste Management Safety Training
- X-ray Safety Training

---

### Awards

- The Western Scholarship of Excellence, *The University of Western Ontario*, **2009**
- Dean's Honor List, *The University of Western Ontario*, **2013**